The Proof-of-Principle of the SABRE experiment for the search of galactic dark matter through annual modulation

PhD candidate:
Ambra Mariani

GRAN SASSO SCIENCE INSTITUTE
SCHOOL OF ADVANCED STUDIES
Scuola Universitaria Superiore

SABRE

Astroparticle Physics - XXXIII cycle
14/05/2020

Advisors:
Aldo Ianni
Claudia Tomei

Outline

- Introduction to dark matter and direct detection
- The SABRE project
- **Characterization of SABRE crystals in the Proof-of-Principle setup**
  - Measurement of potassium contamination
  - Background model of NaI-33 crystal
- Future perspectives
- Summary and conclusions

Evidences of dark matter

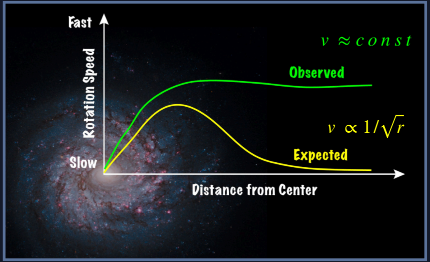

APOD: 2018 March 26 - NASA.

APOD: 2006 August 24 - NASA.

Spiral galaxies velocity rotation curve | **Velocity of galaxies in clusters** | **Clusters collisions**

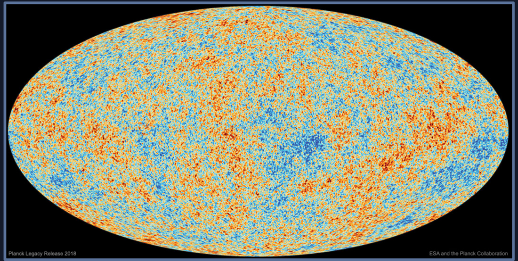

P. A. R. Ade et al., *Astronomy & Astrophysics*, 594:A13, 2016.

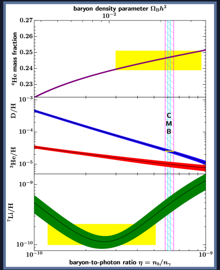

M. Tanabashi et al. , *Phys. Rev. D*, 98(3):030001, 2018.

Cosmic Microwave Background (CMB) | **Big Bang Nucleosynthesis (BBN)** | **Larger scales (older times)…**

"Dark matter is present in the Universe in far greater amount than visible matter."

\- F. Zwicky-

The Universe in mainly “dark”

5 % Visible matter

26 % Dark matter — What is it?

69 % Dark energy

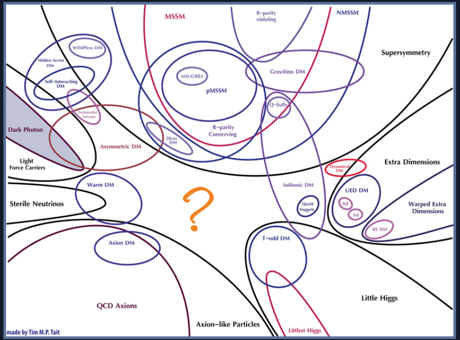

A lot of theories and candidates…

Its nature is still undiscovered, but data tells us that dark matter (DM):

- Makes up almost all the Universe matter
- Interacts very weakly (besides gravitationally)
- Is non-relativistic (“cold”)
- Is non-baryonic
- Is stable (or at least very long-lived)

Some dark matter candidates…

- **Primordial Black Holes**
- **MACHOs**

(Massive Astrophysical Compact Halo Object)

Axions **Thermal relics** **WIMPs**

Masses

Particle Macroscopic

Hypothetical Nambu-Goldstone boson arising as a solution to the strong-CP problem

R. D. Peccei and H. R. Quinn, *Phys. Rev.* D, 16:1791–1797, 1977.

Ruled out as the main DM component

C. Alcock et al., *Astrophys. J.*, 542(1):281–307, 2000.
P. Tisserand et al., *Astronomy & Astrophysics*, 469(2):387–404, 2007.
P. A. R. Ade et al., *Astronomy & Astrophysics,* 594:A13, 2016. M. Zumalacárregui and U. Seljak, *Phys. Rev. Lett.*, 121(14):141101, 2018.

Weakly Interacting Massive Particles

Most popular among the various DM candidates

Direct detection of dark matter

Direct detection experiments look for interactions among DM particles and ordinary matter in Earth-based detectors

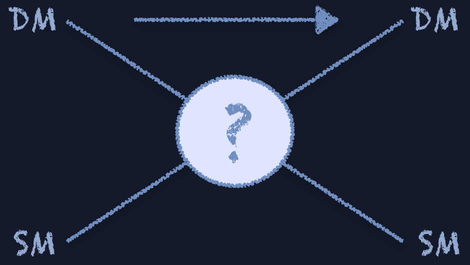

WIMP case (simplest scenario):
elastic scattering off target nuclei

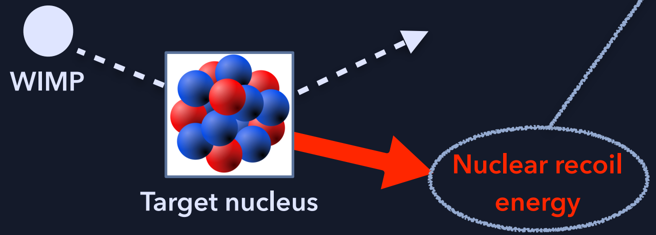

Measurable quantity

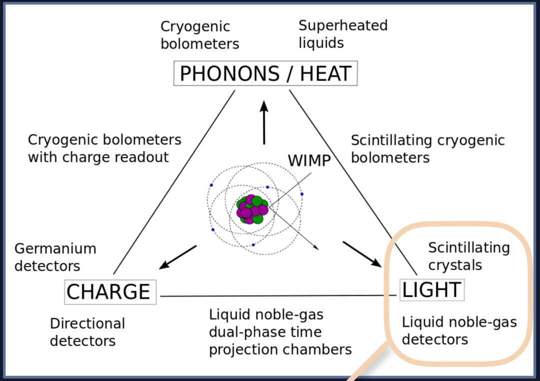

Scintillation light produced by nuclear recoils is reduced w.r.t. electron recoils of the same energy:
$E_{ee} = QF \cdot E_{nr}$
QF (< 1) is the **quenching factor**.

The nuclear recoil energy is 1-100 keV for a 10-1000 GeV/c^2 WIMP

WIMPs event rate

$$\frac{dR}{dE_R}(E_R, t) = \frac{\rho_{DM}}{M_T M_{DM}} \int_{v \geq v_{min}} \frac{d\sigma}{dE_R}(E_R, v) f(v,t)\, v\, d^3v$$

Local dark matter density
Canonical value: ~0.3 GeV/cm^3

Target nucleus mass

Dark matter mass

Cross section
An explicit expression requires arbitrary assumptions on the unknown WIMP-nucleus interaction.

DM velocity distribution in the Earth reference frame
Depends on the DM Halo model.

Widely adopted to present scientific results:
- **Spin-independent cross section** (σ_{SI});
- **Spin-dependent cross section** (σ_{SD}).

Simplest:
Standard Halo Model (SHM)
- Isothermal and isotropic sphere;
- Truncated Maxwell-Boltzmann velocity distribution:
  - Null mean velocity w.r.t. Galactic frame;
  - v_0= 220 km/s;
  - v_{esc} = 544 km/s.

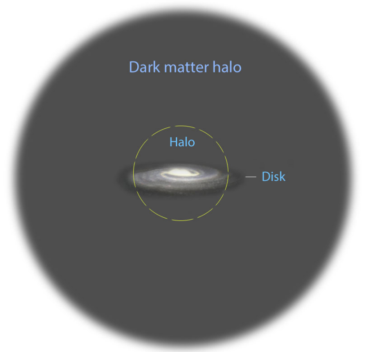

Milky Way model

Spin-independent nuclear recoil spectrum

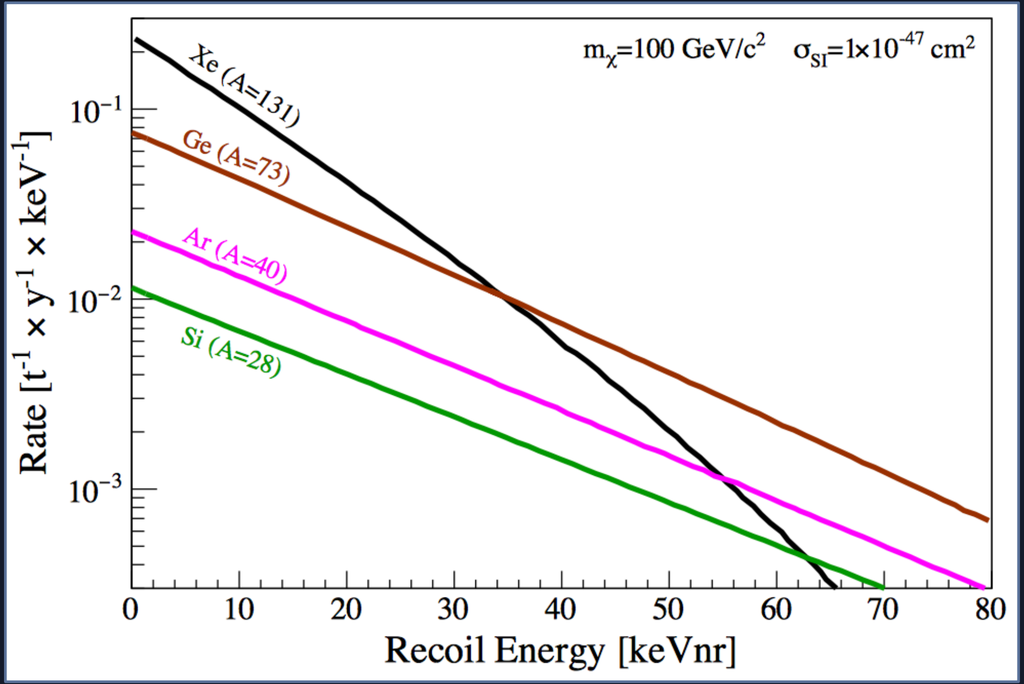

M. Galloway. Dark Matter Direct Detection Techniques and Experiments, *Presentation*, Zürich, 2020.

No features that allow us to distinguish it from background

Expected WIMP event rate:
~0.1-10^{-6} counts/day/kg

Experimental challenge:
Detect rare, featureless and tiny signals over larger background

Background sources

- **Environmental radioactivity**
  - gammas/neutrons from naturally occurring radionuclides (^{40}K, ^{238}U, ^{232}Th and their daughters);
- **Radioactivity of the materials constituting the setup**
  - gammas/neutrons from naturally occurring radionuclides (^{40}K, ^{87}Rb, ^{238}U, ^{232}Th and their daughters);
- **Cosmic rays and cosmic rays-induced processes**
  - Cosmogenically activated isotopes;
  - neutrons.

→ Passive/Active shielding

→ Careful selection of low radioactivity materials

→ Underground laboratories

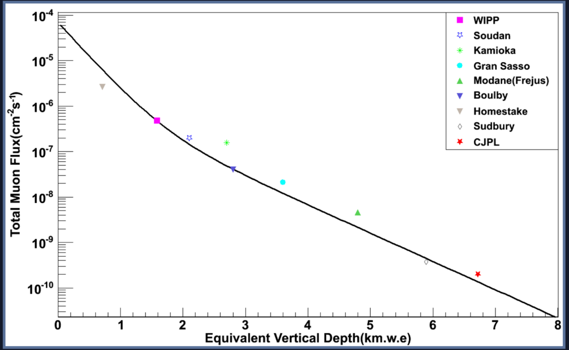

Y.C. Wu et al., *Chin.Phys.C*, 37:086001, 2013.

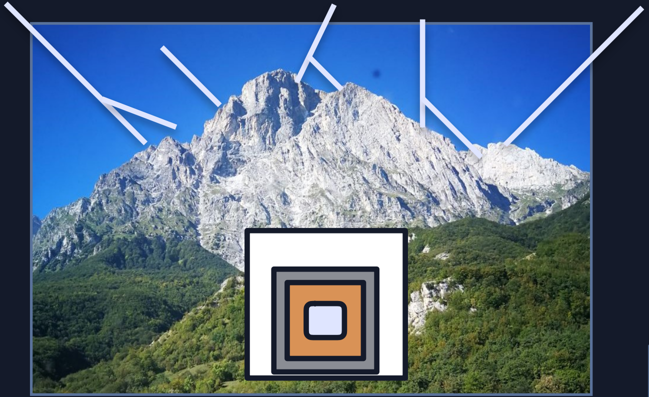

Two experimental approaches

Counting experiments

Excess of DM events in the energy spectrum

Approximately zero background needed

Liquid xenon/argon detectors.

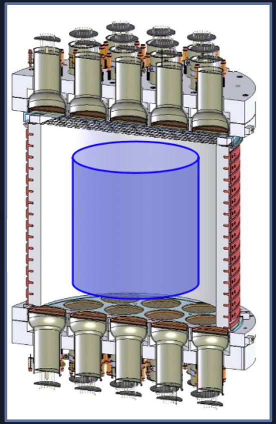

Experiments searching for a peculiar signature

Annual modulation of the DM interaction rate or directionality

Less demanding requirements on the background level

Annual modulation

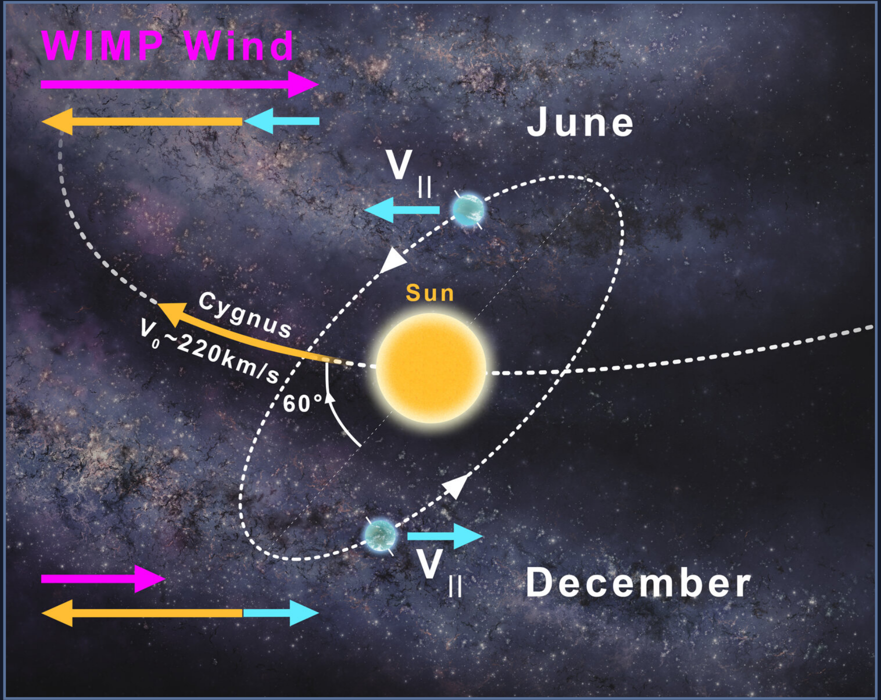

F. Froborg and A. R. Duffy, *J. Phys. G: Nucl. Part. Phys.*, 47:094002, 2020.

Expected DM event rate in an Earth-based detector is modulated due to the combination of the Earth and Sun motion around the Galactic centre

$$\frac{dR}{dE_R} \approx S_0(E_R) + S_m(E_R)cos[\omega(t - t_0)]$$

Period: 1 year; **Phase:** 152.5 days (June 2nd)

Powerful model-independent approach

Only ingredients:

- Halo model;
- DM velocity w.r.t. Earth.

Small modulation fraction S_m/S_0 = O(~few%)

Experimental efforts - current status

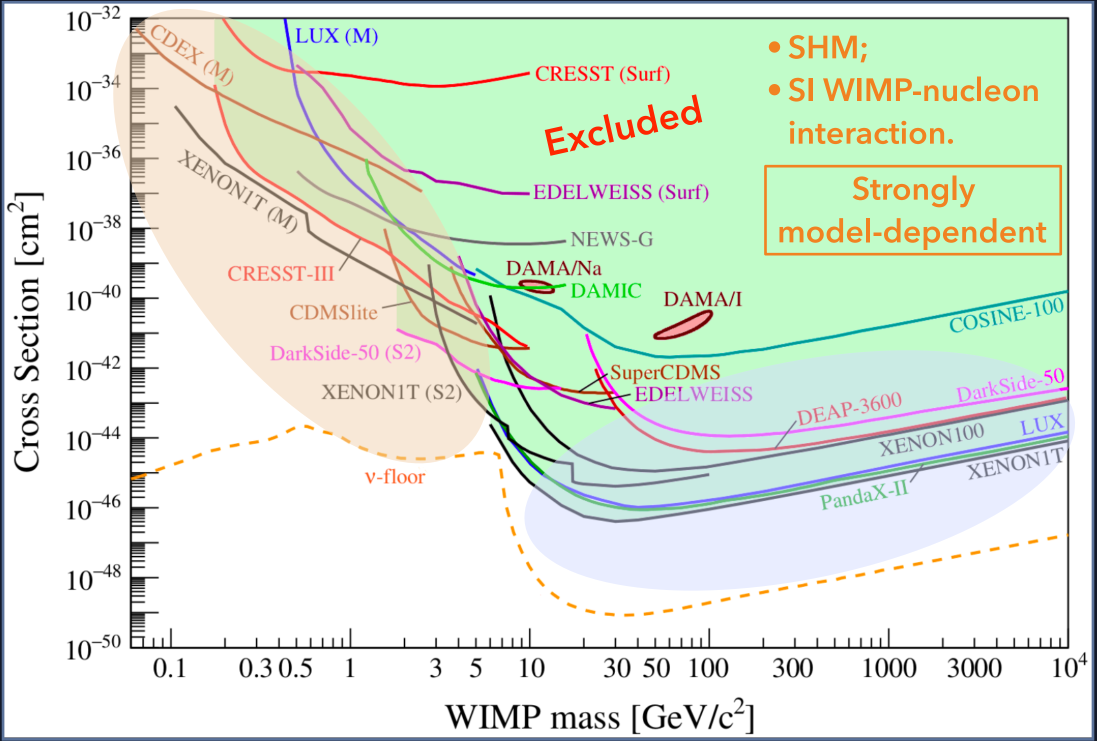

APPEC Committee Report, arXiv:2104.07634, 2021.

Huge experimental effort over the last two decades to detect SI nuclear elastic scattering of WIMPs, using different target materials and techniques

- **"low" mass WIMPs search** leadership held by cryogenic detectors and ton-scale noble liquid detectors (exploiting only scintillation signal S2);
- **"high" mass WIMPs search** leadership held by ton-scale noble liquid detectors.

Several null results have been collected, but…

The case of DAMA/LIBRA

An annually modulated signal has been observed by the DAMA/LIBRA experiment at the Gran Sasso National Laboratory

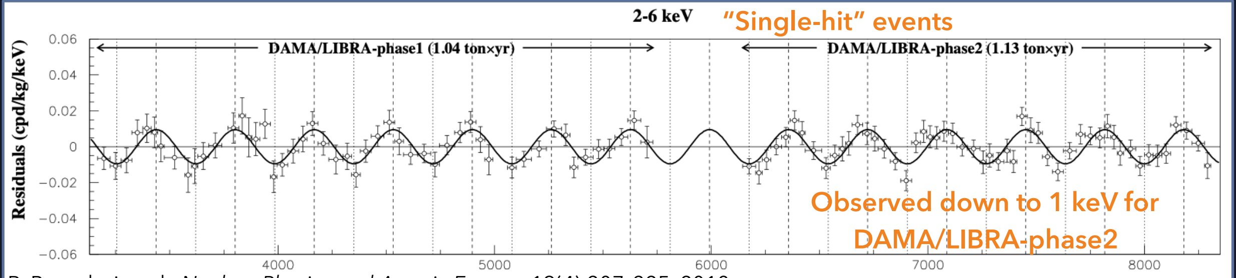

R. Bernabei et al., *Nuclear Physics and Atomic Energy*, 19(4):307-325, 2018.

- Experiments using different targets seem to exclude the interpretation of DAMA signal as due to spin-independent DM scattering off nuclei in the standard WIMP galactic halo hypothesis.
- Currently running experiments using the same target (ANAIS-112 and COSINE-100), have not yet reached the ultra-low background and sensitivity achieved by DAMA.

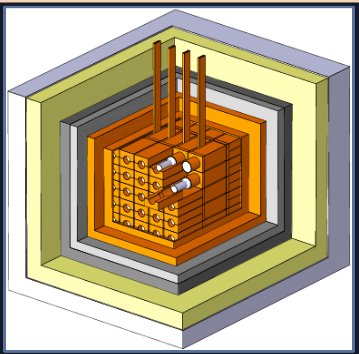

Setup:
~250 kg of NaI(Tl) crystals + passive shielding.
Background level in [1-6] keV:
< 1 count/day/kg/keV (cpd/kg/keV).
Exposure (phase1+phase2):
2.17 ton x yr.
Signal statistical significance (phase1+phase2):
11.9σ C.L.

A new high sensitivity and low background measurement with NaI(Tl) crystals is needed

SABRE: Sodium-iodide with Active Background REjection

WHAT

An experiment based on NaI(Tl) scintillating crystals and focused on the achievement of a very low background

WHERE

At the Gran Sasso National Laboratory (LNGS, Italy) and Stawell Underground Physics Laboratory (SUPL, Australia)

WHY

Search for galactic dark matter through the annual modulation effect and model-independent test of the long-standing DAMA result

The SABRE strategy

1. LOW BACKGROUND
2. LOW ENERGY THRESHOLD
3. ACTIVE VETO
4. DOUBLE LOCATION

1 - Low background

Development of ultra-high purity NaI(Tl) scintillating crystals

Main background is due to crystal internal contaminants:

- *Intrinsic*: ^{238}U, ^{232}Th, ^{40}K, ^{87}Rb, ^{210}Pb
- *Cosmogenically-activated*: ^{3}H, ^{22}Na

A. **Ultra-high purity NaI powder**
B. **Ultra-clean crystal growth method**
C. **Reduced time above ground**

Measured by ICP-MS

Isotope	Astrograde NaI powder [ppb]
^{nat}K	3.5
^{238}U	0.6×10^{-3}
^{232}Th	0.5×10^{-3}
^{87}Rb	0.2

K. E. Shields, PhD Thesis, Princeton University, 2015.

2 - Low energy threshold

Low radioactivity and High Quantum Efficiency (HQE) PhotoMultiplier Tubes (PMTs) directly coupled to the crystal with optical grease

- Reduced light loss;
- Good capacity to convert light into electric charge.

→ **High Light Yield**

Amplified signals and Pulse Shape Discrimination (PSD)

- Reduced noise.

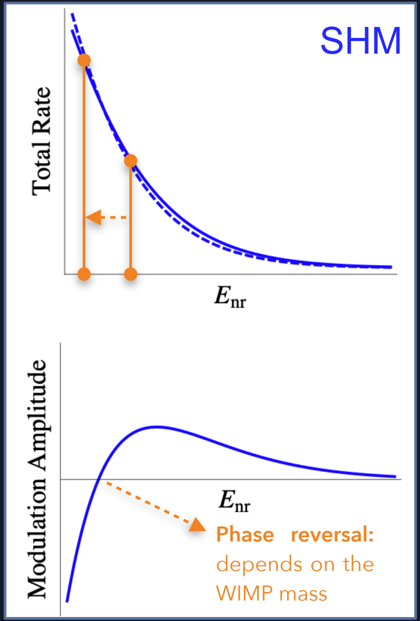

K. Freese et al., *Reviews of Modern Physics*, 85(4):1561-1581, 2013.

Small gain in energy threshold means high gain in total rate and information on the WIMP mass

3 - Active veto

NaI(Tl) crystals surrounded by liquid scintillator (LS) veto (PC+PPO mixture from Borexino plant)

Tag and reject internal and external backgrounds such as:

- Radioactive decays in the crystal due to ^{40}K and ^{22}Na;
- Cosmic rays related processes.

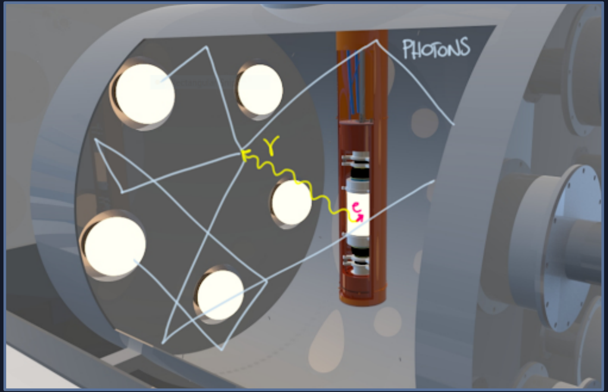

Events which deposit energy in both crystal and LS veto are certainly background

^{40}K simplified decay scheme

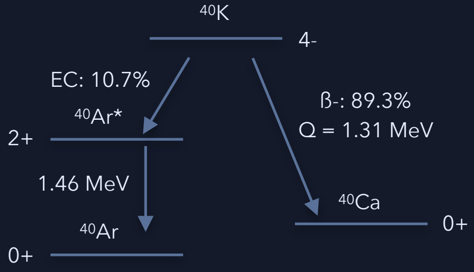

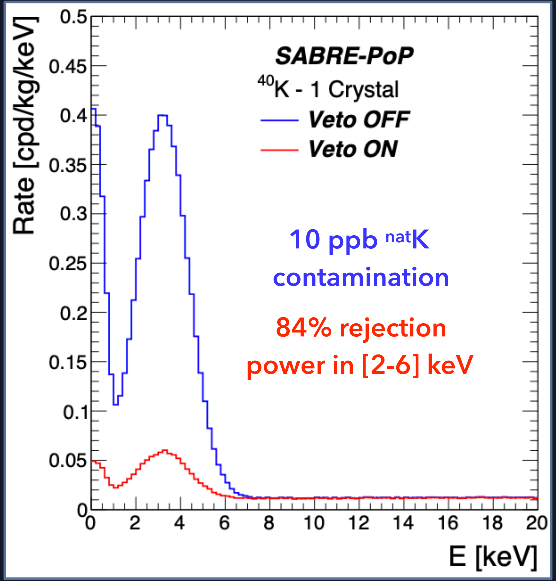

M. Antonello et al., *Astropart. Phys.*, 106:1-9, 2019.

4 - Double location

Two detectors in both the Northern and Southern hemispheres

https://www.lngs.infn.it

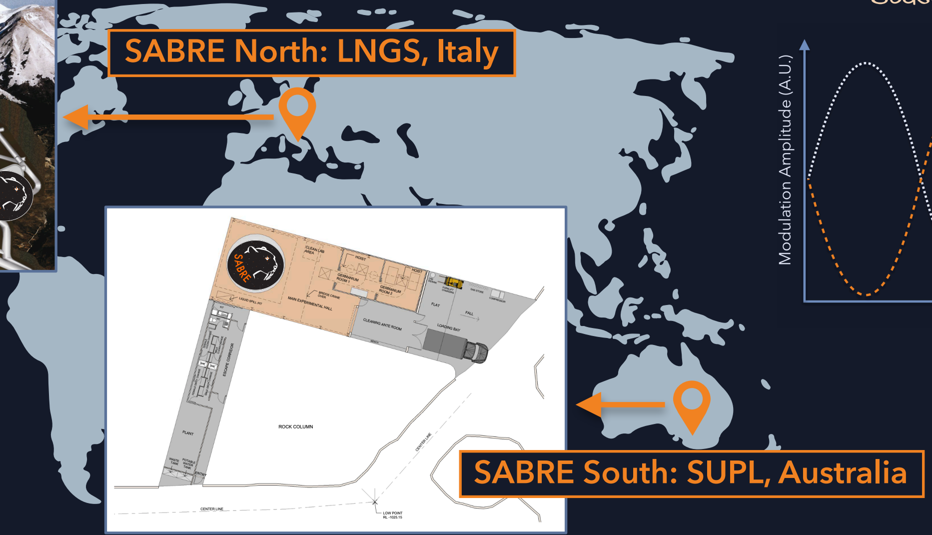

P. Urquijo, *arXiv:1605.03299*, 2016.

Seasonal effect

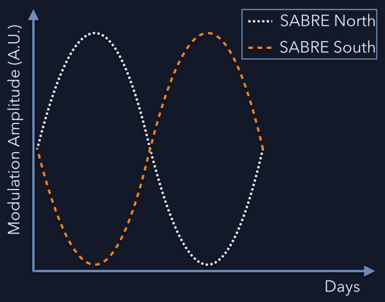

Dark Matter

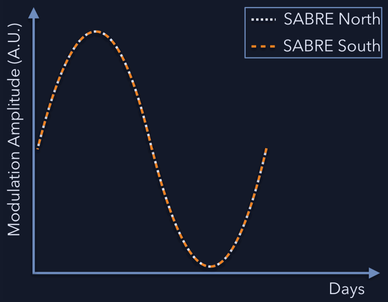

It is possible to disentangle seasonal or site-related effects from DM modulated signal

Development of ultra-high purity NaI(Tl) crystals

NaI-31

- 6 kg **Astrograde NaI powder** in a **fused quartz** crucible;
- Grown at RMD (Radiation Monitoring Devices) using the Vertical Bridgman (VB) method;
- Crystal growth completed in June 2018;
- **Octagonal shape**, **Mass ~3 kg** after cut and polishing;
- Arrived @LNGS on April 24, 2019 - **transported by plane**.

NaI-31 before cut and polishing

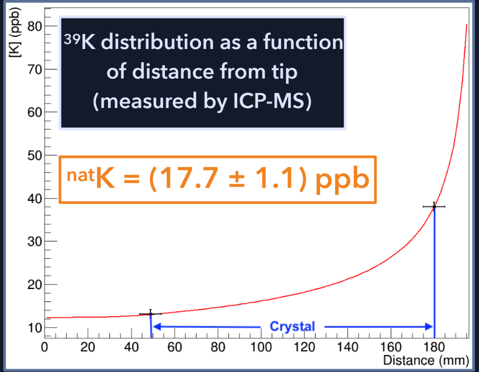

^{39}K distribution as a function of distance from tip (measured by ICP-MS)

$^{nat}K = (17.7 \pm 1.1)$ ppb

Same level of DAMA and ANAIS and COSINE best crystals

B. Suerfu, PhD thesis, Princeton University, 2018.

NaI-33

- 6 kg **Astrograde NaI powder** in a **synthetic fused silica** crucible;
- Grown at RMD using the VB method;
- Crystal growth completed in October 2018;
- **Octagonal shape**, **Mass ~3.4 kg** after cut and polishing;
- Arrived @LNGS on August 6, 2019 - **transported by boat**.

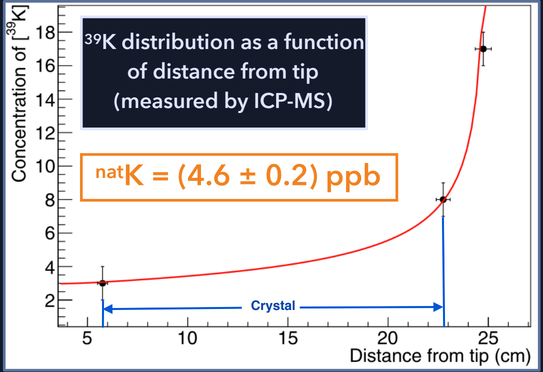

^{39}K distribution as a function of distance from tip (measured by ICP-MS)

$^{nat}K = (4.6 \pm 0.2)$ ppb

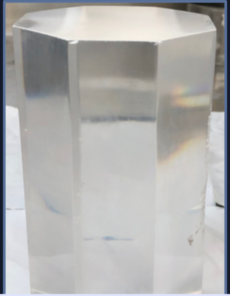

NaI-33 after cut and polishing

Lowest level ever achieved

B. Suerfu et al., Phys. Rev. Research, 2:013223, 2020.

Detector modules assembly

The two SABRE detector modules were assembled in a glove box inside a cleanroom at Princeton University

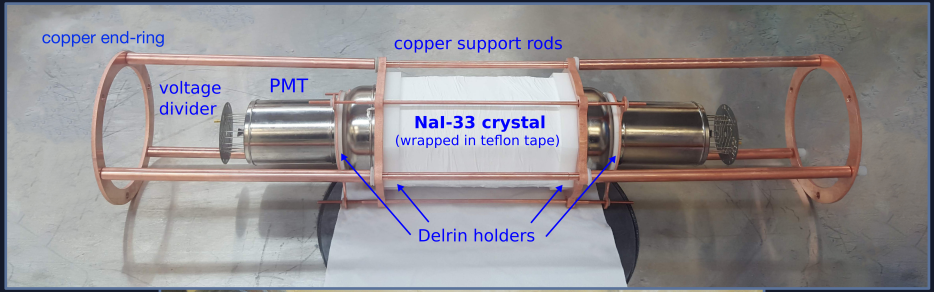

Same procedure followed for both NaI-31 and NaI-33

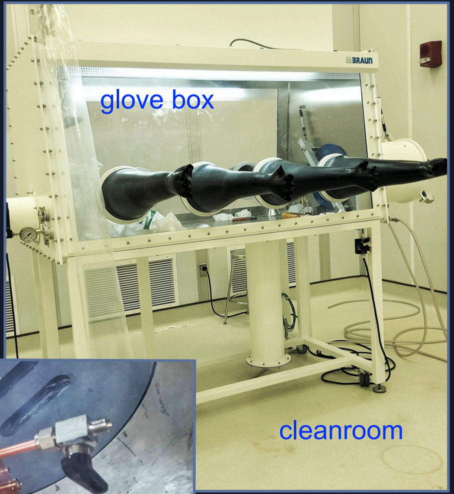

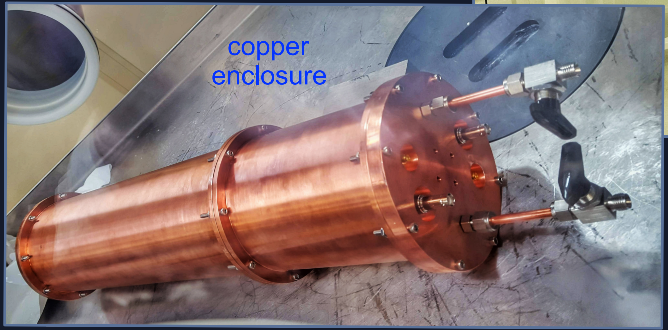

Characterization of NaI-33 in Hall B

A first characterization of the NaI-33 crystal was performed in an underground testing facility located in Hall B

Experimental setup

- Passive shielding made of **low radioactivity copper** + **lead**;
- It is enclosed in a Lexan box that can be sealed and flushed with high purity N_2 gas;
- Refurbishment of the passive shielding to increase the copper thickness.

Shield 1
5 cm of Cu
17.5 cm of Pb

Shield 2
10 cm of Cu
17.5 cm of Pb

Measurements

- **Light yield** and **energy resolution**;
- **Alpha rate** and **build-up of ^{210}Po**;
- ^{238}**U** and ^{232}**Th** content;
- Study of **cosmogenic activation**.

Results published
Eur. Phys. J. C, 81(4):299, 2021

Data acquisition

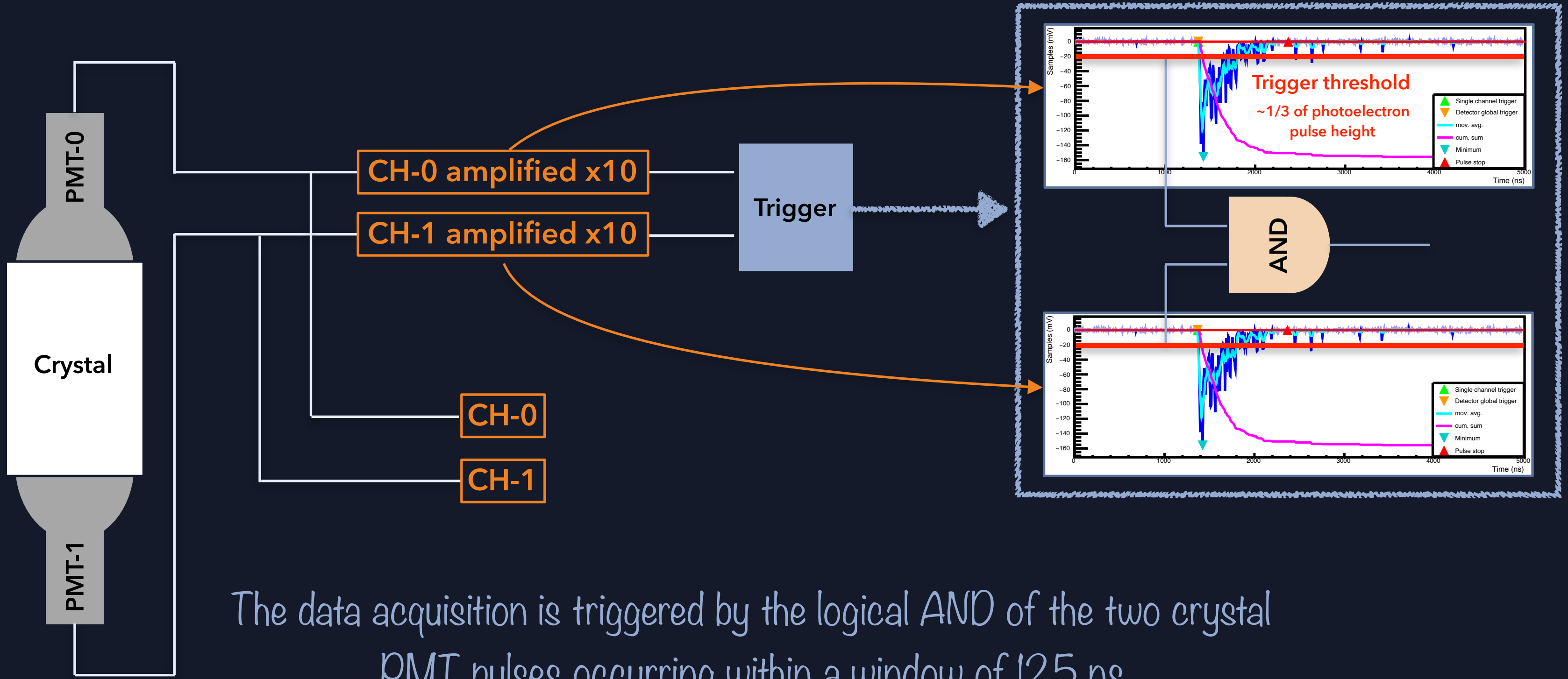

The data acquisition is triggered by the logical AND of the two crystal PMT pulses occurring within a window of 125 ns

Light yield and energy resolution

^{241}Am source to measure light yield (LY) and energy resolution (R) on the 59.5 keV gamma line

- Source positioned on the copper enclosure in correspondence with the crystal centre.

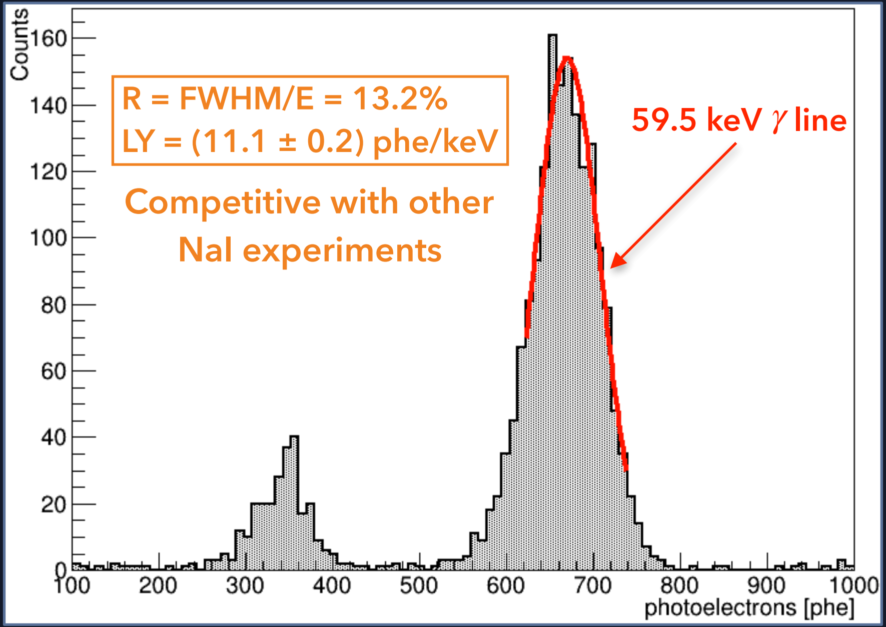

For comparison:

	LY [phe/keV]	R @59.5 keV
DAMA/LIBRA-phase2	6-10	15.8%
ANAIS-112	15	11.2%
COSINE-100	15	11.8%
NaI-33 (Hall B)	11.1	13.2%

R. Bernabei et al., The DAMA project: Achievements, implications and perspectives. Progress in Particle and Nuclear Physics, 114, 2020.

J. Amaré et al., Performance of anais-112 experiment after the first year of data taking. The European Physical Journal C, 79(3), 2019.

G. Adhikari et al., Initial Performance of the COSINE-100 Experiment. Eur. Phys. J. C, 78(2):107, 2018.

Measurement of the alpha rate

PSD: Amplitude weighted Mean Time ($< t >_{600}$)

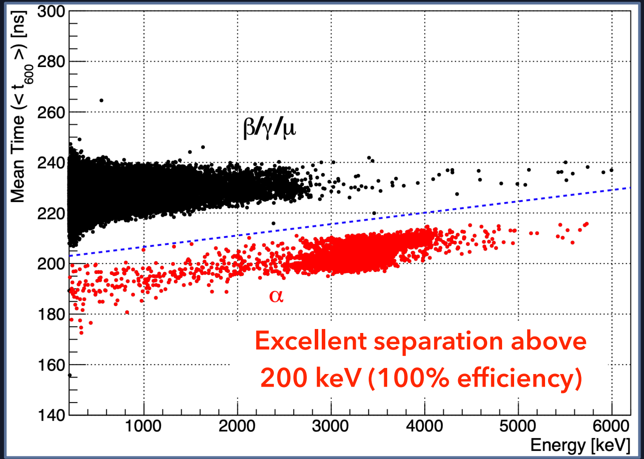

- In NaI(Tl) crystals, signals induced by α decays are faster than β/γ ones.

$$< t >_{600} = \frac{\sum_{t_i<600\ ns} h_i t_i}{\sum_{t_i<600\ ns} h_i}$$

h_i: pulse amplitude in mV
t_i: time of the i-th sample (starting from the trigger t_0)

Also lower than NaI-31: (1.02 ± 0.07) mBq/kg

α rate = (0.54 ± 0.01) mBq/kg
Still higher than DAMA but lower than other NaI competitors

Alpha spectrum

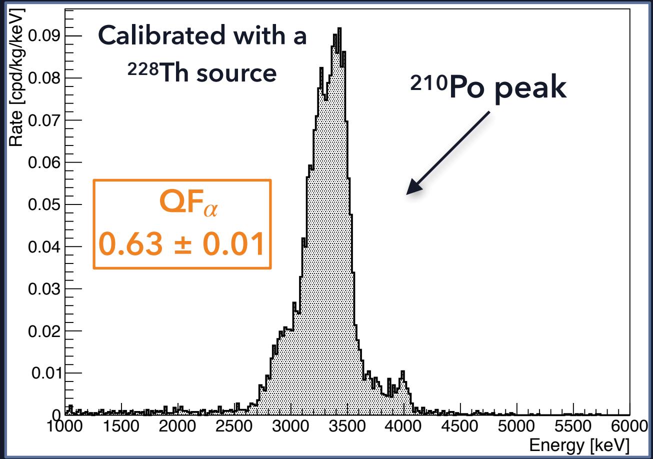

^{238}U and ^{232}Th content estimation

$T_{1/2}$	Isotope	E_α(MeV)
$4.468 \cdot 10^9\,y$	^{238}U	
	$\downarrow \alpha$	4.18
$24.1\,d$	^{234}Th	
	$\downarrow \beta$	
$1.17\,m$	^{234m}Pa	
	$\downarrow \beta$	
$2.455 \cdot 10^5\,y$	^{234}U	
	$\downarrow \alpha$	4.75
$7.538 \cdot 10^4\,y$	^{230}Th	
	$\downarrow \alpha$	4.66
$1600\,y$	^{226}Ra	
	$\downarrow \alpha$	4.78
$3.8\,d$	^{222}Rn	
	$\downarrow \alpha$	5.49
$3.10\,m$	^{218}Po	
	$\downarrow \alpha$	6.00
$26.8\,m$	^{214}Pb	
	$\downarrow \beta$	
$19.9\,m$	^{214}Bi	
	$\downarrow \beta$	
$164.3\mu s(*)$	^{214}Po	
	$\downarrow \alpha$	7.69
$22.3\,y$	^{210}Pb	
	$\downarrow \beta$	
$5.01\,d$	^{210}Bi	
	$\downarrow \beta$	
$138.4\,d$	^{210}Po	
	$\downarrow \alpha$	5.30
Stable	^{206}Pb	

Bi-Po-214

$T_{1/2}$	Isotope	E_α(MeV)
$1.405 \cdot 10^{11}\,y$	^{232}Th	
	$\downarrow \alpha$	3.99
$5.75\,y$	^{228}Ra	
	$\downarrow \beta$	
$6.15\,h$	^{228}Ac	
	$\downarrow \beta$	
$1.9116\,y$	^{228}Th	
	$\downarrow \alpha$	5.37
$3.66\,d$	^{224}Ra	
	$\downarrow \alpha$	5.69
$55.6\,s$	^{220}Rn	
	$\downarrow \alpha$	6.29
$0.145\,s$	^{216}Po	
	$\downarrow \alpha$	6.78
$10.64\,h$	^{212}Pb	
	$\downarrow \beta$	
$60.55\,m$	^{212}Bi	
	$\downarrow \alpha_{36\%}$	6.06
	$\downarrow \beta_{64\%}$	
$0.299\,\mu s(*)$	^{212}Po	
	$\downarrow \alpha$	8.78
$3.053\,m$	^{208}Tl	
	$\downarrow \beta$	
Stable	^{208}Pb	

α triplet

Bi-Po-212

C. Cuesta, PhD thesis, University of Zaragoza, 2013.

β decays from U and Th decay chains are possible background in the ROI for DM searches.

Fast β-α sequences (Bi-Po) and fast α decays were used to measure the activity (A) of primordial radioactive chains in NaI-33

- ^{238}U chain
  - Bi-Po-214 (τ = 237 μs) –> A_{226Ra} = (5.9 ± 0.6) μBq/kg
- ^{232}Th chain
  - Bi-Po-212 (τ = 431 ns) –> A_{228Th} = (1.6 ± 0.3) μBq/kg
  - α triplet (τ_1 = 80.2 s, τ_2 = 209 ms) –> A_{228Th} = (1.7 ± 0.3) μBq/kg

If secular equilibrium held, U/Th contamination < 0.5 ppt

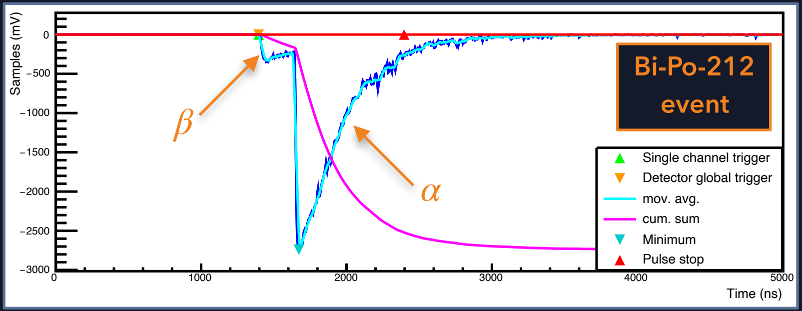

Alpha rate vs. time: build-up of ^{210}Po

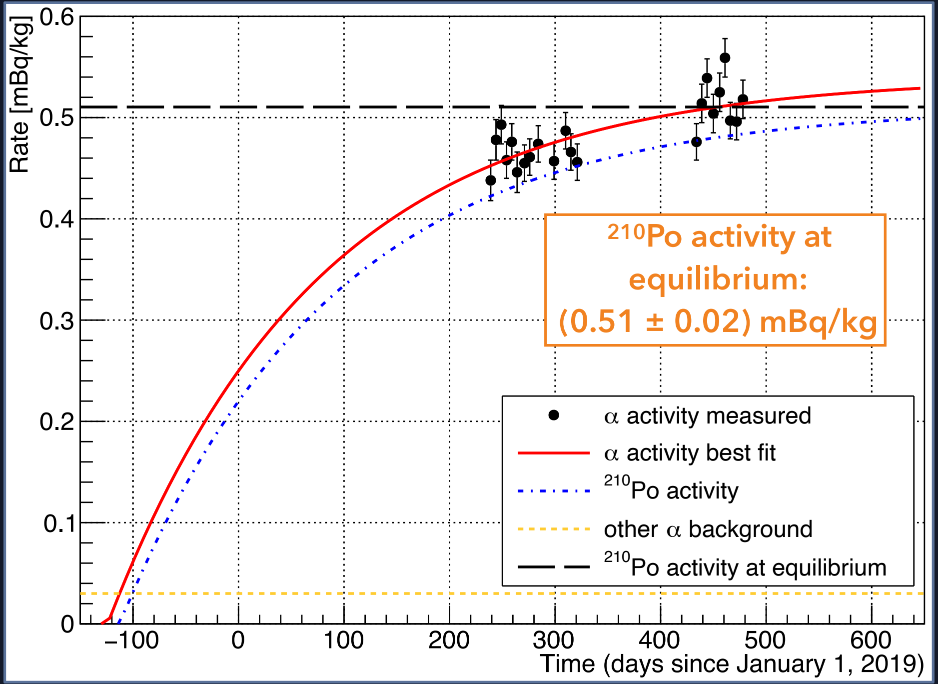

The alpha rate in the ^{210}Po energy region was studied over a period of several months

$\tau \sim 200\ days$ (Mean-life of ^{210}Po)

Out-of-equilibrium contamination of ^{210}Pb accidentally introduced in the crystal during the manufacturing process or already in the powder

Study of cosmogenic activation

The NaI-33 crystal was exposed to cosmic rays (at sea level) for a total of 279 days

- Experimental spectra acquired at different time periods after the arrival of the detector underground were compared.
- Cosmogenic peaks due to ^{125}**I** and ^{126}**I** are clearly visible.
- Matching activities extracted by comparison with Monte Carlo simulated spectra.

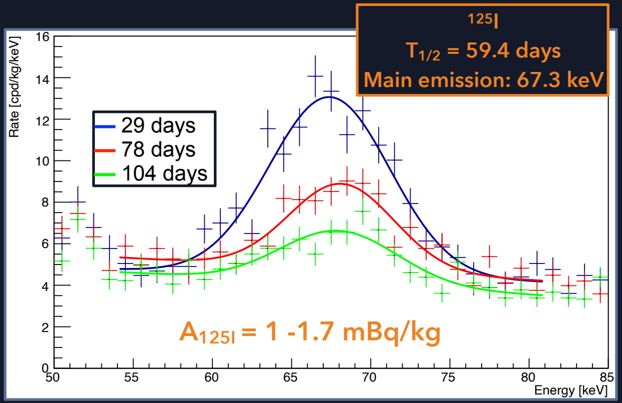

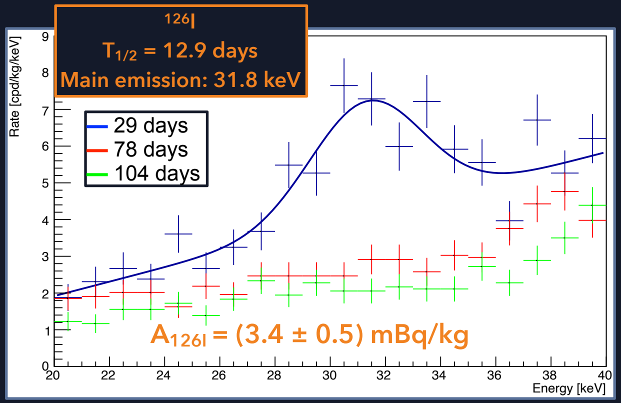

Upper limits on tellurium isotopes activities

Isotope	γ line [keV]	Limit [mBq/kg]
^{127m}Te	88.3	0.14
^{125m}Te	144.8	0.10
^{123m}Te	247.6	0.09
^{121m}Te	294.0	0.15

The SABRE Proof-of-Principle (PoP)

Goal: assess the radiopurity of SABRE crystals and test the active veto performance

Measurements
- **Veto** detector **characterization**;
- **Potassium direct counting**;
- **Low energy analysis** of **NaI-33** data;
- **Background model** of **NaI-33**.

Results about to be submitted for publication to Physical Review Letters


Application of Lumirror inside the veto vessel


Veto PMTs mounting

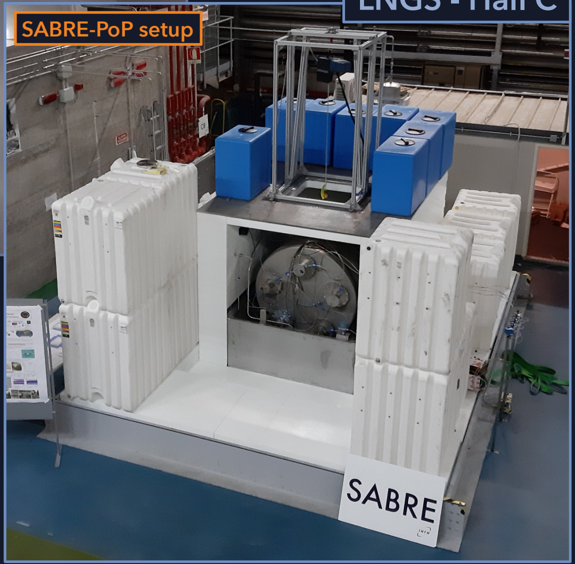

SABRE-PoP setup

LNGS - Hall C

The SABRE-PoP setup

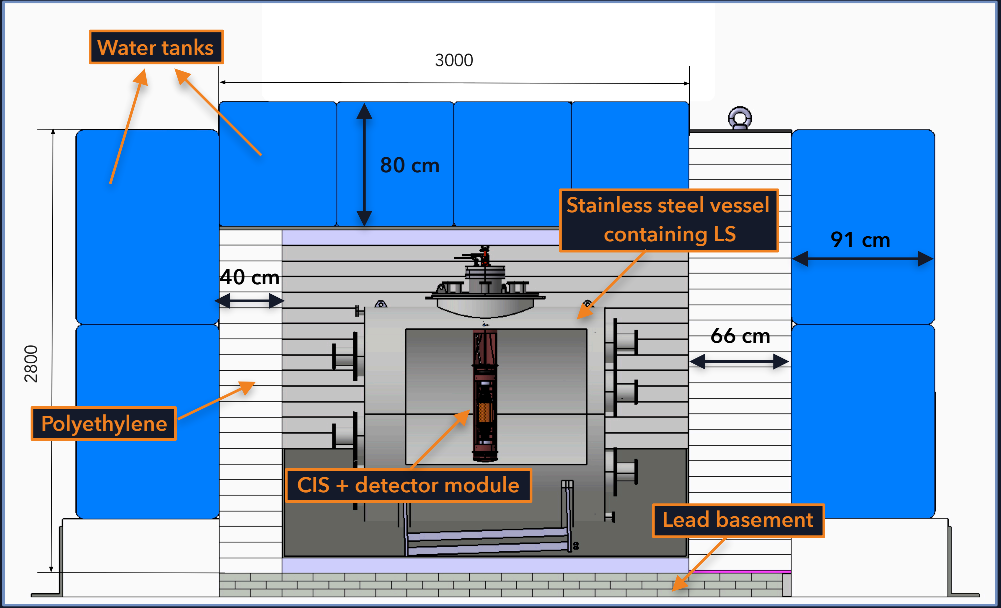

- **Stainless steel vessel** equipped with ten 8″ Hamamatsu R5912 PMTs containing ~2 tons of LS;
- **1 detector module** per time:
  - high purity copper enclosure containing the crystal directly coupled to two 3″ Hamamatsu R11065-20 PMTs;
- **Crystal insertion system (CIS):**
  - blind-end copper tube purged with high purity N_2 gas housing the detector module;
- External passive shielding (**lead, polyethylene** and **water**) sealed and purged with N_2 gas.

GSSI

GSSI

SABRE-PoP commissioning

2020

Start	NaI-31 insertion		Water tanks filling	End
May 26	June 16	June 30 - July 3	July 6-14	July 14
Veto water filling		Water displacement with LS		

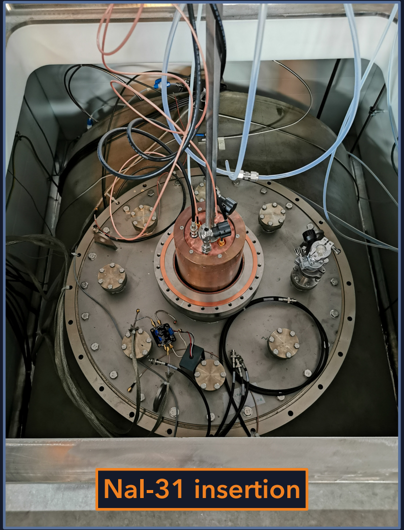
NaI-31 insertion

Water tanks filling


SABRE-PoP

GSSI

GSSI

Veto detector characterization

^{228}Th source to measure LY, energy resolution and quenching

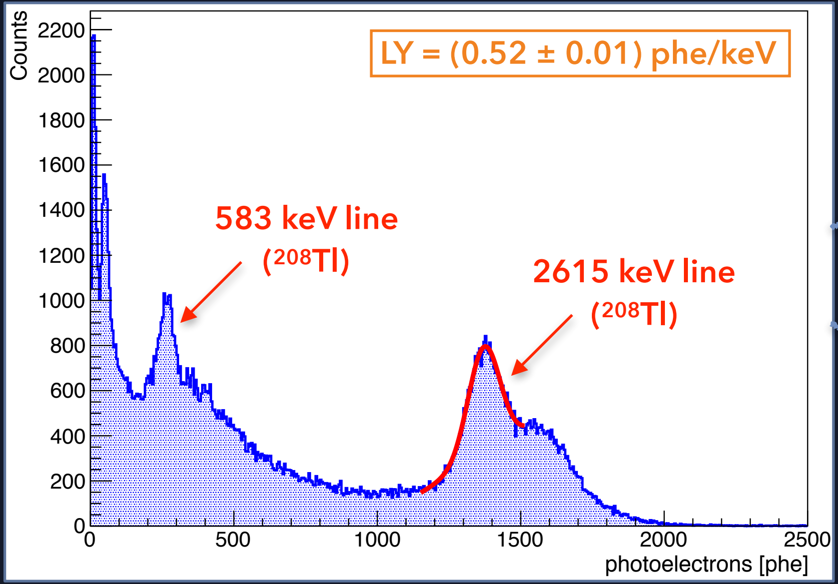

σ

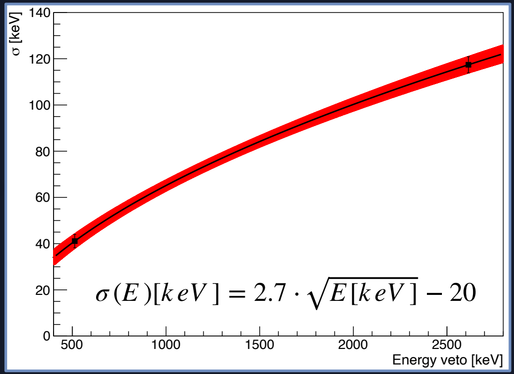

E_{vis}/E_γ

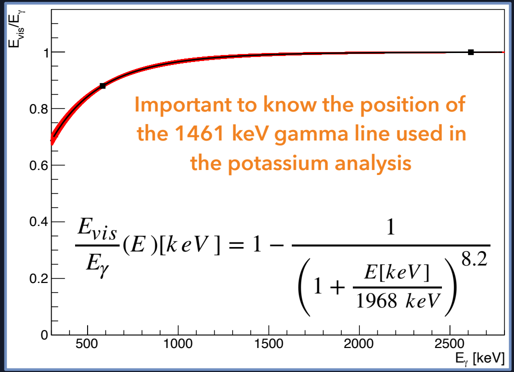

The excellent LY allowed us to set the veto threshold at 50 keV

Potassium measurement mode (KMM)

Coincidence analysis between crystal and veto detector

Requirements:

- A crystal energy deposition within $\pm 1\sigma_c$ around the 3.2 keV peak (σ_c energy resolution of the crystal);
- A veto energy deposition within $\pm 2\sigma_v$ around the 1461 keV γ peak (σ_v energy resolution of the veto).

To subtract accidental coincidences, I determine the average number of events in two sideband intervals in the crystal, adjacent to the signal band, and accompanied by the same veto signature.

Efficiency of the selection taken into account and calculated by MC

$$\epsilon_{MC} = N_{coin}/N_{tot}$$

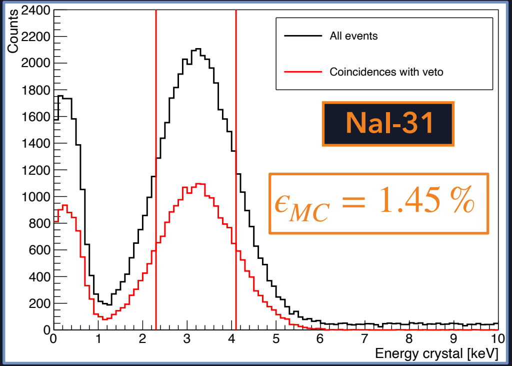

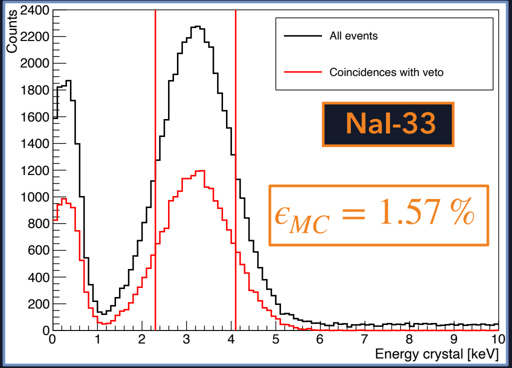

KMM- noise vs. real scintillation pulses

Residual noise events (especially spikes) are removed by applying the Charge over Maximum (CoM) cut

$$CoM = \frac{C_{(0,1000)}}{h_{max}}$$

$C_{(0,1000)}$ → pulse area between 0 and 1000 ns

h_{max} → absolute value of the maximum pulse amplitude in mV

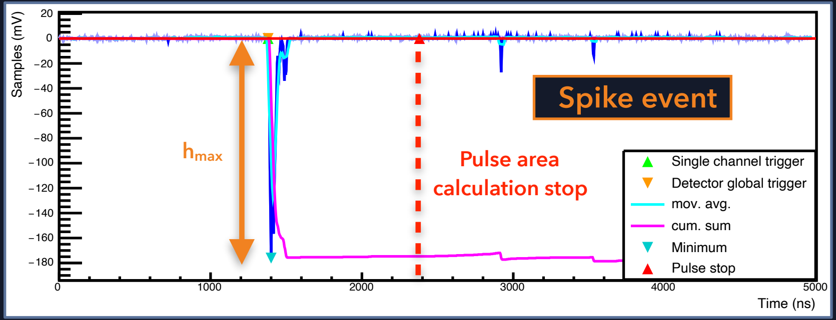

Events with CoM < 50 ns are rejected

Signal acceptance evaluated with a ^{228}Th calibration run and taken into account for the analysis.

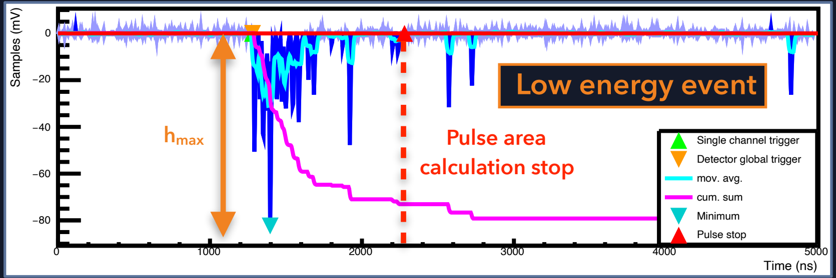

KMM - energy crystal vs. energy veto

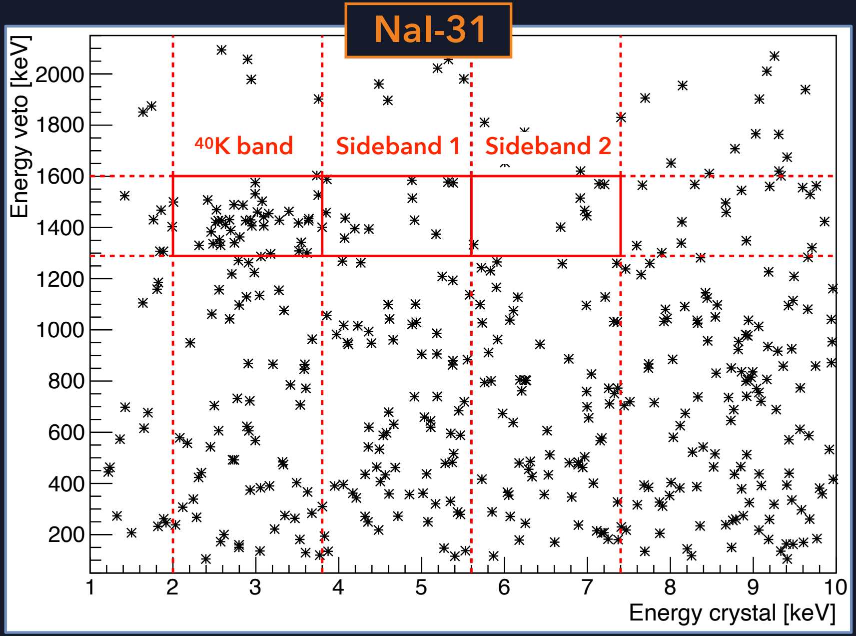

Exposure: ~60 kg · days

(as scheduled)

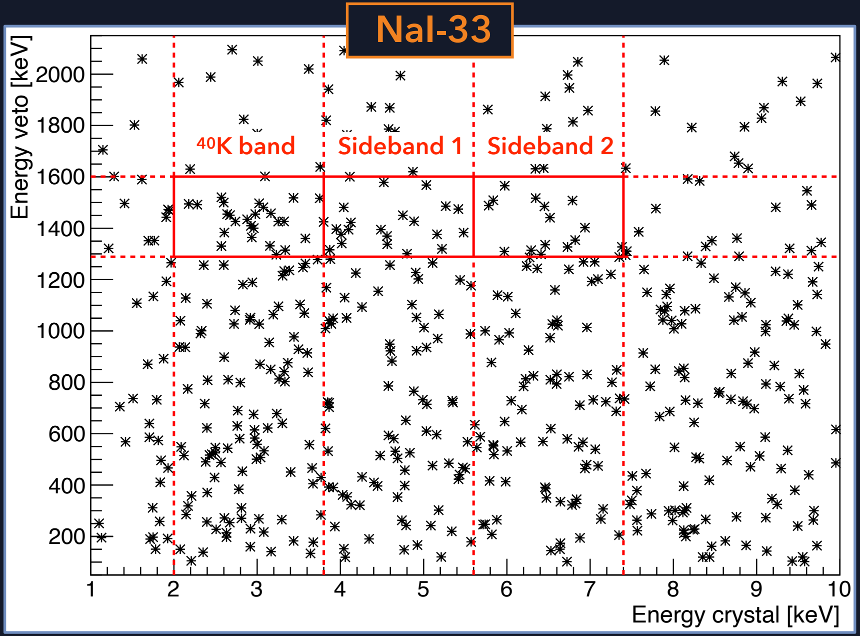

Exposure: ~90 kg · days

(run interrupted due to a technical problem)

KMM spectra - NaI-31

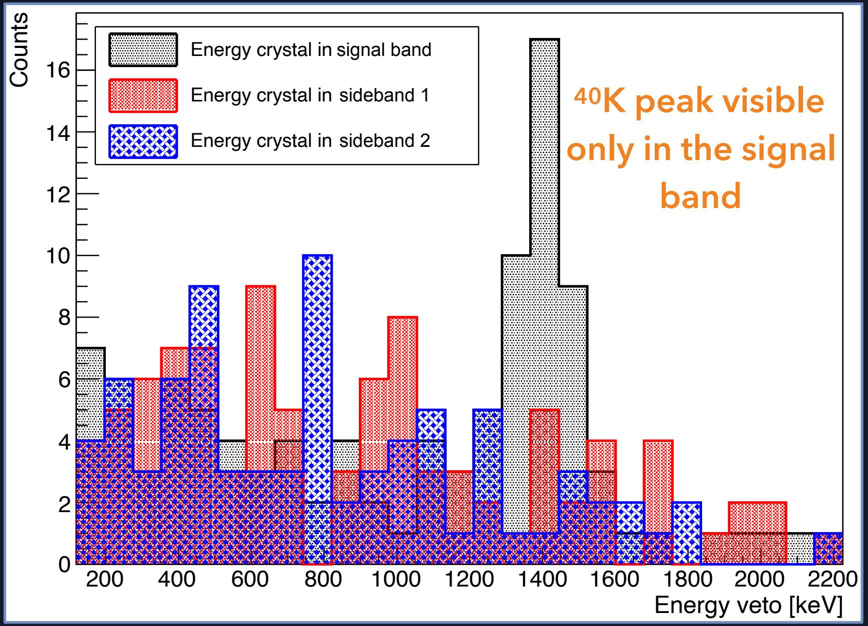

Veto energy spectra

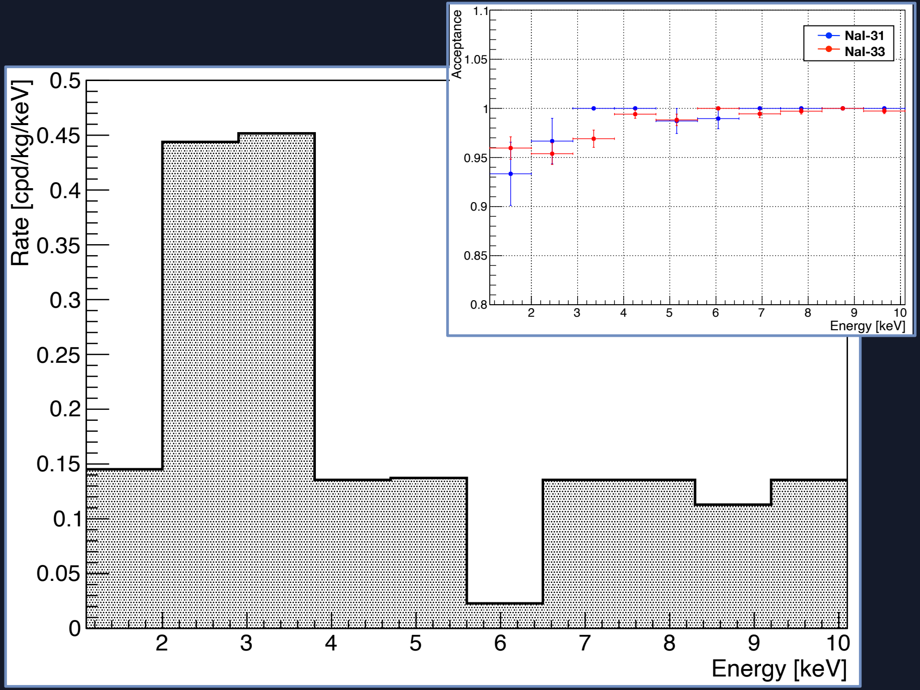

Crystal energy spectrum efficiency-corrected

KMM spectra - NaI-33

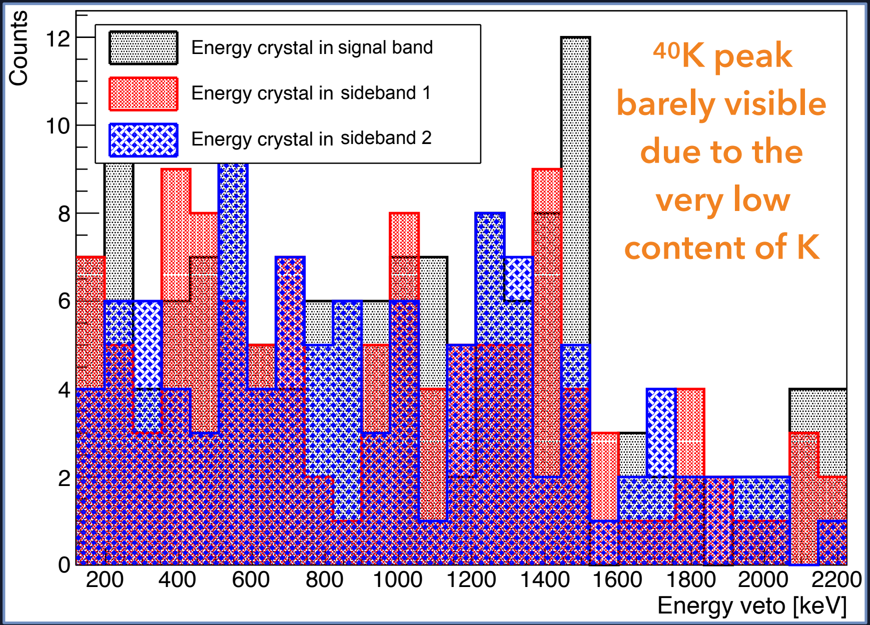

Veto energy spectra

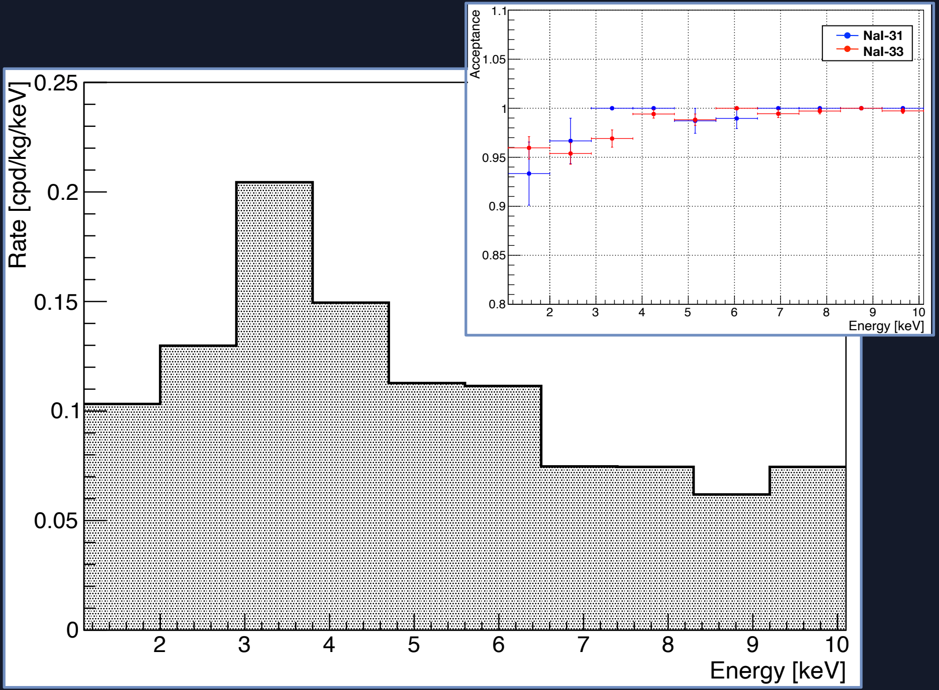

Crystal energy spectrum efficiency-corrected

KMM results

	NaI-31	NaI-33
N_{S+B}	48 ± 7	27 ± 5
N_{B1}	15 ± 4	21 ± 5
N_{B2}	9 ± 3	15 ± 4
N_{40K}	37 ± 7	9 ± 6
^{40}K activity [mBq/kg]	0.49 ± 0.10	0.07 ± 0.05
^{nat}K contamination [ppb]	15.7 ± 3.2	2.2 ± 1.5
^{nat}K contamination by ICP-MS [ppb]	17.7 ± 1.1	4.6 ± 0.2

Upper limits for NaI-33 (90% C.L.):

- **^{40}K activity:** < 0.15 mBq/kg;
- **^{nat}K contamination:** < 4.7 ppb.

PoP setup sensitive to a ppb-level ^{nat}K contamination in the crystal and results from direct counting in agreement with ICP-MS measurements

$$N_{40K} = N_{S+B} - \frac{N_{B_1} + N_{B_2}}{2} \pm \sqrt{\sigma^2_{N_{S+B}} + \frac{1}{4}(\sigma^2_{N_{B_1}} + \sigma^2_{N_{B_2}})} \longrightarrow A_{40K}[Bq/kg] = \frac{N_{40K} \pm \sigma_{N_{40K}}}{t[s] \cdot m[kg] \cdot \epsilon_{MC}}$$

- N_{S+B}: number of events in signal band;
- N_{B1} (N_{B2}): number of events in sideband 1 (sideband 2);
- $\sigma_{N_i} = \sqrt{N_i}$, with i = S+B, B_1, B_2.

- t[s]: live time;
- m[kg]: crystal mass;
- ϵ_{MC}: Monte Carlo efficiency.

Low energy spectrum - noise vs. real scintillation pulses

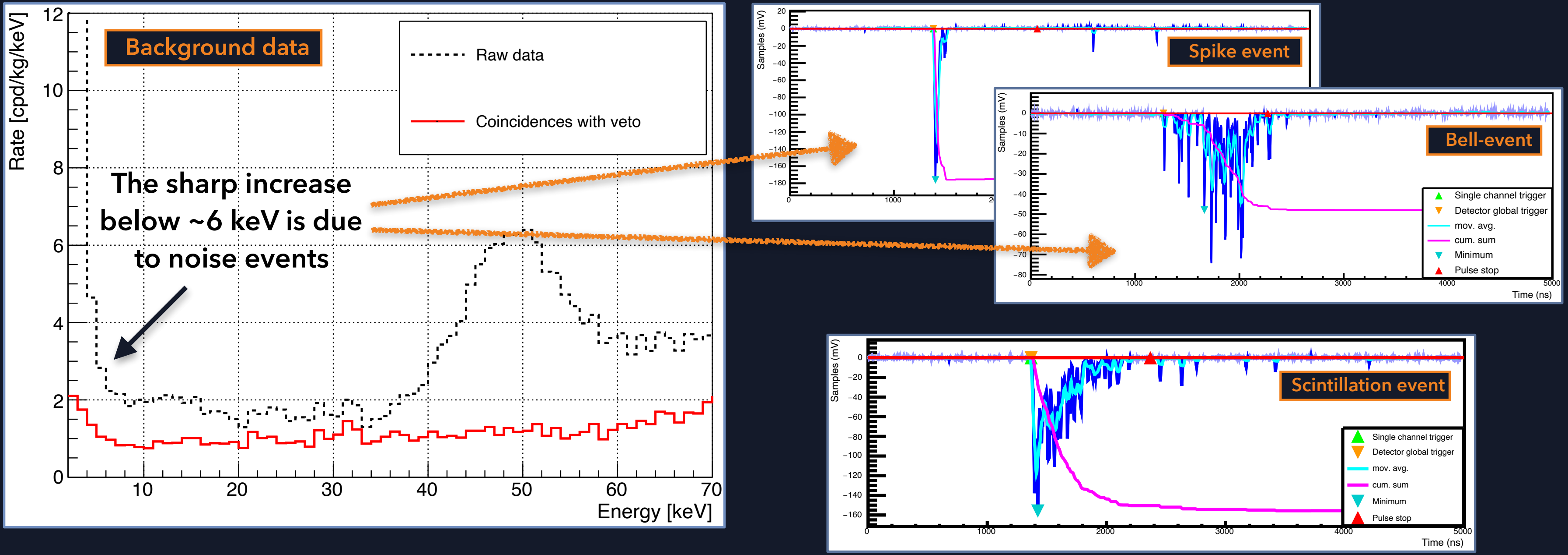

Pulse Shape Discrimination (PSD) parameters used to select scintillation events

Cut-based analysis - Amplitude weighted Mean Time

Amplitude weighted Mean Time ($< t >_{600}$) distribution (^{228}Th dataset)

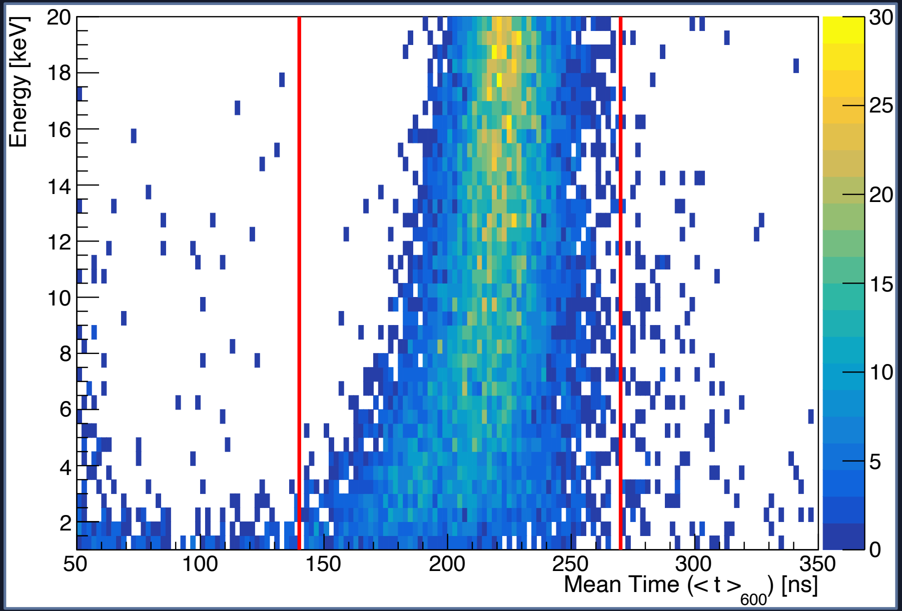

140 ns < $< t >_{600}$ < 270 ns

$$< t >_{600} = \frac{\sum_{t_i < 600\ ns} h_i t_i}{\sum_{t_i < 600\ ns} h_i}$$

t_i: time of the i-th sample (starting from the trigger t_0)

h_i: pulse amplitude in mV

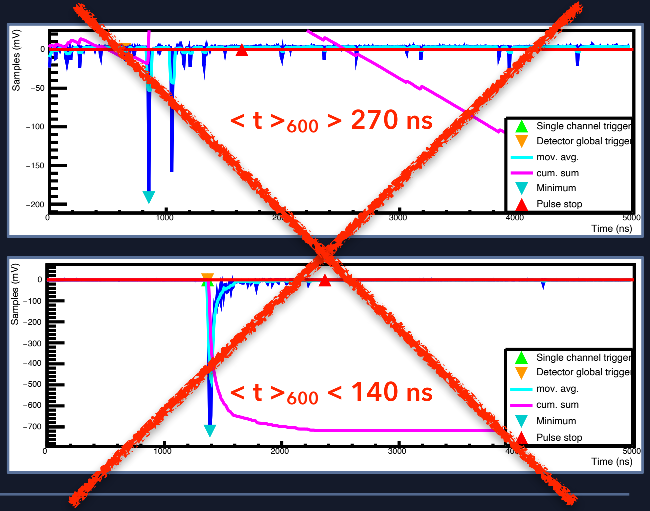

Cut-based analysis - Charge over Maximum

Charge over Maximum (CoM) distribution (^{228}Th dataset)

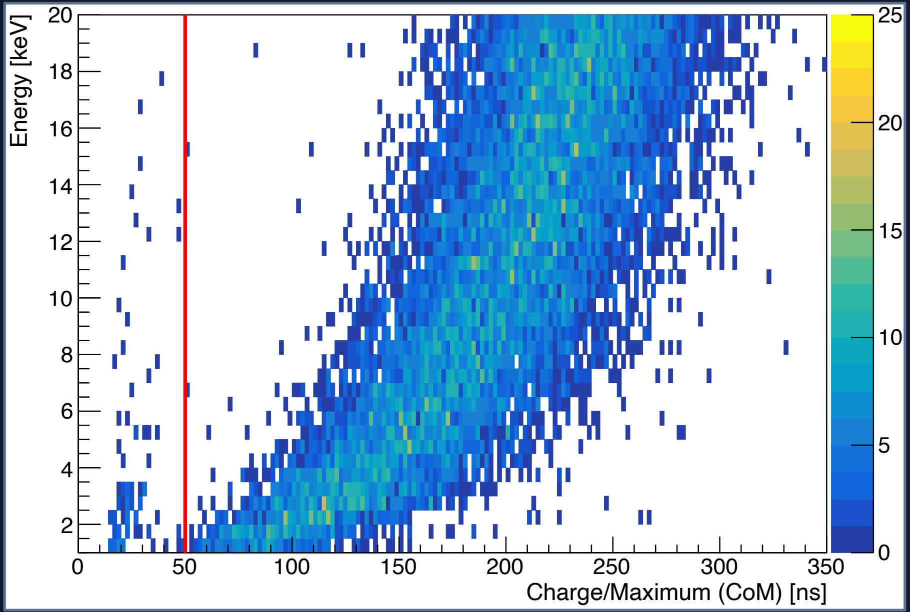

CoM > 50 ns

$$CoM = \frac{C_{(0,1000)}}{h_{max}}$$

pulse area between 0 and 1000 ns

absolute value of the maximum pulse amplitude in mV

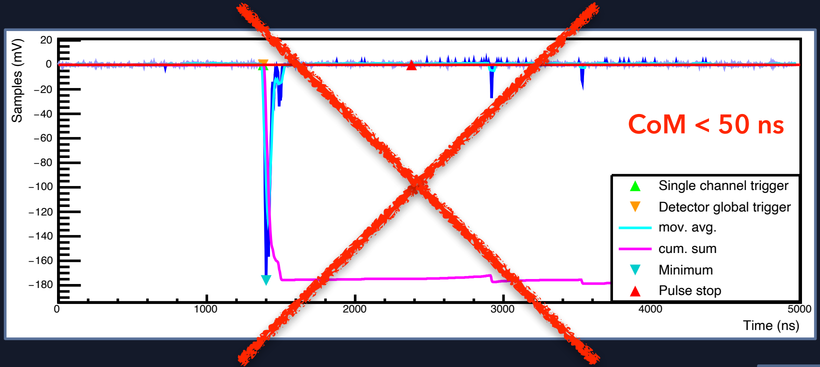

Cut-based analysis - Head-to-middle pulse shape

Head-to-middle pulse shape (C_2/C_1) distribution (^{228}Th dataset)

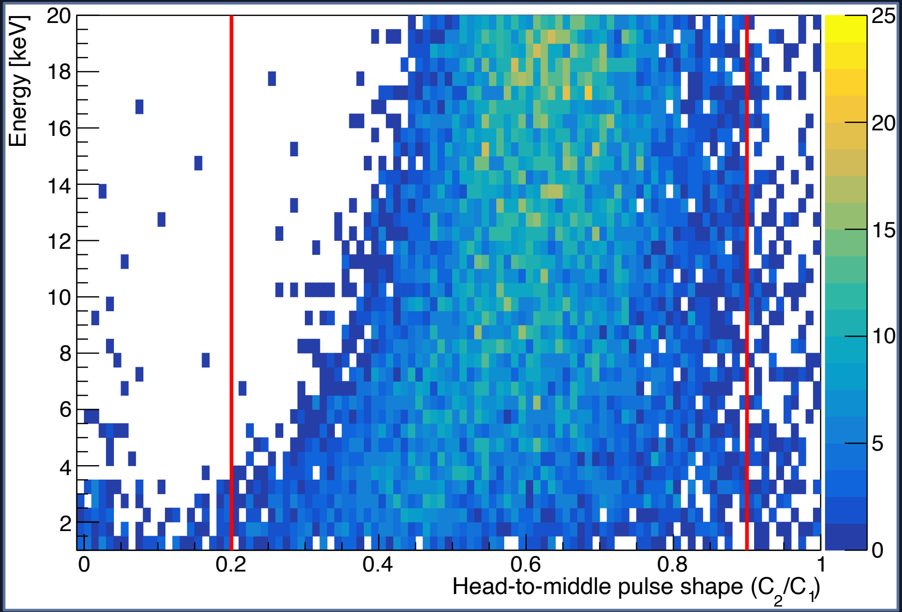

$$C_2/C_1 = \frac{C_{(200,400)}}{C_{(0,200)}}$$

pulse area between 200 and 400 ns

pulse area between 0 and 200 ns

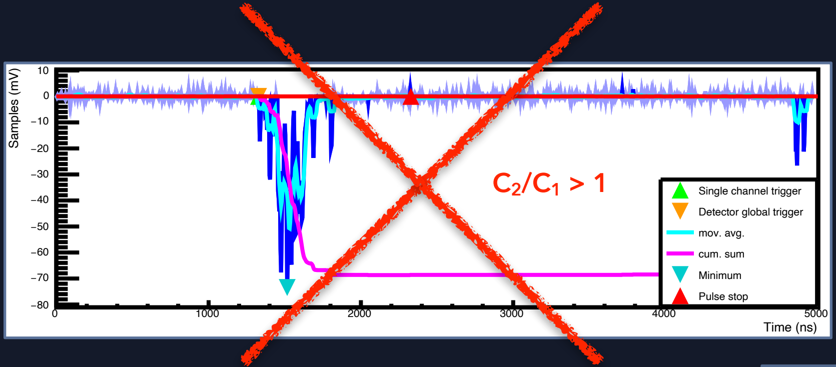

$0.2 < C_2/C_1 < 0.9$

Cut-based analysis - Middle-to-tail pulse shape

Middle-to-tail pulse shape (C_3/C_2) distribution (^{228}Th dataset)

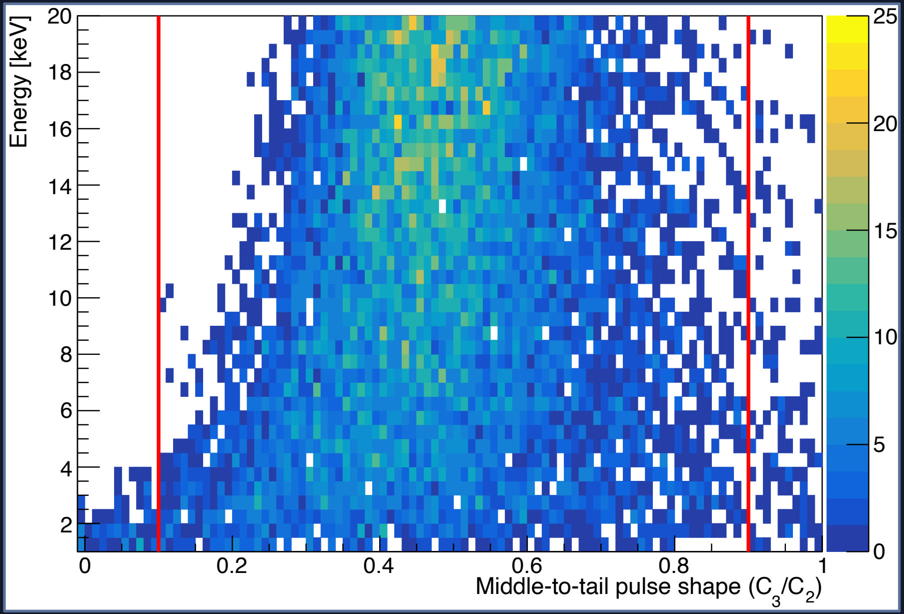

0.1 < C_3/C_2 < 0.9

$$C_3/C_2 = \frac{C_{(400,600)}}{C_{(200,400)}}$$

pulse area between 400 and 600 ns

pulse area between 200 and 400 ns

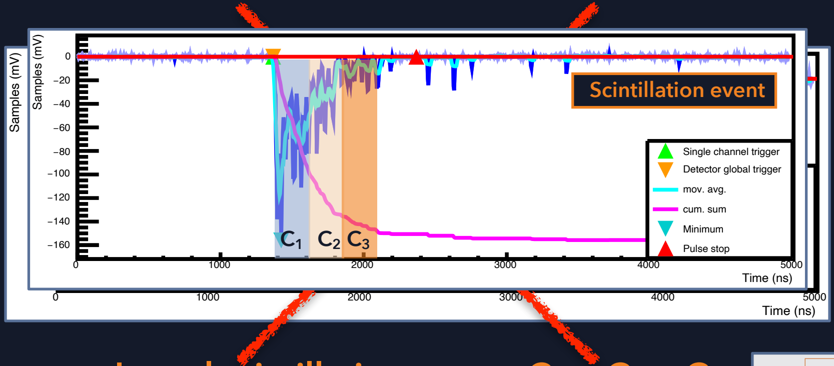

In real scintillation events $C_1 > C_2 > C_3$

Cut-based analysis - Trigger Time Delay

Trigger Time Delay (TTD) distribution (^{228}Th dataset)

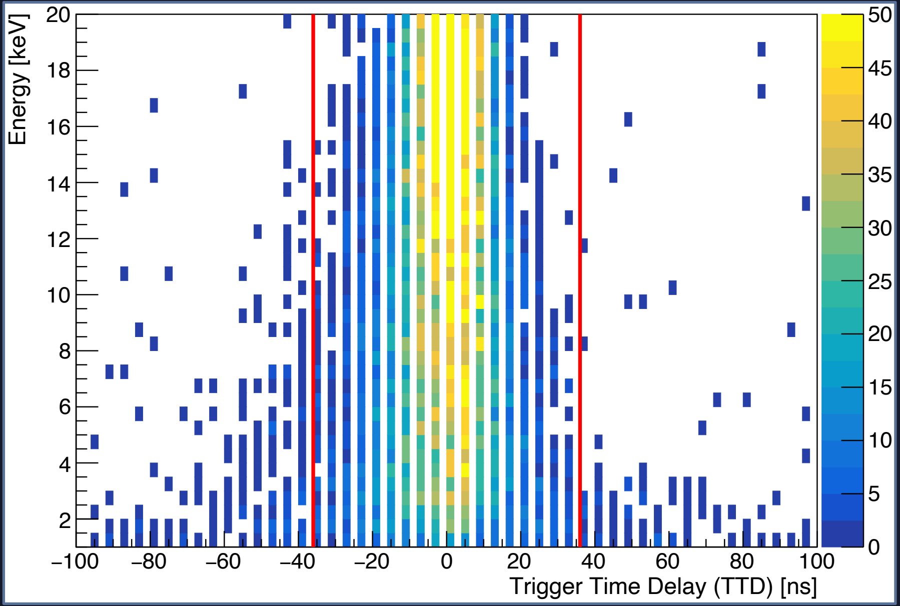

-36 ns < TTD < 36 ns

TTD: *Difference in time between the triggers of the 1st and 2nd channel, respectively.*

Useful to remove afterglows in PMTs

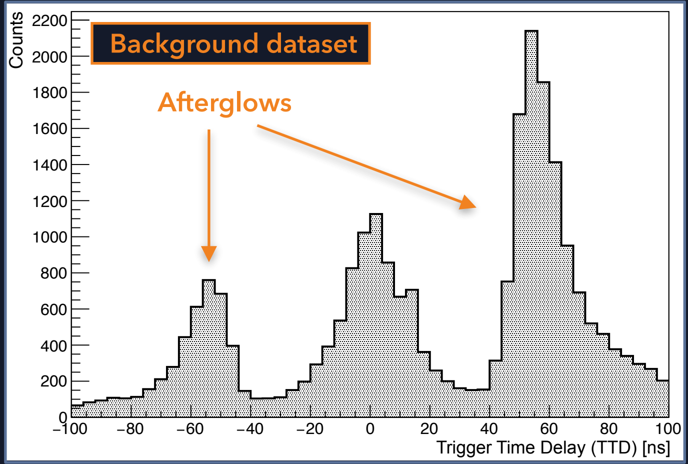

Cut criteria and signal acceptance

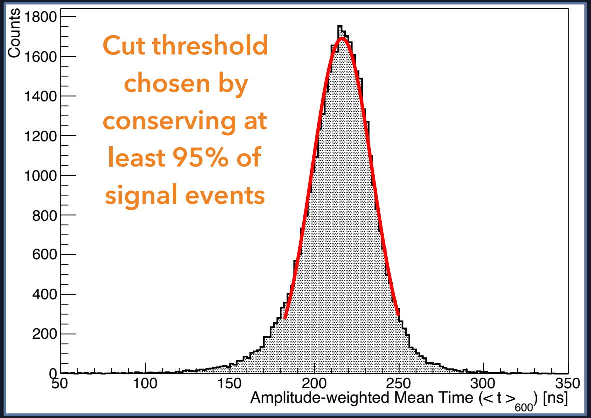

2D parameters distributions in [1-20] keV are projected in 1D histograms and fitted with a Gaussian function.

Cut	Number of events	Acceptance
None	11354	100%
TTD	11092	97.7%
$< t >_{600}$	11148	98.2%
CoM	11254	99.1%
C_2/C_1	10736	94.6%
C_3/C_2	10837	95.4%

Single cuts acceptance in [1-20] keV (^{228}Th dataset)

Combined acceptance (^{228}Th dataset)

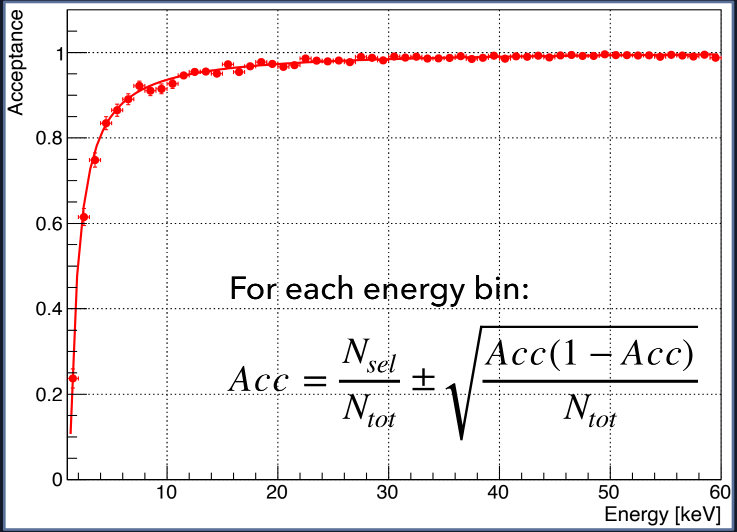

$$Acc = \frac{N_{sel}}{N_{tot}} \pm \sqrt{\frac{Acc(1-Acc)}{N_{tot}}}$$

Low energy spectrum - [1-100] keV

Anti-coincidence spectrum (efficiency-corrected)

- Events which deposit energy in the crystal, but not in the veto detector (LS threshold = 50 keV).

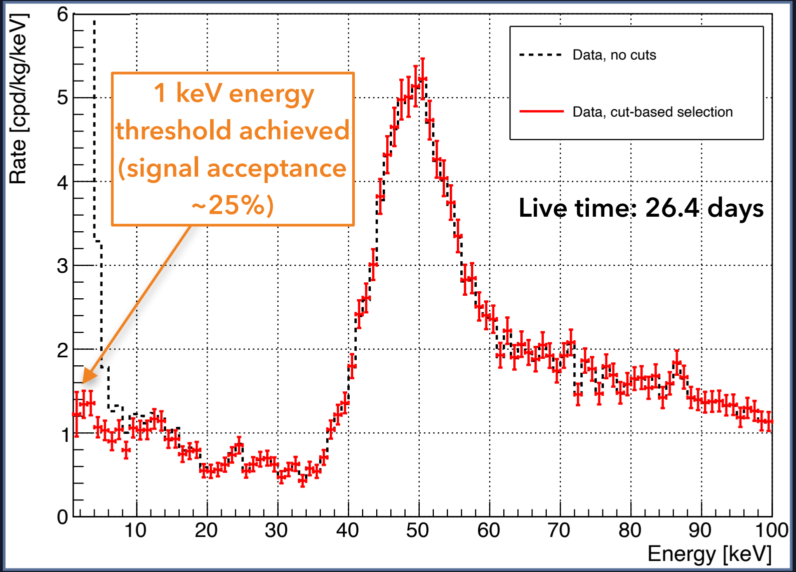

Veto rejection power

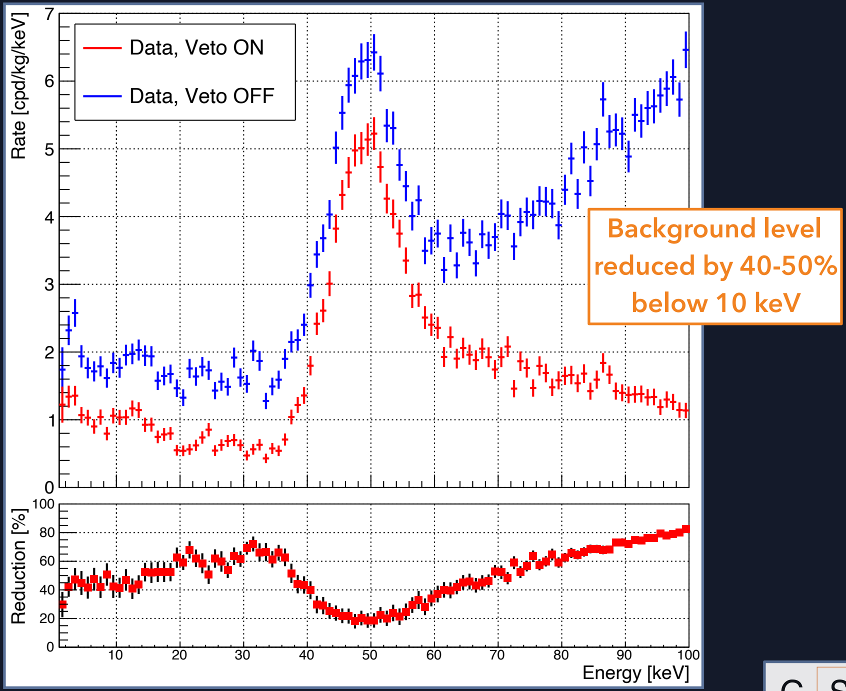

Low energy spectrum - [1-20] keV

Anti-coincidence spectrum (efficiency-corrected)

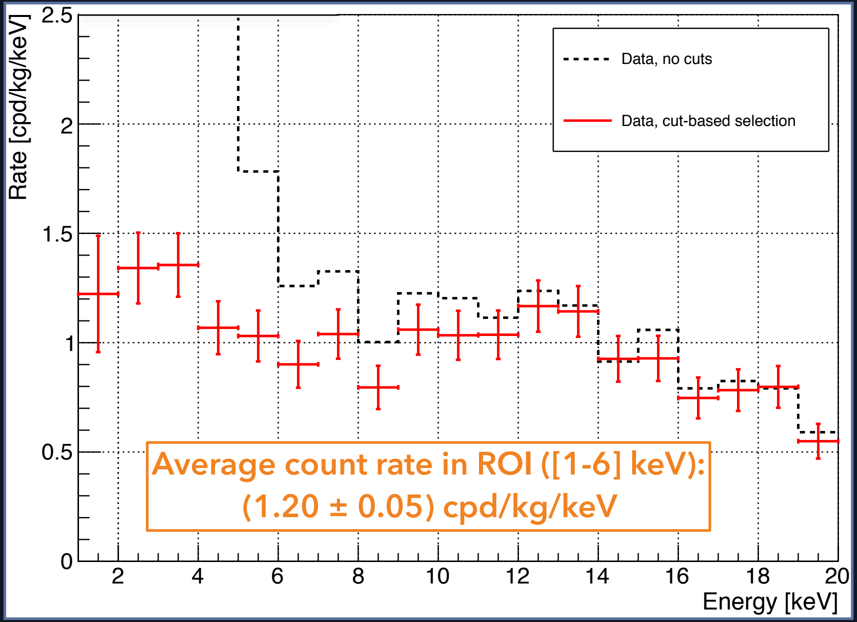

Comparison with other NaI(Tl) experiments

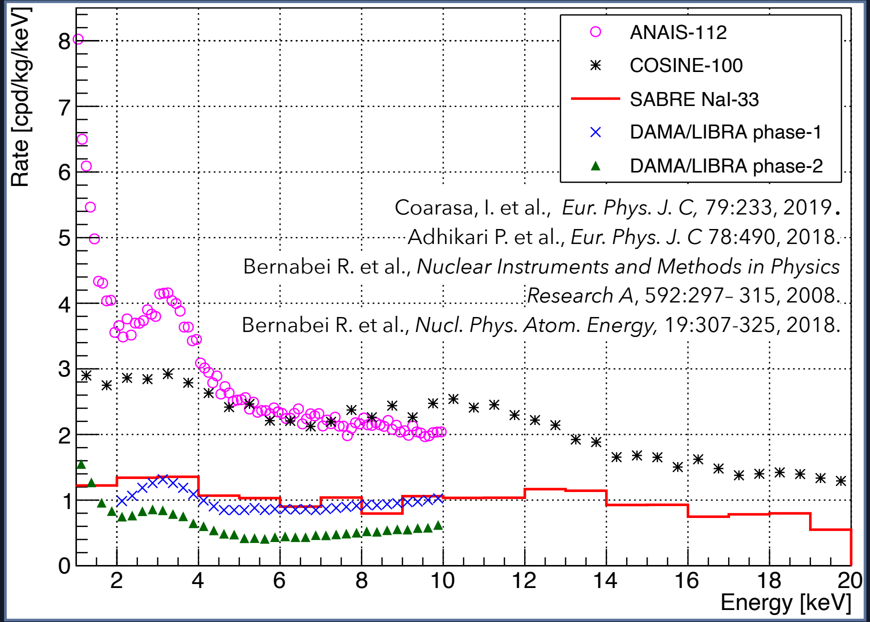

The NaI-33 is the best crystal ever produced after DAMA/LIBRA

Background model

SABRE Monte Carlo code (based on Geant4 v.10.05) used to simulate radioactive decays of the main background sources and build the background model of the NaI-33 crystal

- Listed isotopes are used as input of the background model.

Crystal intrinsic:

1) ^{40}K
2) ^{226}Ra chain
3) ^{232}Th chain
4) ^{210}Pb (bulk)

Crystal cosmogenics:

5) ^{3}H
6) ^{22}Na
7) ^{125}I
8) ^{129}I
9) ^{121m}Te
10) ^{123m}Te
11) ^{125m}Te
12) ^{127m}Te
13) ^{113}Sn
14) ^{109}Cd

Surface contamination:

15) ^{210}Pb (reflector)
16) ^{210}Pb (crystal surface)

Internal + External contamination:

17) Flat component

→ e.g. low energy tail of background contributions dominant at high energy, and internal beta spectra such as ^{87}Rb

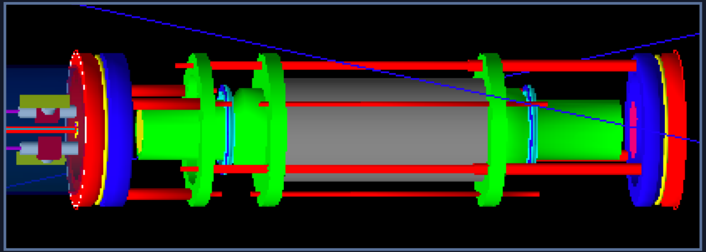

Energy range: [2-100] keV

Background model - Spectral fit

C++ code (based on TMinuit ROOT class) developed to perform the spectral fit of NaI-33 anti-coincidence data

- For each energy bin, the **fitting function** is the sum of the simulated spectra, each multiplied with a scale factor (f_k) to be determined from the fit:

$$\sum_{k=1}^{10} f_k \cdot \left(\sum_{i=1}^{N_{bins}} y_{k,i} \right)$$

Content of the i-th bin for the k component spectrum

Background components included in the best-fit:

1) ^{40}K
2) ^{226}Ra chain
3) ^{232}Th chain

Results from independent measurements exploited to constrain their activities in the spectral fit

4) ^{210}Pb (bulk)
5) ^{3}H
6) ^{129}I
7) ^{121m}Te
8) ^{127m}Te
9) ^{210}Pb (reflector)
10) Flat component

Background model - results

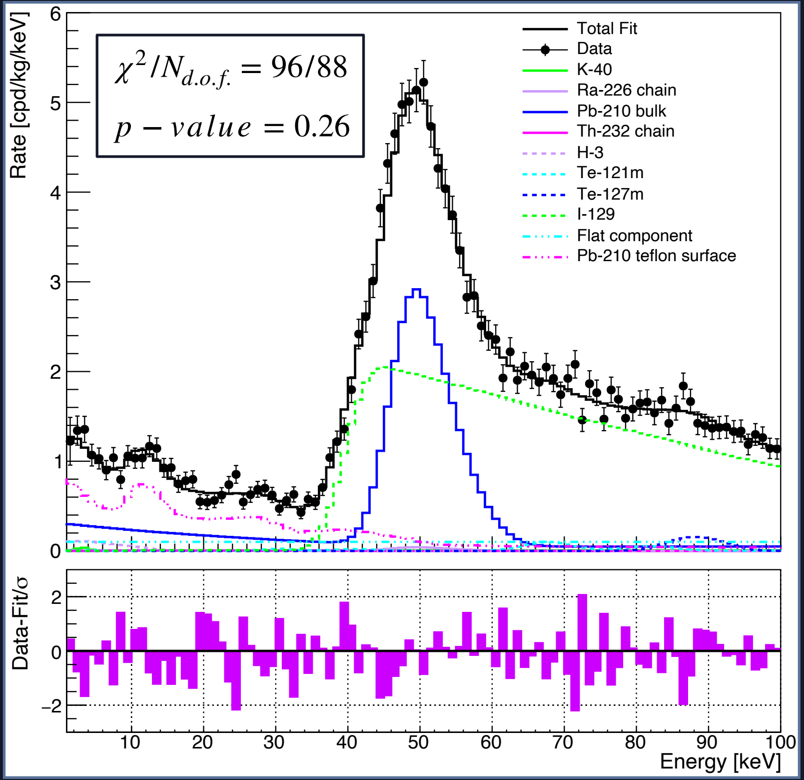

Source	Activity (or rate)
^{40}K	(0.14 ± 0.01) mBq/kg
^{226}Ra	(5.9 ± 0.6) μBq/kg
^{232}Th	(1.6 ± 0.3) μBq/kg
^{210}Pb (bulk)	(0.41 ± 0.02) mBq/kg
^{3}H	(12 ± 7) μBq/kg
^{129}I	(1.34 ± 0.04) mBq/kg
^{121m}Te	≤ 84 μBq/kg
^{127m}Te	(16 ± 6) μBq/kg
^{210}Pb (reflector)	(1.1 ± 0.2) mBq
Flat component	(0.10 ± 0.05) cpd/kg/keV

Background model - [1-20] keV

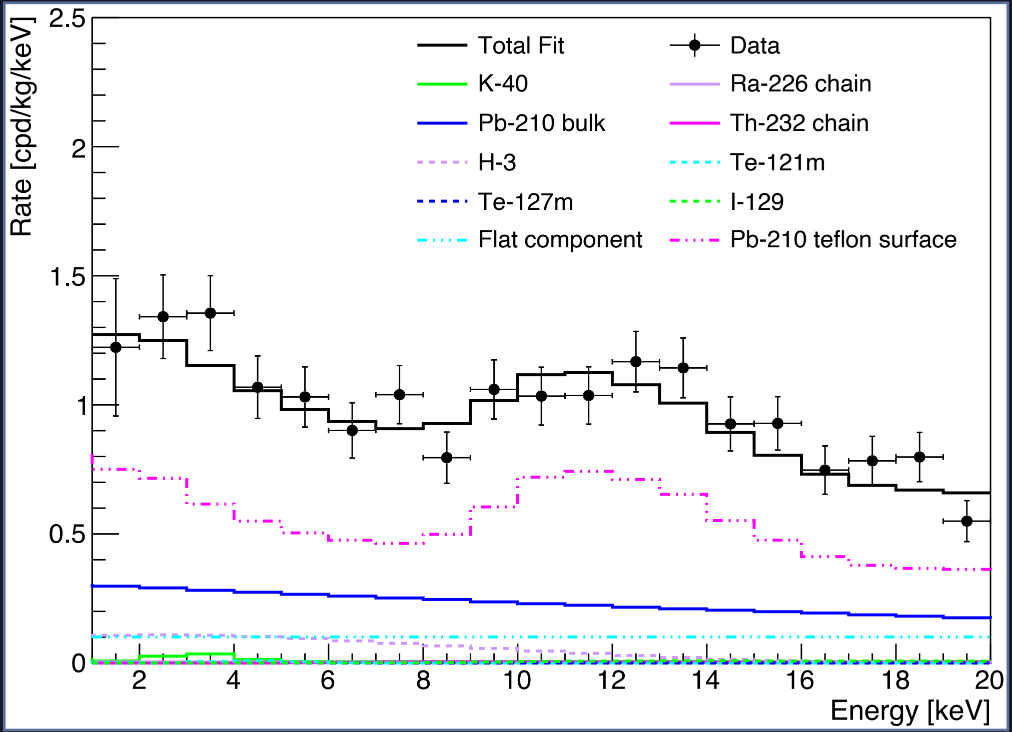

The dominant background contributions are from internal ^{210}Pb and ^{210}Pb in the teflon reflector wrapped around the crystal

A careful screening and selection of the reflector will be fundamental in view of the SABRE full-scale experiment.

^{3}H activity in NaI-33 seems to be about one order of magnitude lower than measured in ANAIS and COSINE crystals

Coarasa, I. et al., *Eur. Phys. J. C*, 79:233, 2019.
Adhikari P. et al., *Eur. Phys. J. C* 78:490, 2018.

Zone Refining (ZR) purification tests on NaI powder

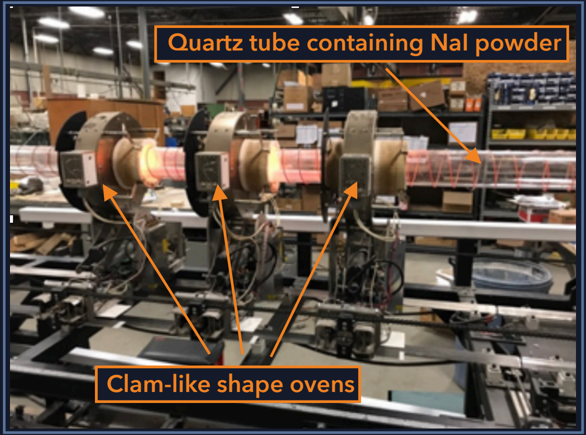

Zone refining system developed in collaboration with the Mellen Company.

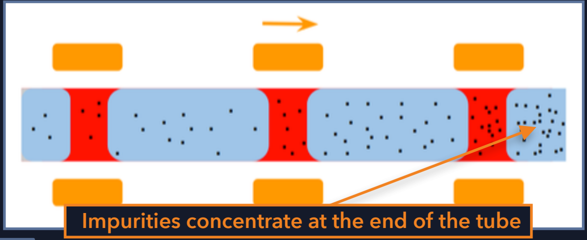

B. Suerfu, PhD thesis, Princeton University, 2018.

Further improvements on the crystals radiopurity are under investigation

- ZR is a purification process in which impurities in the powder are moved, together with the molten material, in the same direction as the ovens move.
- Test operation made in 2019: samples taken from five successive sectors along the tube to perform ICP-MS measurements.

Ovens motion direction →

Isotope	Powder [ppm]	S_1 [ppm]	S_2 [ppm]	S_3 [ppm]	S_4 [ppm]	S_5 [ppm]
^{39}K	0.0085	< 0.0008	< 0.0008	0.001	0.016	0.46
^{208}Pb	0.0012	0.0004	0.0004	0.0004	0.0005	0.0005
^{85}Rb	< 0.0002	< 0.0002	< 0.0002	< 0.0002	< 0.0002	0.0007

ZR reduces ^{40}K and ^{87}Rb (from ^{39}K and ^{85}Rb measurements) to negligible levels, and ^{208}Pb by at least a factor of three

Future perspectives

NaI-33 count rate in ROI ([1-6] keV) calculated from background model vs. projected count rate in ROI for future SABRE crystals

Source	Rate in ROI [cpd/kg/keV]	Projected rate in ROI [cpd/kg/keV]
^{40}K	0.018 ± 0.001	≤ 0.004
^{210}Pb (bulk)	0.28 ± 0.01	0.093 ± 0.003
Other intrinsic(*)	(4.4 ± 0.5) x 10^{-3}	(4.4 ± 0.5) x 10^{-3}
^{3}H	≤ 0.12	~0
Other cosmogenics(**)	≤ 1.1 x 10^{-2}	~0
^{210}Pb (reflector)	0.63 ± 0.09	6.6 x 10^{-3}
Flat component	0.10 ± 0.05	0.10 ± 0.05
Total	1.16 ± 0.10	0.21 ± 0.05

(*) ^{226}Ra and ^{232}Th chains. (**) ^{129}I, ^{121m}Te and ^{127m}Te.

Assumed NaI-33 contamination after scaling for the reduction factors observed in ZR tests

Assumed crystal growth in an underground facility which reduces to zero cosmogenic activation

Assumed an upper limit of 38 mBq/kg_{teflon} (90%C.L.) measured for teflon used in the framework of DarkSide-50

P. Agnes et al. , Physics Letters B, 743:456-466, 2015.
M. Laubenstein and P. Meyer, private comunication.

This result would mark a significant improvement in the quest for DM induced annual modulation with NaI(Tl) crystals

SABRE sensitivity for annual modulation signal

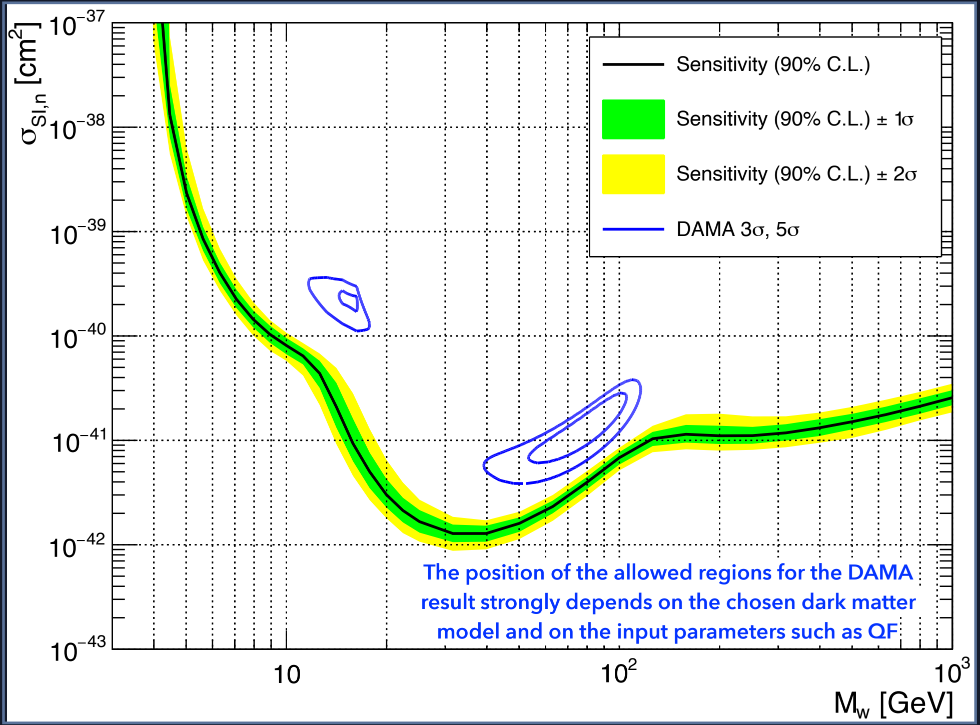

Assumptions:

- **Standard Halo Model**;
- **Spin-independent WIMP-nucleon interaction**;
- **50 kg** of NaI(Tl) crystals;
- **3 years** of data taking;
- Background level in the ROI of **0.2 cpd/kg/keV**.
- **QF** for **Na** measured by **Xu et al.**;
  J. Xu et al., *Phys. Rev. C*, 92(1):015807, 2015.
- **QF** for **I** measured by **DAMA** (0.09);
  R. Bernabei et al., *Phys. Lett. B*, 389:757-766, 1996.

The SABRE experiment is expected to be sensitive to WIMP-nucleon scattering cross sections down to 1.3×10^{-42} cm² (for a WIMP mass of 30–40 GeV)

GSSI GSSI

Summary and conclusions

Summary and conclusions

The SABRE crystals were fully characterized at LNGS using two setups: a passive shielding testing facility in Hall B and the SABRE-PoP in Hall C

	NaI-31	NaI-33	DAMA/LIBRA crystals	ANAIS crystals	COSINE crystals
LY [phe/keV]	9.1 ± 0.1	12.1 ± 0.2	6-10	15	15
FWHM/E @59.5 keV	14.1%	13.5%	15.8%	11.2%	11.8%
^{40}K activity [mBq/kg] (direct counting)	0.49 ± 0.10	< 0.15	< 0.62	0.70-1.33	0.58-2.5
^{238}U content [ppt] (Bi-Po-214 direct counting)	-	< 0.5	0.7-10	0.2-0.8	< 0.02-0.12
^{232}Th content [ppt] (Bi-Po-212 direct counting)	-	< 0.5	0.5-7.5	0.1-1	0.3-2.4
Alpha rate [mBq/kg]	1.02 ± 0.07	0.54 ± 0.01	0.08-0.12	-	0.74-3.20
^{210}Pb activity [mBq/kg] (^{210}Po build-up)	-	0.51 ± 0.02	0.005-0.03	0.7-3.15	-
^{3}H activity [mBq/kg] (spectral fit)	-	0.012 ± 0.007	< 0.09	0.09-0.20	0.05-0.12
Exposure	60 kg·days	90 kg·days	2.17 ton·yr	313.95 kg·yr	97.7 kg·yr
Average rate in [1-6] keV [cpd/kg/keV]	-	1.20 ± 0.05	< 1	3.605 ± 0.003	2.73 ± 0.14

Summary and conclusions

My major contributions to these results can be divided in the following areas:

Detector design, deployment, commissioning and operation

- **MC simulations** to evaluate the expected background;
- **Assembly and testing** of the two SABRE **detector modules**;
- SABRE-PoP **commissioning**;
- **Tests and calibrations** of the detectors (both **crystals** and **veto**);
- **Co-responsibility** for the **management** of **data taking**;
- **Off-line processing** and **analysis**.

Development of software tools for data processing and data analysis

- **Implementation** and **validation** of some **modules** of the **reconstruction software**;
- **Algorithms** for **PSD** and **Bi-Po selection;**
- **Development** and **implementation** of **data filtering procedures**;
- **Development** of the **code** to perform the **spectral fit** of **NaI-33 data**.

Physics results

- **LY** and **energy resolution;**
- ^{238}**U** and ^{232}**Th content**;
- α **rate** and ^{210}**Pb activity**;
- ^{40}**K activity**;
- **1 keV energy threshold achieved** for NaI-33 data analysis;
- **Background level in the ROI** for DM search;
- **Background model**;
- **SABRE projected sensitivity** to spin-independent WIMP-nucleon elastic scattering.

Credits

This presentation template was created by **Slidesgo**, including icons by **Flaticon,** infographics & images by **Freepik**

Backup I

Evidences of dark matter at galactic scale

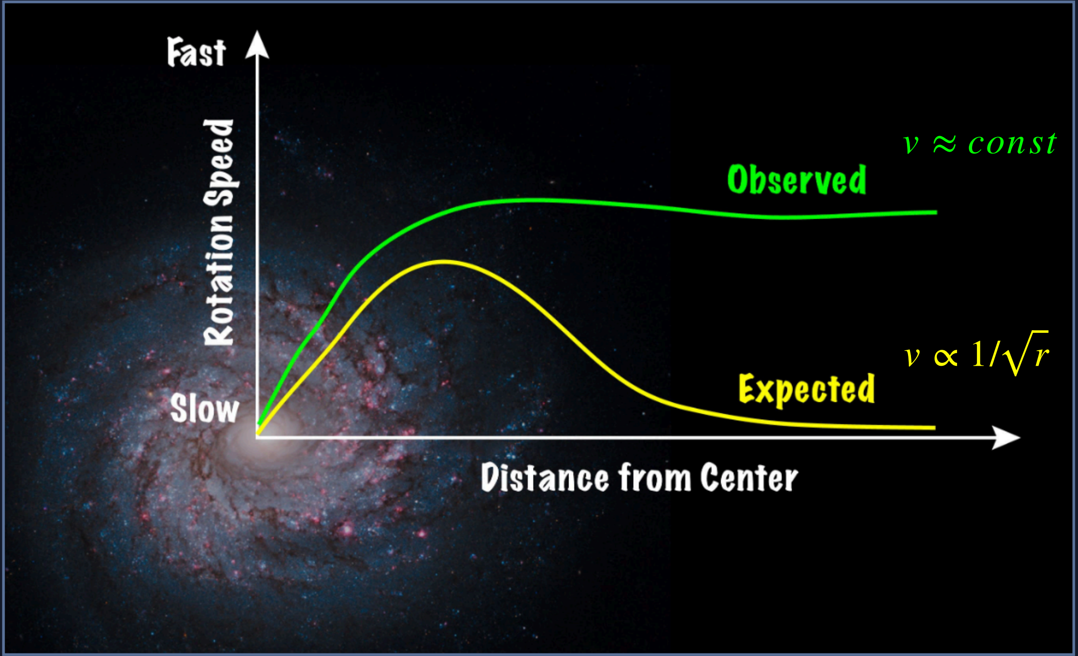

Spiral galaxies velocity rotation curve

Boundary stars are feeling the gravitational effect of an **unseen mass** distributed in a **halo** around the galaxy.

Evidences of dark matter at clusters scale

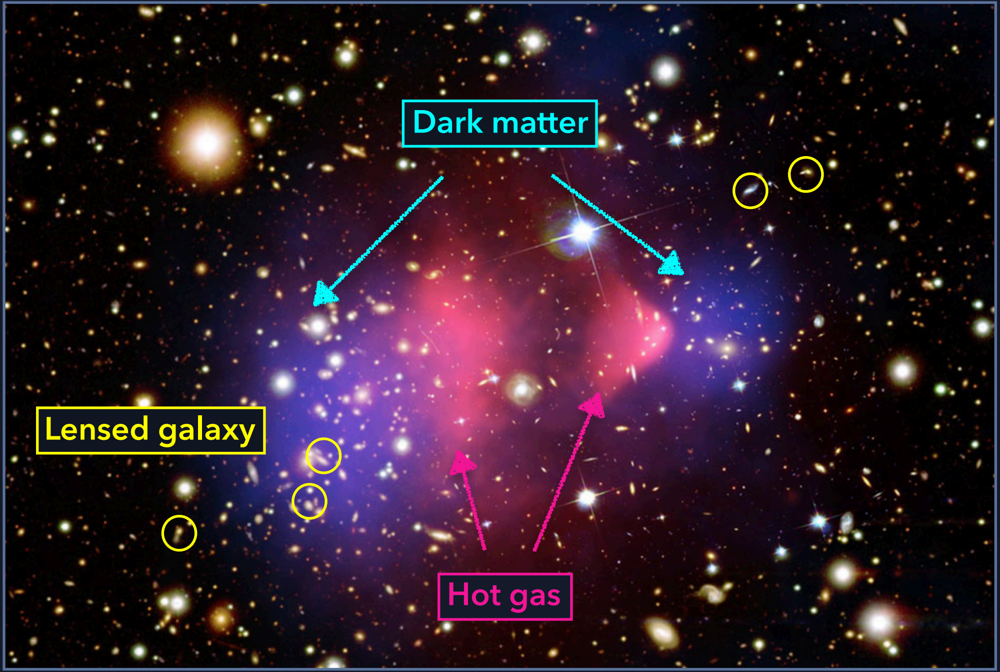

APOD: 2006 August 24 - NASA

Bullet Cluster

Collision between two clusters of galaxies.

The largest matter component is **collisionless** and has **non-luminous** nature.

Evidences of dark matter at larger scale

Cosmic Microwave Background (CMB)

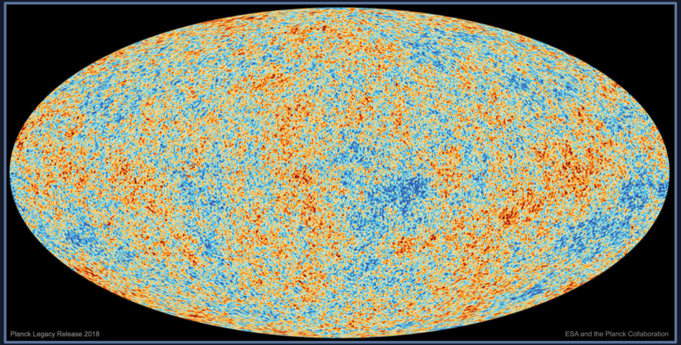

P. A. R. Ade et al., *Astronomy & Astrophysics*, 594:A13, 2016.

Black body spectrum → $\frac{\delta T}{T}(\theta, \phi) = \sum_{lm} a_{lm} Y_{lm}(\theta, \phi)$

$\Omega_m h^2 = 0.1427 \pm 0.0014$

$\Omega_b h^2 = 0.02225 \pm 0.00016$

$\Omega_m > \Omega_b$

Ω_m: Total matter density parameter

Ω_b: Baryonic matter density parameter

Angular power spectrum

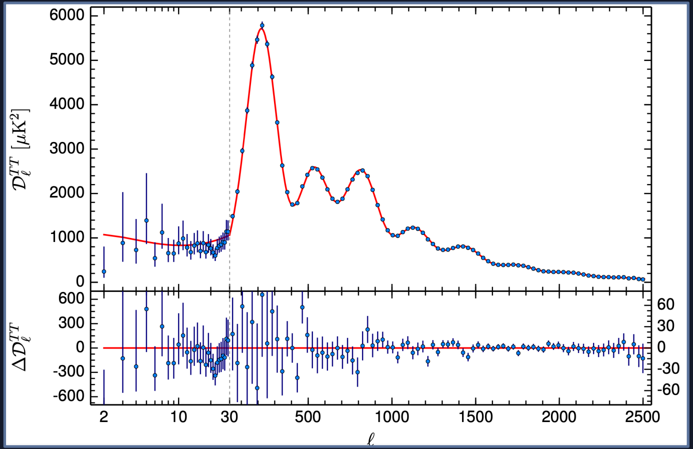

P. A. R. Ade et al., *Astronomy & Astrophysics*, 594:A13, 2016.

$D_l^{TT} \equiv l(l+1)C_l/2\pi \quad (C_l \equiv <|a_{lm}|^2>)$

Dark matter relic density

- A heavy particle χ is initially in **thermal equilibrium**

$$\chi\chi \leftrightarrows q\bar{q}$$

- The **Universe cools down**

$$\chi\chi \not\leftrightarrows q\bar{q}$$

- The Universe expands: "**freeze-out**"

$$\chi\chi \not\leftrightarrows q\bar{q}$$

- And this is the **density of DM today**

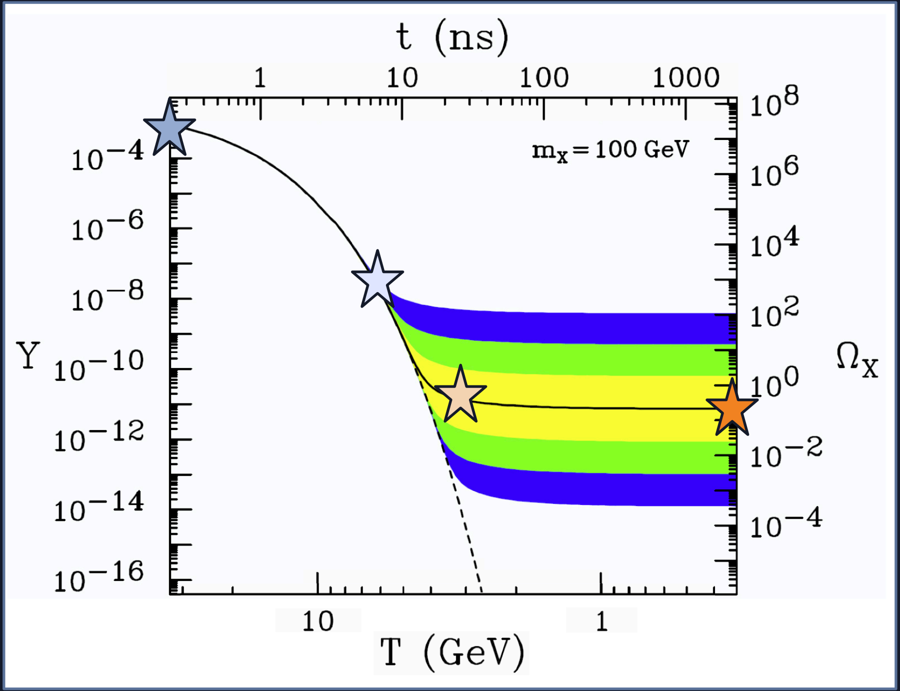

J. L. Feng, *Ann. Rev. Astron. Astrophys*, 48: 495, 2010.

G S S I

G S S I

Missing mass problem

Modification of gravity

MOND

Modification of Newtonian dynamics which account for observed rotation curves

M. Milgrom, *Astrophys. J.*, 270:365–370, 1983.

$$\frac{ma^2}{a_0} = \frac{GmM}{r^2} \Rightarrow v = (GMa_0)^{1/4} = const \quad (a << a_0)$$

No fundamental theory of modified gravity have been found yet which can explain all the gravitational anomalies at the same time

Dark matter

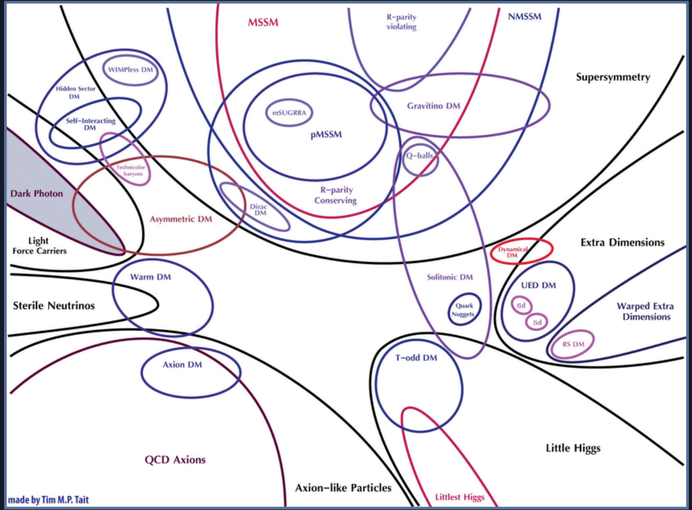

A lot of theories and candidates...

ANAIS-112

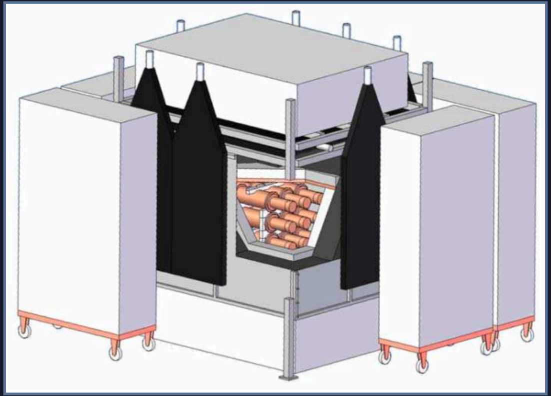

- Located at **Canfranc Underground Laboratory**
- ~112 kg of **NaI(Tl) crystals**;
- **Passive shielding** (lead, water tanks and polyethylene);
- **Active muon veto** (plastic scintillators);
- Taking data since 2017.

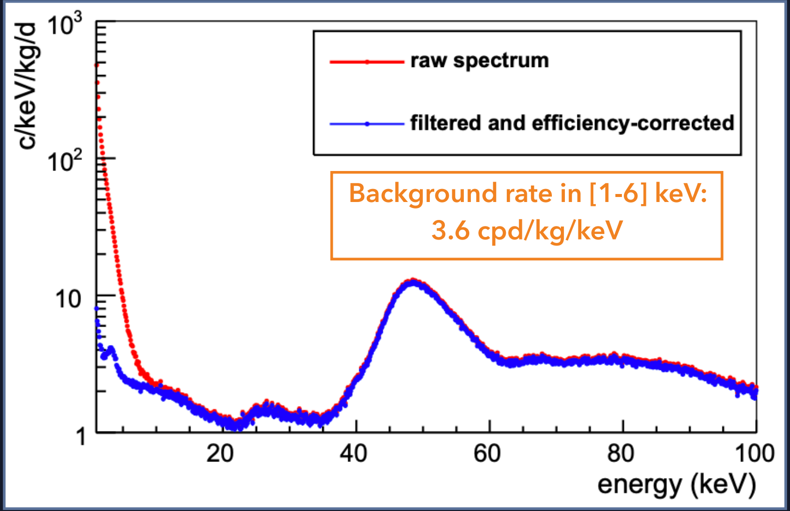

- **^{40}K** ~ 0.96 mBq/kg (~32 ppb of ^{nat}K) on average;
- **^{210}Pb:** 3.15-0.70 mBq/kg;
- **^{3}H:** 0.20-0.09 mBq/kg.

J. Amaré et al.,The European Physical Journal C, 79(3), 2019.
J. Amaré et al., The European Physical Journal C, 79(5), 2019.

ANAIS-112 - annual modulation results

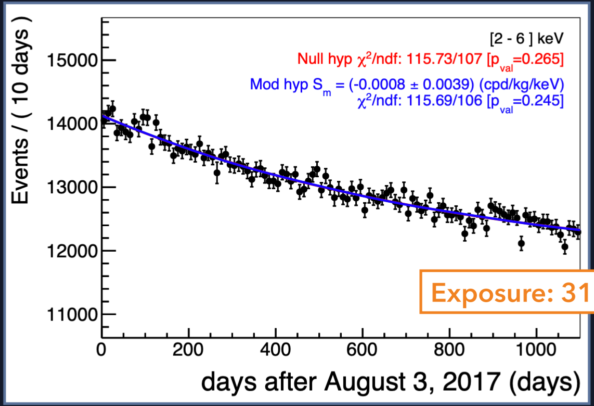

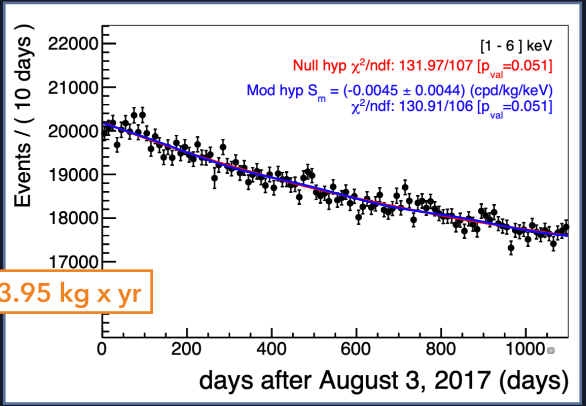

Exposure: 313.95 kg x yr

arXiv:2103.01175

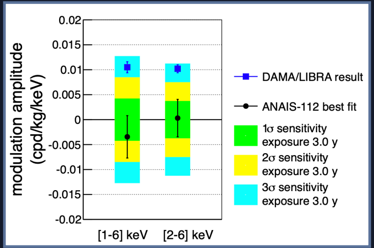

Sensitivity

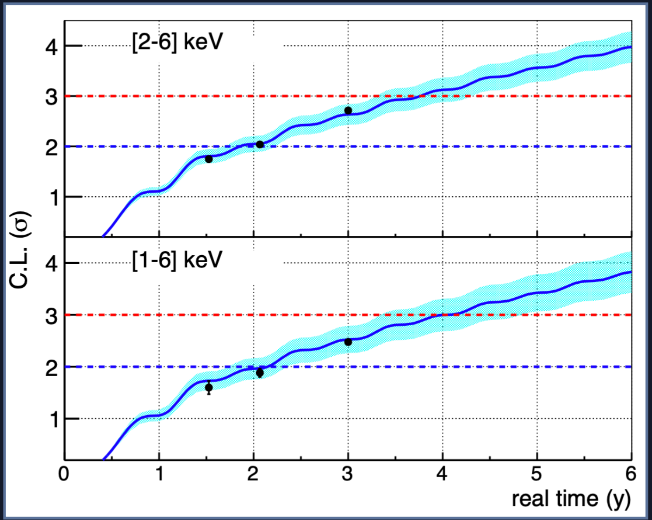

Best-fit in the [1-6] keV ([2-6] keV) energy region supports the absence of modulation in ANAIS data, and is incompatible with DAMA/LIBRA result at 3.3 (2.6) σ, for a sensitivity of 2.5 (2.7) σ

COSINE-100

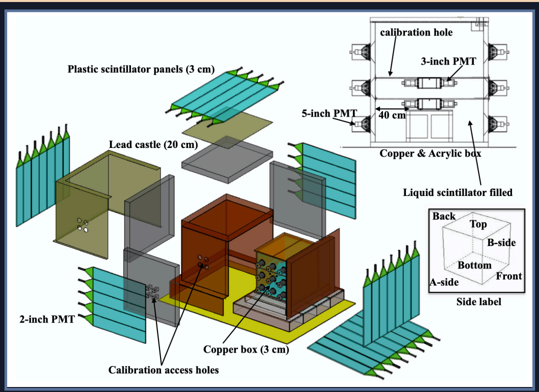

- Located at **Yangyang Underground Laboratory**
- ~106 kg of **NaI(Tl) crystals**;
- LAB-based **LS veto**;
- **Passive shielding** (copper and lead);
- **Active muon veto** (plastic scintillators);
- Taking data since 2016.

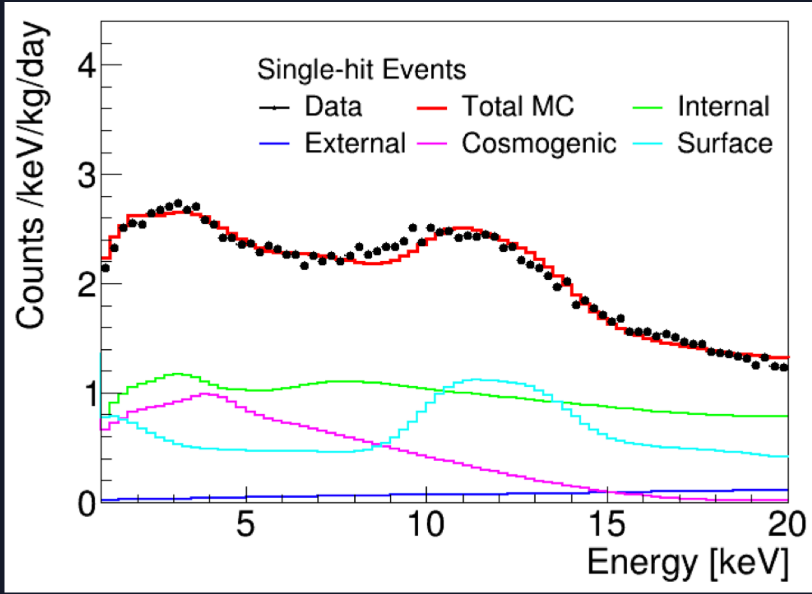

arXiv:2101.11377

Background rate in [1-6] keV: 2.73 cpd/kg/keV

- ^{nat}**K** ~42 ppb on average;
- ^{210}**Pb:** 3.20-0.74 mBq/kg;
- ^{3}**H:** ~0.20 mBq/kg.

COSINE-100 - annual modulation results

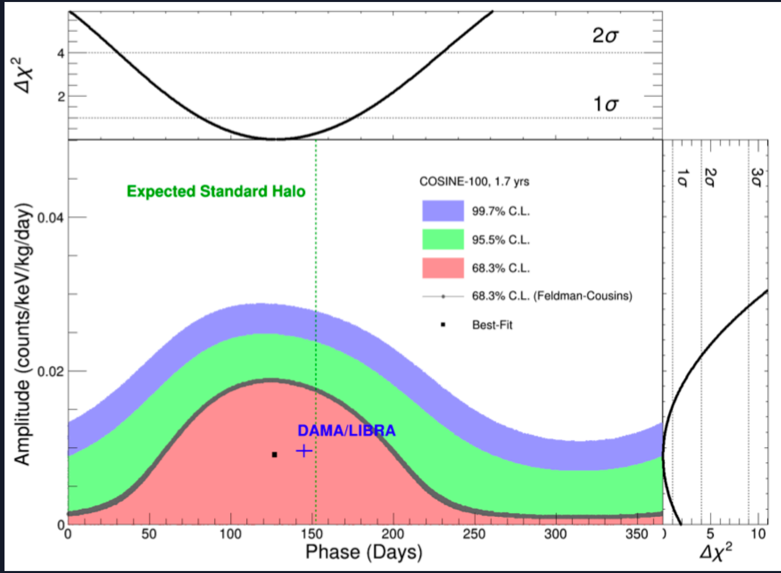

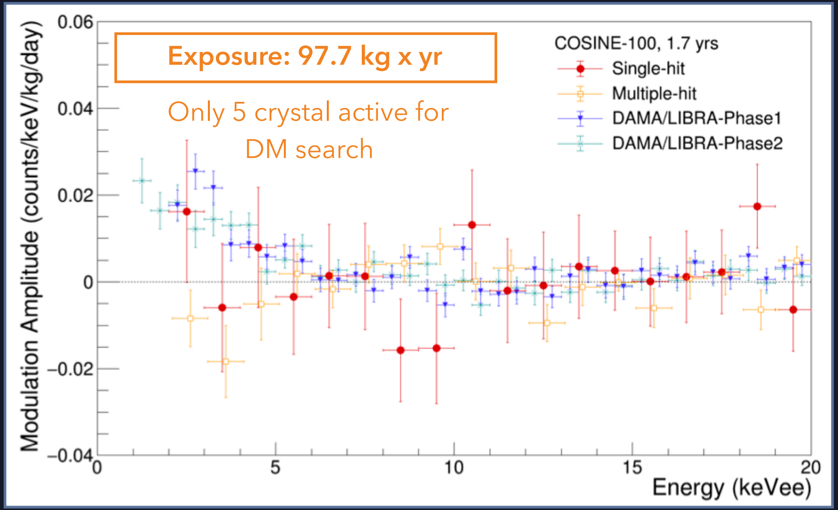

G. Adhikari et al., *Phys. Rev. Lett.*, 123(3):031302, 2019.

Current data from COSINE are consistent with both the DAMA/LIBRA annual modulation result and the null hypothesis of no modulation at the 68.3% C.L.

Growth of ultra-high purity SABRE crystals

SABRE crystals were grown by the RMD (Radiation Monitoring Devices) company using the Vertical Bridgman method

- The NaI powder is melted and slowly cooled through a thermal gradient;
- The crucible can be completely sealed.

A. Possibility of contamination during the growth phase drastically reduced

B. The crystal radiopurity depends only on the purity of the starting powder and crucible

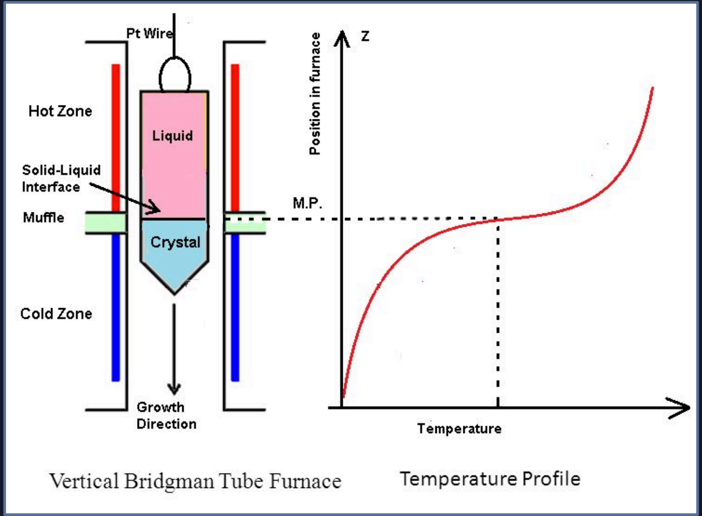

A. S. M. J. Islam. Float Zone and Bridgman Crystal Growth Techniques. *Presentation*, Khulna University, May 2019.

Detector module cleaning protocols

All the components close to the crystal must be extremely clean to avoid the introduction of additional impurities

The SABRE **detector modules** are mainly made of two materials: **copper** (Cu) and **Delrin.**

Cleaning procedure:

- **Ultrasonic bath** (~30 min):
  - de-ionized water + 2% v/v of Alconox Detergent 8 (both **Cu** and **Delrin**);
  - de-ionized water + 4% m/m of citric acid (**Cu** only);
- **Rinsing** with de-ionized water;
- **Vacuum baking** (~1 day):
  - T ~100°C (**Cu**);
  - T ~60°C (**Delrin**).

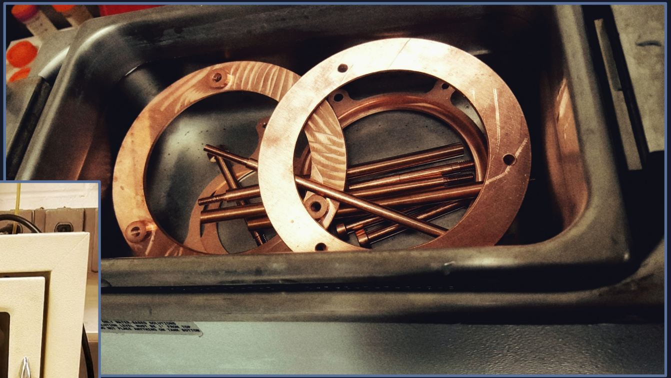

NaI(Tl) crystals are highly hygroscopic, so it is necessary to remove any moisture trace

Detector module testing

Both the detector modules were tested before the shipment to LNGS

Lead bricks shielding

NaI-33 detector module

- Small **lead bricks shielding** (~4″ in all directions) used to reduce environmental background radiation;
- Data acquired with uncollimated **^{137}Cs** and **^{22}Na** sources.

Characteristic peaks in the energy spectra are properly reconstructed

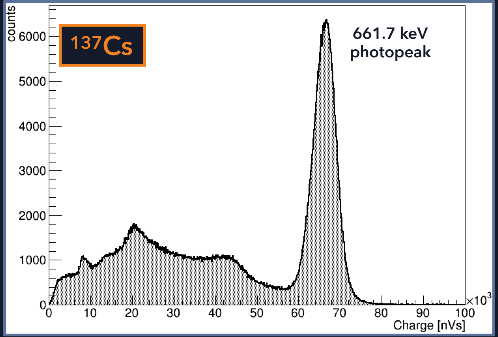

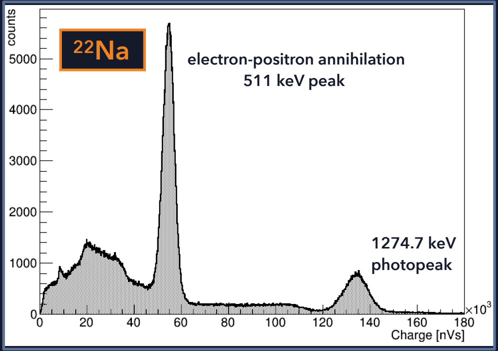

Data acquisition system (DAQ) scheme

Digitize and record signals
(250 MS/s with 12 bit-resolution)

Manage communication with PC through optical link

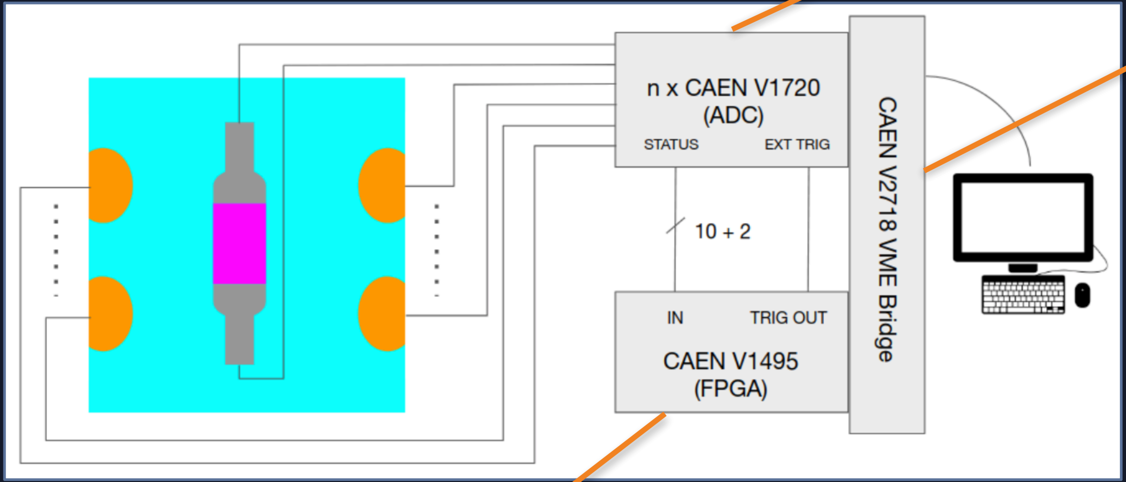

B. Suerfu, PhD thesis, Princeton University, 2018.

Trigger logic

Crystal PMT signals amplification:

- **Hall B**:
  - Custom-made THS3001 based amplifier on a NIM crate;
- **Hall C**:
  - Pre-amplifier module mounted on the CIS top flange to maximize signal-to-noise ratio (due to the very long cables).

Bi-Po sequences selection efficiency

$$\epsilon = \int_{t_{min}}^{t_{max}} \frac{1}{\tau} e^{-t/\tau} dt = e^{-t_{min}/\tau} - e^{-t_{max}/\tau}$$

Bi-Po-212

t_{max} = 3 τ, where τ = 431 ns (^{212}Po mean-life)

t_{min} = 0.15 τ, to avoid re-triggering phenomena

$$\epsilon = 81\ \%$$

Bi-Po-214

t_{max} = 3 τ , where τ = 237 μs (^{214}Po mean-life)

t_{min} = 0.02 τ, to take into account the possibility that the alpha event could be lost because it occurs in the pre-trigger or post-trigger interval, or due to the acquisition dead time (~1 μs)

$$\epsilon = 93\ \%$$

Data quality cuts - tail events

Before analyzing data, events that cannot be considered "valid" are rejected —> live time reduction

- Tail-events following very high energy interactions.

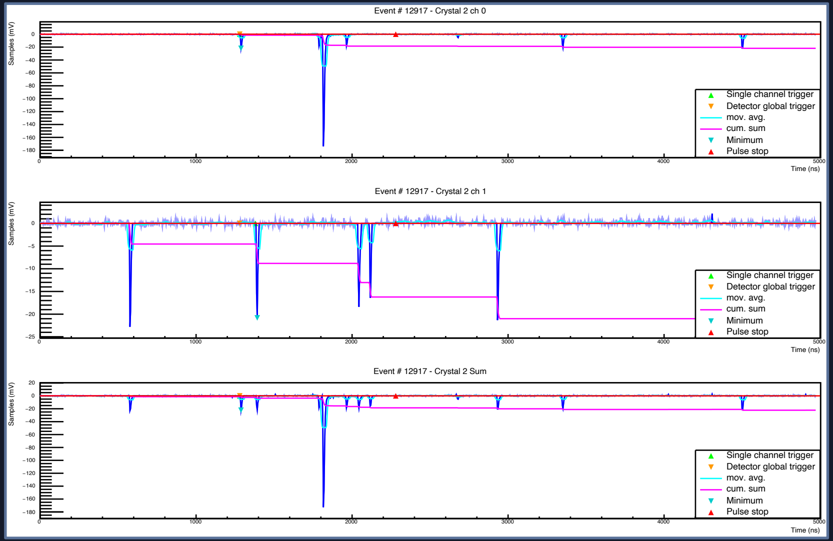

Probability of DM interactions occurring in short time periods is negligible (true also for scintillation events caused by radioactivity due to the very low background).

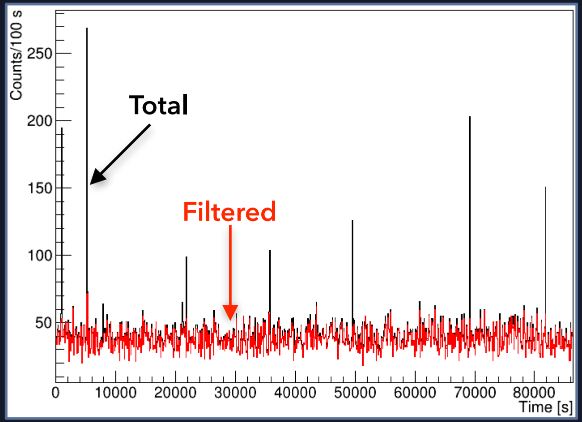

Events arriving in a time interval < 500 μs after the preceding trigger are rejected

Data quality cuts - events with anomalous baseline estimation

- Events with anomalous baseline estimation (tail-events not removed by the previous cut or dark current photons).

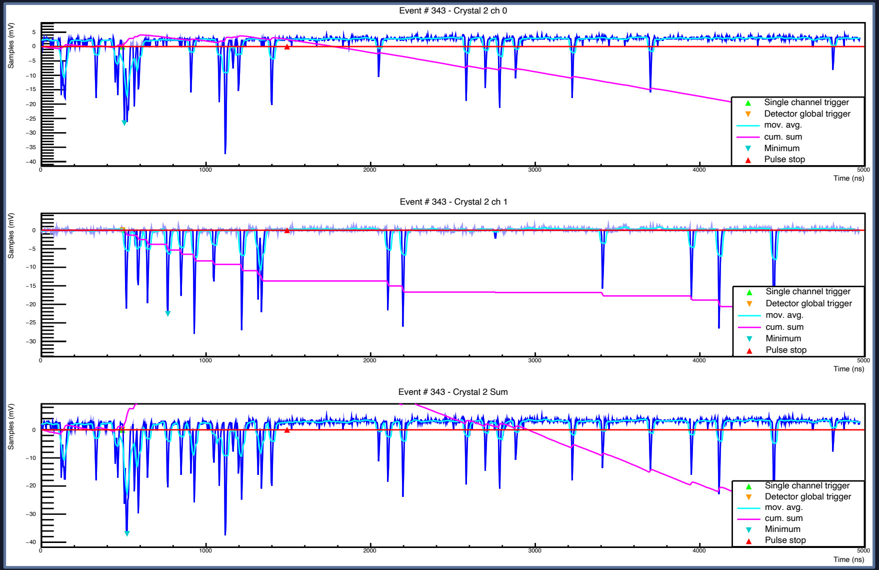

The baseline is calculated by averaging the first 125 samples before the beginning of the pulse. If one or more photons appear in the pre-trigger region, the baseline (and other related pulse parameters) won't be properly calculated.

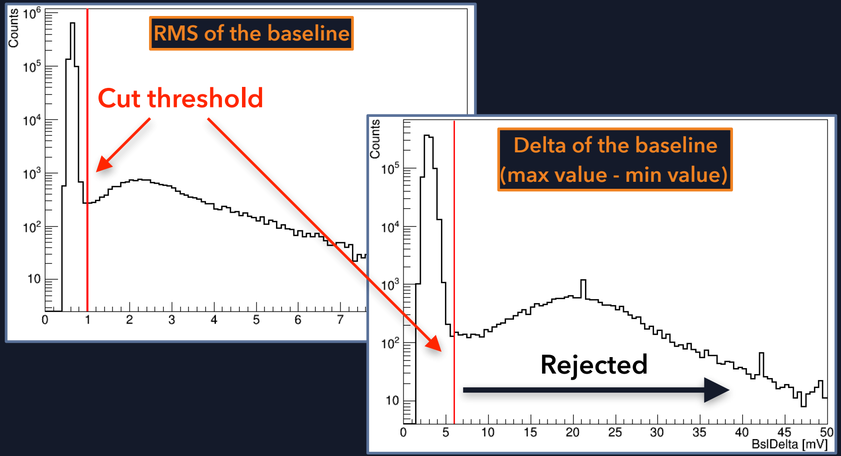

Cut threshold ~8σ away from the mean value of the peak

Data quality cuts - bipolar events

- Events affected by electromagnetic noise.

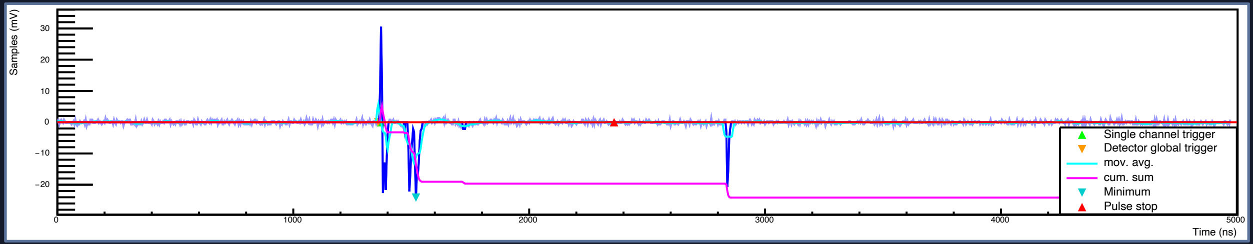

Cut threshold ~8σ away from the mean value of the peak

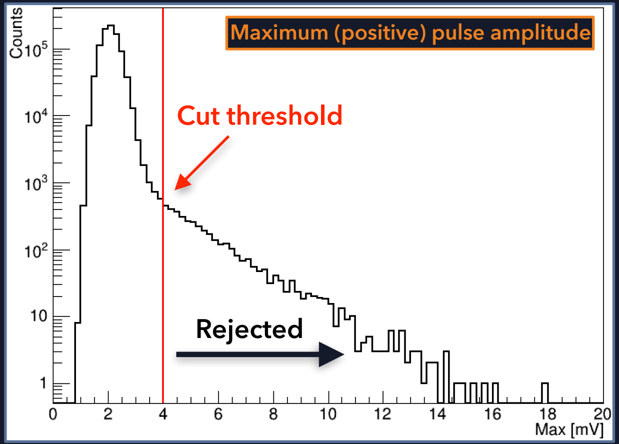

The total dead time introduced by all the data quality cuts is ~0.2%
(almost entirely due to the cut on tail-events)

Effect of data quality cuts on live time

Cut	Number of events	Dead time [s]	Live time [s]
None	980043	-	2280444.0
Tail-events	900442	450.2	2279993.8
Wrong-Bsl events	925015	0.3	2280443.7
Bipolar events	954215	0.2	2280443.8
All	897679	450.7	2279993.3

NaI-33 high energy spectrum

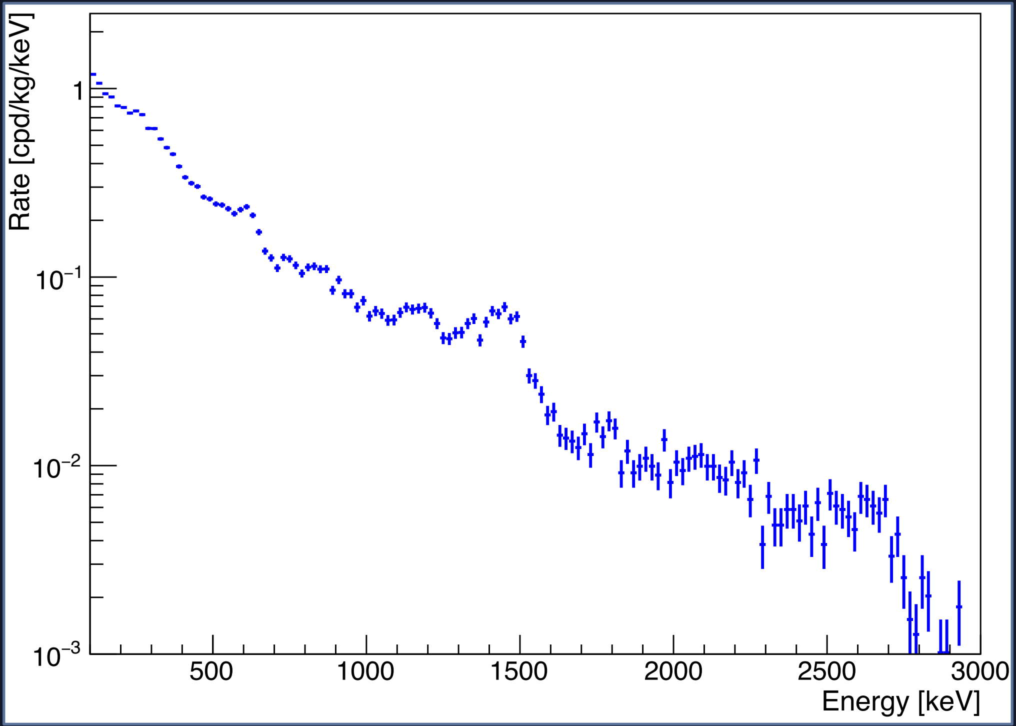

Crystals characterization within the PoP setup

^{214}Am source to measure light yield (LY) and energy resolution (R) on the 59.5 keV gamma line

- Source positioned next to the copper enclosure in correspondence with the crystal centre.

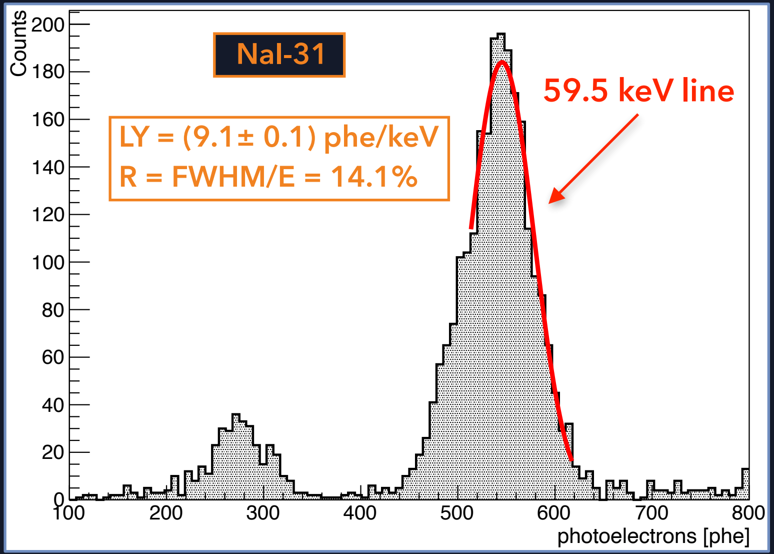

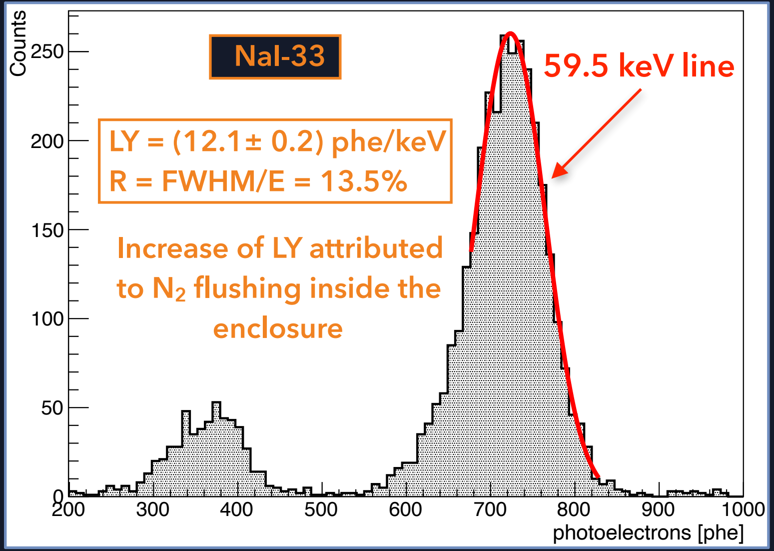

Events selection: ^{228}Th calibration run

Selection criteria tuned on data acquired with a ^{228}Th source (without veto)

- **Pros:** very intense source –> rich dataset in short time;
- **Cons:** so intense that emitted γs frequently hit crystal PMTs –> a lot of additional noise.

Noise has to be efficiently removed before using this dataset to tune selection criteria and evaluate signal acceptance

Additional data quality cuts included to this aim.

- They are based on three parameters:
  - Amplitude weighted mean time ($\langle t \rangle_{600}$); → Same used for particles discrimination
  - Trigger Time Delay between the two PMTs signals (TTD); → Difference in time between the triggers of the 1st and 2nd channel
  - Number of Cluster in each PMT (NC). → A cluster is defined by the waveform exceeding an amplitude threshold corresponding to ~1 phe

Study of quality cuts acceptance with pulse simulation

Cut threshold for $< t >_{600}$ and TTD parameters chosen using a MC simulation of the scintillation pulses

"Synthetic" waveforms generated by randomly sampling from the time distribution of a reference pulse built using a ^{241}Am calibration run.

- 1 entry = 1 photoelectron;
- Energy range: [1-20] keV.

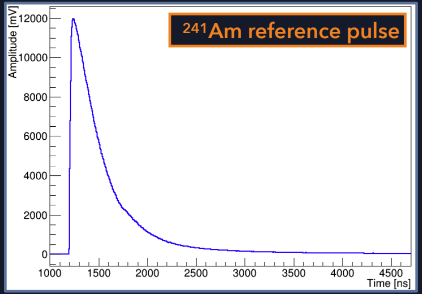

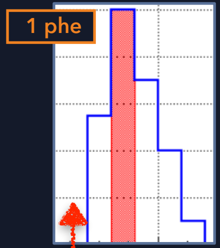

Probability of having a phe in the 1st channel

$p_0 = LY_0/LY_1$

N_{phe} → $B(N_{phe}, p_0)$ → $N_1 = N_{phe} - N_0$

Total number of phe at a given energy — Binomial distribution — Number of phe in the 2nd channel

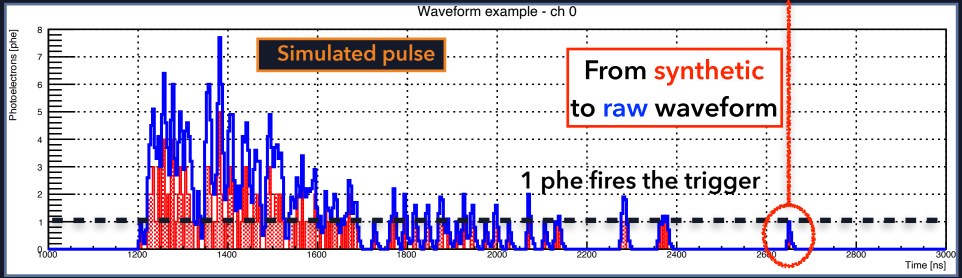

$< t >_{600}$ and TTD calculated in the same way as in the experimental data

Study of quality cuts acceptance with pulse simulation

$< t >_{600}$ and TTD distributions for simulated pulses and corresponding signal acceptance after the cut

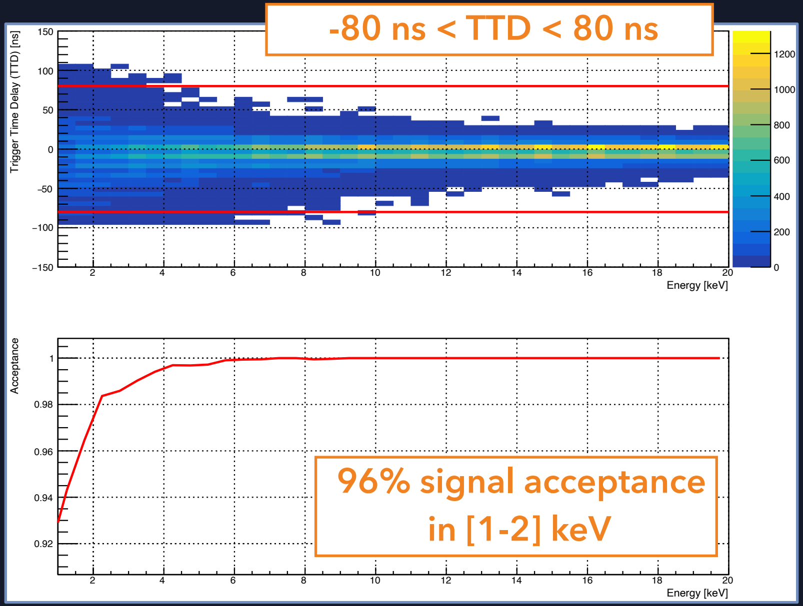

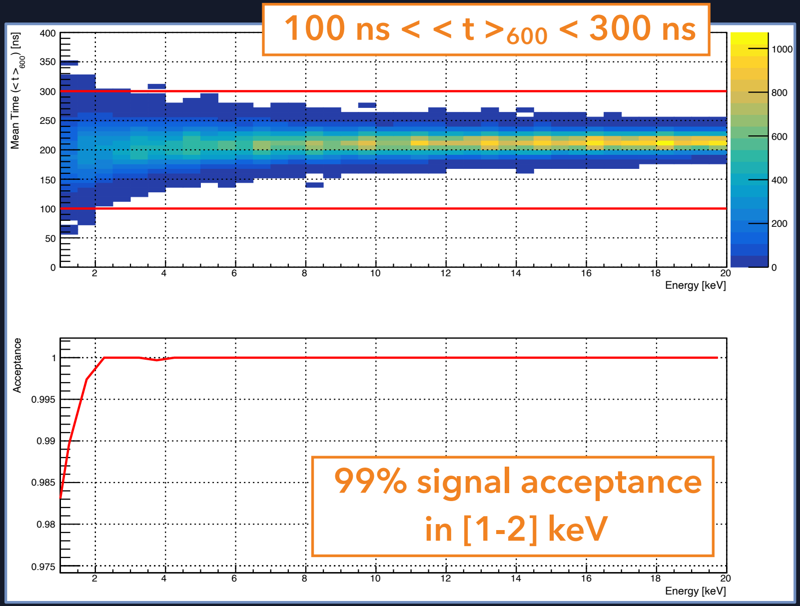

Asymmetric events and NC cut

Events with asymmetry in the energy partition between the two PMTs constitute a noise population below 4 keV

- Identified by the difference in the number of clusters (NC) in the two PMT channels.

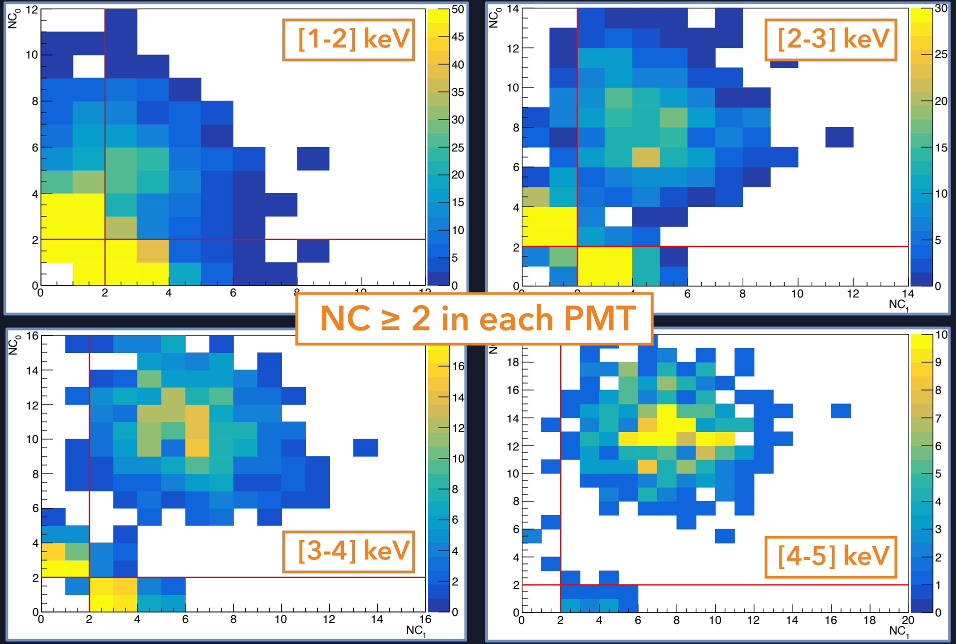

Examples of rejected events…

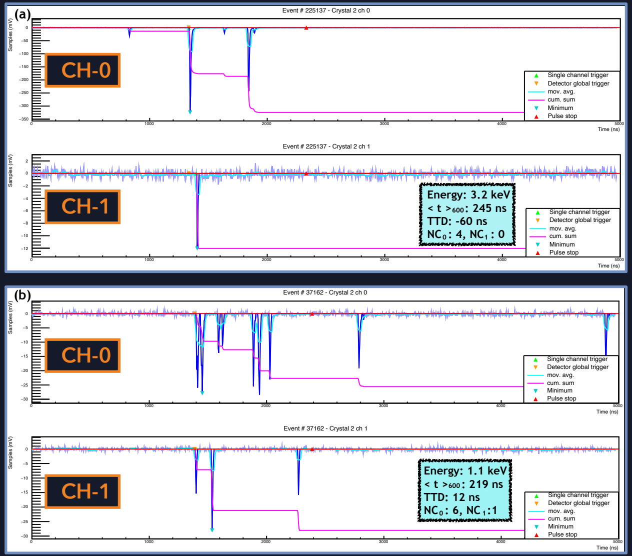

NaI-33 low energy correction

Proper reconstruction of small energy deposits is necessary to build the low energy spectrum of the crystal

- Slight non-linearity observed between calibration with the 59.5 keV line of ^{241}Am and 3.2 keV line of ^{40}K.

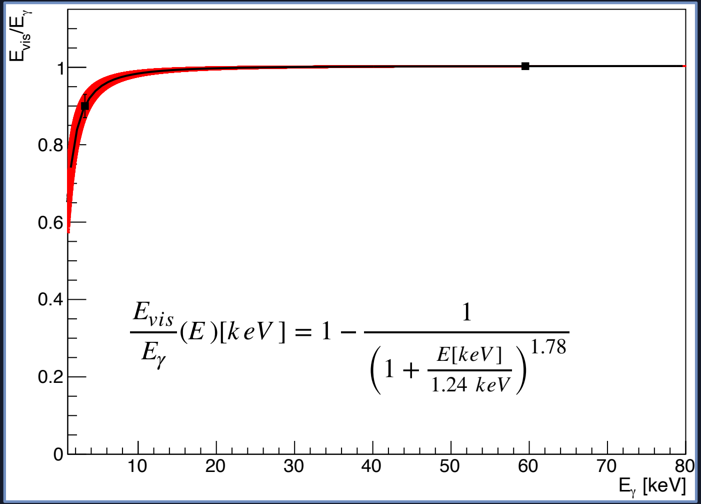

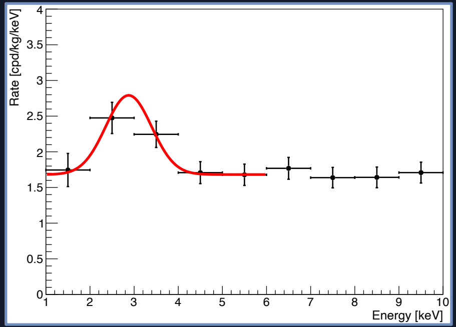

Before calibration

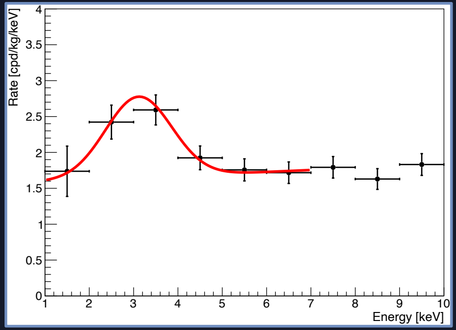

After calibration

^{210}Pb surface contaminations study

Teflon reflector

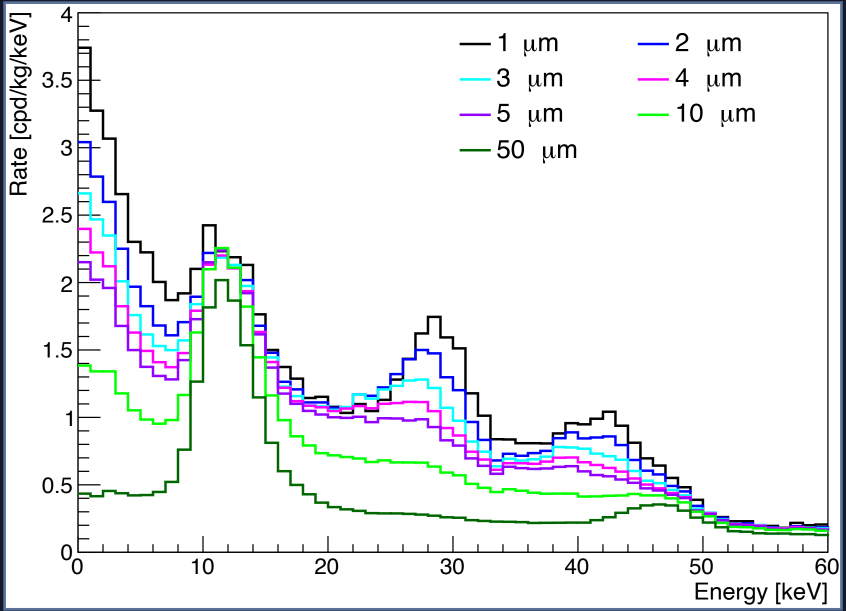

Crystal (surface layer)

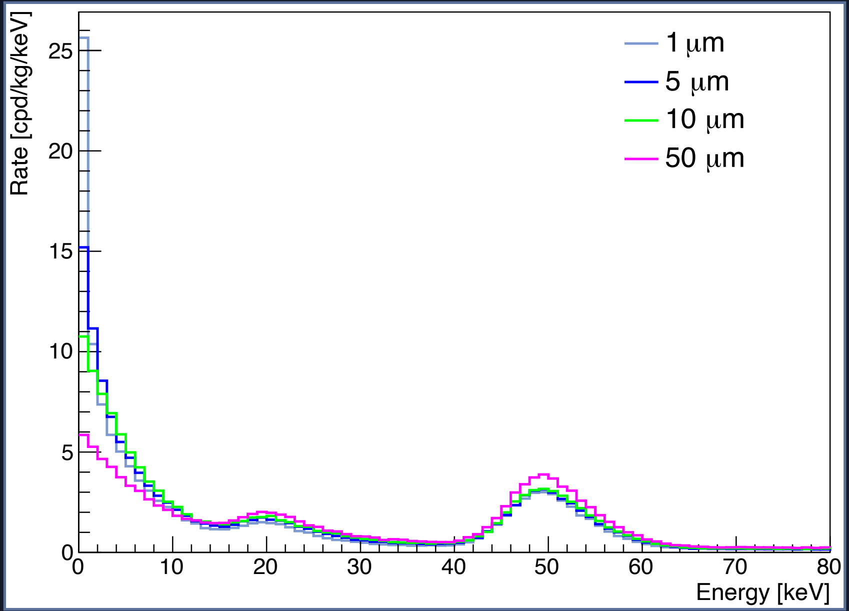

GSSI

Background model - [1-100] keV

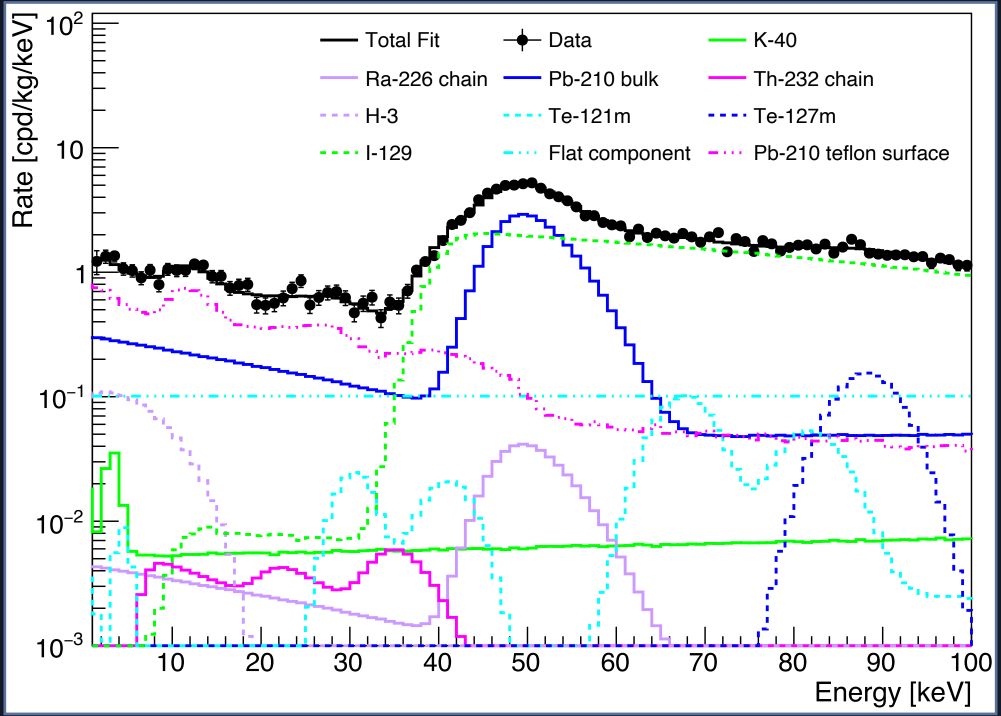

SABRE sensitivity - method

For every couple of M_W in the range [1-1000] GeV and $\sigma_{SI,n}$ between 10^{-42} and 10^{-38} cm^2:

- **1000 pseudo-experimental distributions** of rate as a function of time:
  - Monthly rate randomly extracted from a Poisson distribution with mean value **unmodulated rate+background**;
  - Energy varying from 1 to 6 keV in ten 0.5 keV bins.

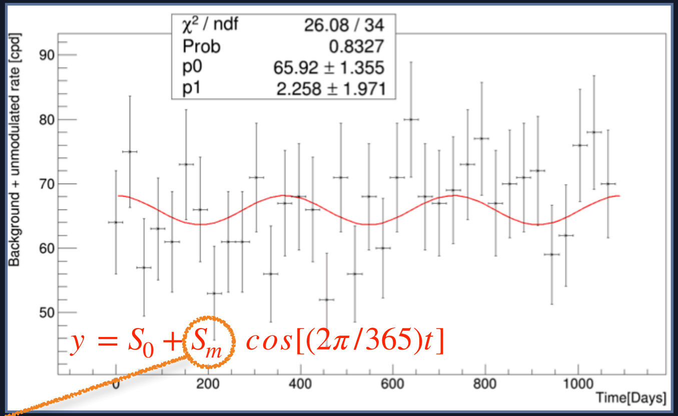

V. Toso, Master thesis, Università degli Studi di Milano, 2017.

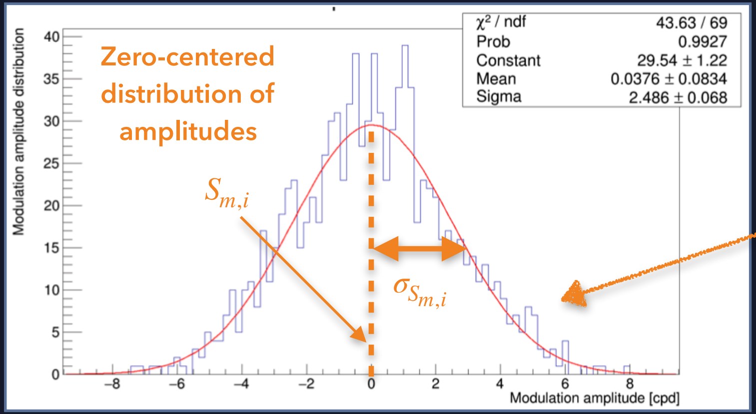

V. Toso, Master thesis, Università degli Studi di Milano, 2017.

$$\chi^2(M_W, \sigma_{SI,n}) = \sum_{i=1}^{N_{bins}} \left(\frac{S^{th}_{m,i} - S_{m,i}}{\sigma_{S_{m,i}}} \right)^2$$

90% C.L. sensitivity limit obtained cutting at $\chi^2 = 2.71$

SABRE sensitivity for different background levels

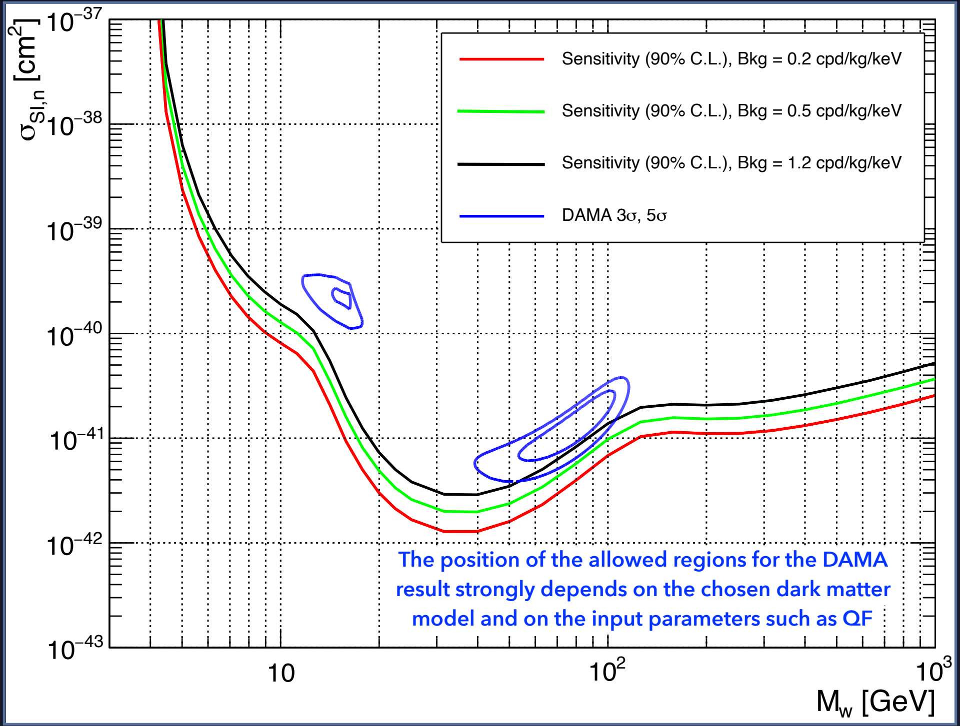

Assumptions:

- Standard Halo Model;
- Spin-independent WIMP-nucleon interaction;
- **50 kg** of NaI(Tl) crystals;
- **3 years** of data taking.

SABRE sensitivity - systematics

The effect of the uncertainties on different parameters was considered:

1) Energy resolution;
2) Detector efficiency;
3) Quenching factor for Na;
4) Quenching factor for I;
5) Background level in the ROI.

→ Simultaneously varied by randomly sampling 200 times from their expected distributions (Gaussian distributions assumed).

1) $\sigma(E)/E = 0.454/\sqrt{E}$ –> $\mu = 0.454$, $\sigma = 25\%$;
2) $\varepsilon(E) = 1.013 - 0.91/E$ –> $\mu_1 = 1.013$, $\sigma_1 = 0.1\%$; $\mu_2 = 0.91$, $\sigma_2 = 2\%$;
3) Xu et al. measurement (energy-dependent) –> $\mu_{1,2}$ and $\sigma_{1,2}$ determined from a linear fit to data;
4) DAMA measurement –> $\mu = 0.09$, $\sigma = 1\%$;
5) 0.2 cpd/kg/keV –> $\mu = 0.2$, $\sigma = 30\%$.

Each set of sampled values was used to build the distribution of sensitivity limits.

The ±1σ and ±2σ error bands are defined as the 16° and 84° percentile, and the 2.25° and 97.75° percentile of the sensitivity limits distribution, respectively

GSSI

GSSI

Backup 2

WIMPs

Generic class of DM candidates

- Weakly interacting with ordinary matter (besides gravitationally)
- Neutral
- Non-relativistic ("cold")
- Massive
- Stable (or at least very long-lived)

$$\Omega_{DM} \approx 0.1 \frac{3 \times 10^{-26} cm^3/s}{< \sigma v >}$$

Weak cross section: $\sigma \sim G_F^2 M_{DM}^2$

$$if \quad M_{DM} = 100\ GeV \Rightarrow < \sigma v > \sim 10^{-26} cm^3/s$$

"WIMP Miracle"

Three ways for the “dark side” of the Universe

https://www.lngs.infn.it

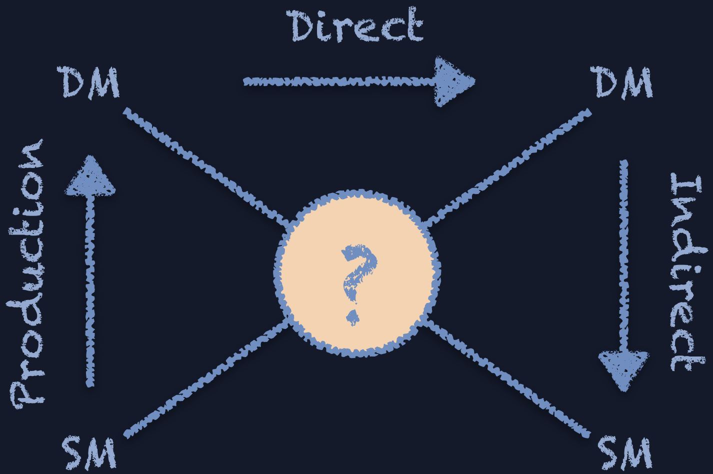

R. E. Allen, *Phys. Scr.*, 89:018001, 2014.

NASA.

Monitoring of the operations

Commercial NaI placed inside the passive shielding to monitor the environmental background

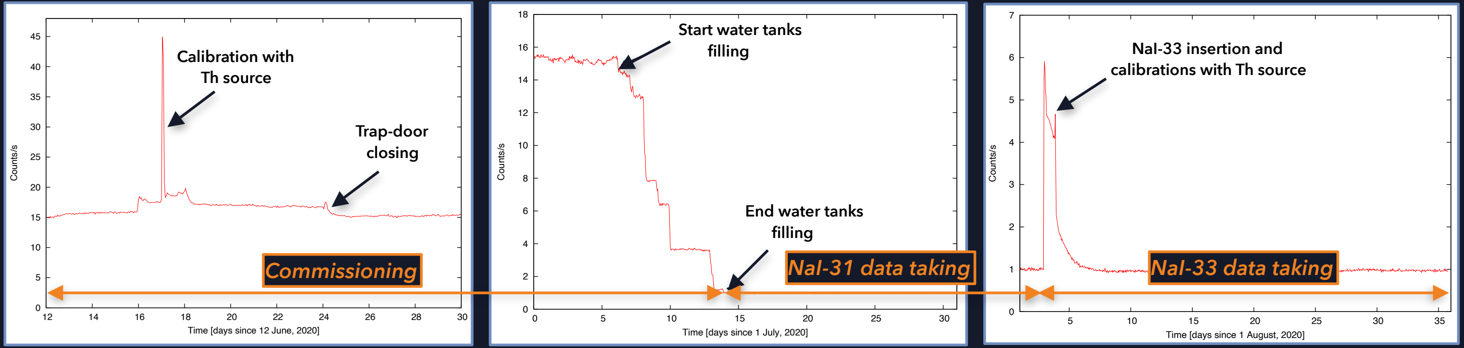

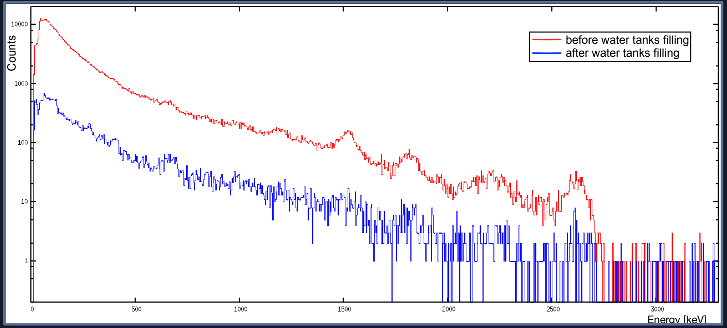

Reliable, stable and precise monitoring during the whole period

Rate ~1 counts/s (water tanks filled)

↓

Reduction of about one order of magnitude

PMTs operating conditions

Single Electron Response (S.E.R) and Gain (G) evaluated as a function of the voltage applied

- 12-bit ADC resolution **Teledyne LeCroy HDO6104 scope** digitizing at 2.5 GS/s;
- Signal pulse integrated over an interval of 150 ns starting from the trigger as well as the baseline in a pre-trigger region of the same length;
- PMTs charge spectrum built after baseline subtraction –> **Single phe peak easily recognizable and dominant over multiple phe structures.**
- **Gaussian fit** to extract **mean value of S.E.R. peak area** for each voltage applied.

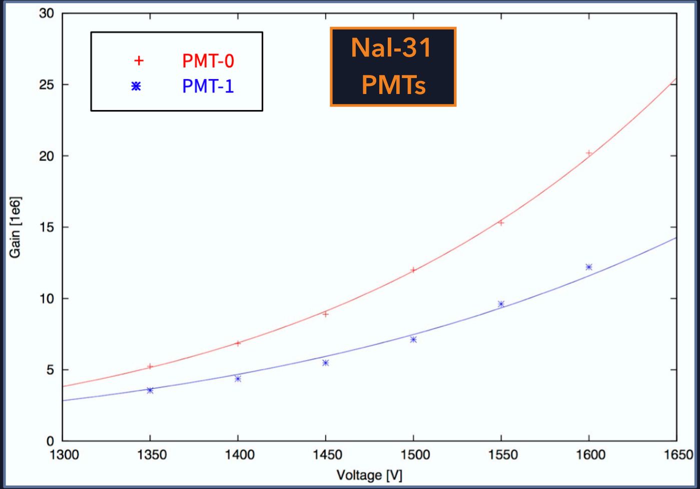

$$G = \frac{Q_{tot}}{e} = \frac{\int_{0\,ns}^{150\,ns} V(t)dt}{eR}$$

e = 1.602x10^{-19} C; R = 25 Ω (load resistance seen by PMTs)

- **NaI-31:** S.E.R. ~28 pV·s, G ~7x10^{6};
- **NaI-33:** S.E.R. ~20 pV·s, G ~5x10^{6}.

Cosmogenic contaminants in NaI(Tl) crystals

Source	Half-life [days]	Decay mode	Main emissions energy [keV]	Estimated activity at t_0 [mBq/kg]
^{126}I	12.9	EC, β^+, β^-	31.8	3.4 ± 0.5
^{125}I	59.4	EC	$35.5 + 31.8 = 67.3$	1.0-1.7
^{121m}Te	154	IT, EC	294.0	< 0.15
^{123m}Te	119	IT	247.6	< 0.09
^{125m}Te	57.4	IT	144.8	< 0.10
^{127m}Te	107	IT, β^-	88.3	< 0.14
^{113}Sn	115	EC	27.9	-
^{3}H	4500	β^-	-	-
^{129}I	$1.57 \cdot 10^7$ yr	β^-	-	-
^{22}Na	950	EC, $\beta+$	0.87, 511 and 1274.6	-

Events selection in Hall B data: ^{108m}Ag calibration run

- Twofold selection strategy: **cut-based selection** and a **Boosted Decision Trees (BDT) analysis**.
- The event selection is based on several variables which are common to both approaches.
- Selection criteria tuned on a calibration run with a ^{108m}Ag source.

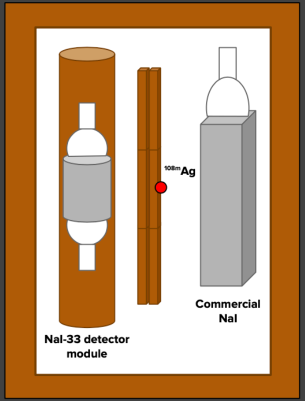

Schematic view of the setup

The ^{108m}Ag source produces three simultaneous gamma rays of 434 keV, 614 keV and 723 keV. Coincident signals are observed in two crystals: NaI-33 and a commercial NaI detector.
Copper between the source and the NaI-33 was used to degrade the gamma energies and increase the statistics of low energy depositions in the NaI-33.

Pulse Shape Discrimination (PSD) parameters

Amplitude weighted mean time	$\langle t\rangle_{600}$	$= \dfrac{\sum_{t_i<600\text{ ns}} h_i t_i}{\sum_{t_i<600\text{ ns}} h_i}$
Charge over maximum	CoM	$= \dfrac{C_{(0,1000)}}{h_{max}}$
Tail-to-total pulse shape	X_1	$= \dfrac{C_{(100,600)}}{C_{(0,600)}}$
Head-to-total pulse shape	X_2	$= \dfrac{C_{(0,50)}}{C_{(0,600)}}$
Asymmetry	A	$= \dfrac{E_0 - E_1}{E_0 + E_1}$
Head-to-middle pulse shape	C_2/C_1	$= \dfrac{C_{(200,400)}}{C_{(0,200)}}$
Middle-to-tail pulse shape	C_3/C_2	$= \dfrac{C_{(400,600)}}{C_{(200,400)}}$
Time Variance	Var[t]	$= \langle t^2\rangle_{600} - \langle t\rangle^2_{600}$
Skewness	Skw[t]	$= \dfrac{\langle t^3\rangle_{2000}}{(\langle t^2\rangle_{2000})^{3/2}}$
Kurtosis	Krt[t]	$= \dfrac{\langle t^4\rangle_{2000}}{(\langle t^2\rangle_{2000})^2} - 3$
Combination of X_1 and X_2	ES	$= \dfrac{1-(X_2-X_1)}{2}$
Combination of Skw[t] and Krt[t]	SK	$= (a\cdot \text{Skw}[t] - b\cdot \text{Krt}[t] - c)^2 + (\text{Krt}[t] - d)^2$

a = 30, b = 5.2, c = 50 and d = 2

- h_i and t_i are the pulse amplitude in mV and the time of the i-th sample (starting from the trigger, t_0);
- h_{max} is the absolute value of the maximum pulse amplitude in mV;
- $C(t_i, t_f)$ is the pulse area between t_i and t_f in ns;
- E_0 and E_1 correspond to the energy measured by each of the two PMTs in the 1000 ns following the trigger;
- Energy estimated for each channel as C(0, 1000)/(S.E.R. x LY_{ch}).

Kolmogorov-Smirnov (KS) distance from a ^{241}Am reference pulse

KS is the maximum distance between the CDF of data samples and a ^{241}Am reference pulse

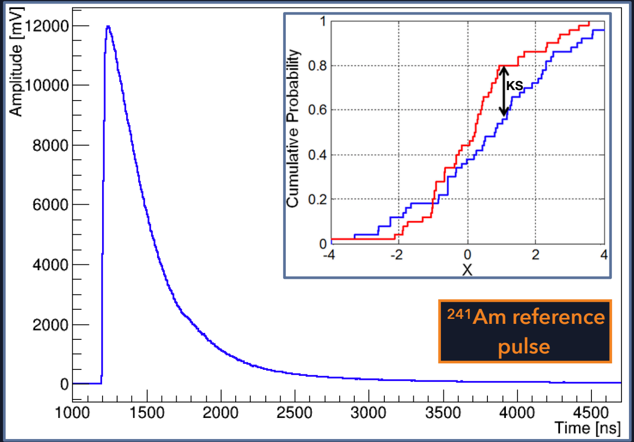

Cut-based analysis Hall B

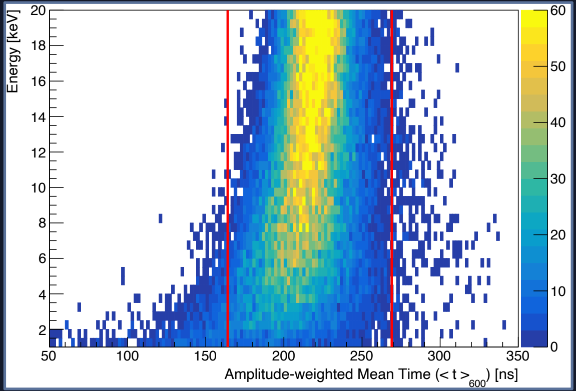

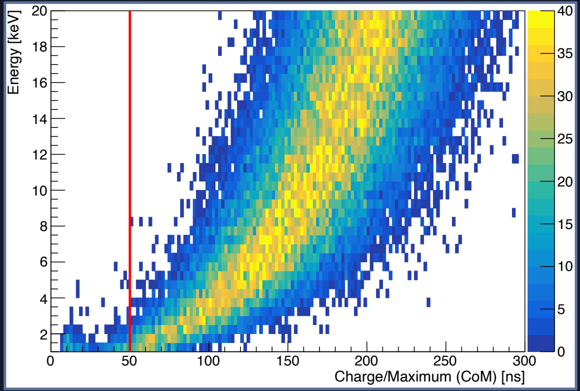

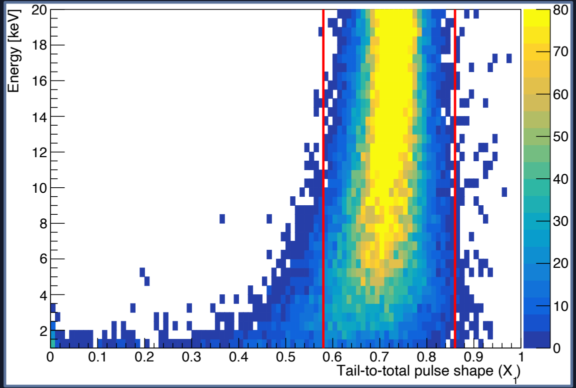

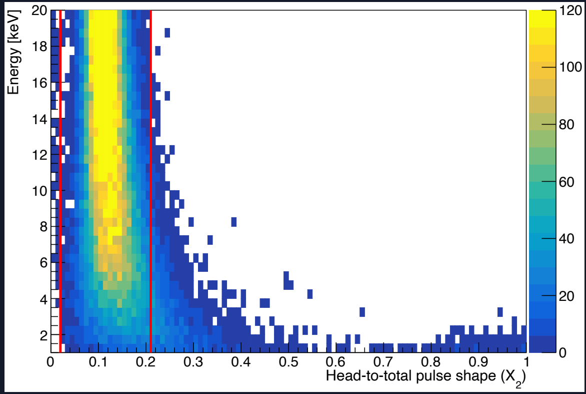

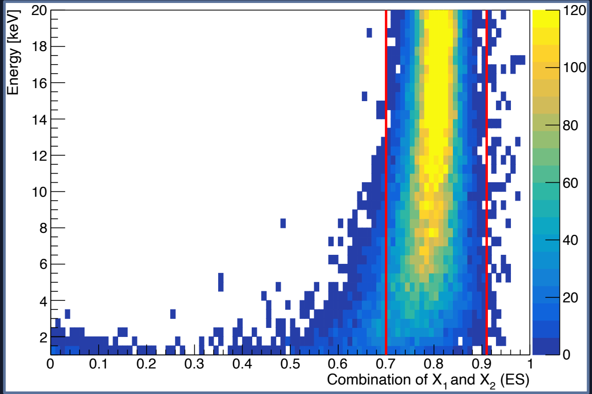

Cut-based analysis Hall B

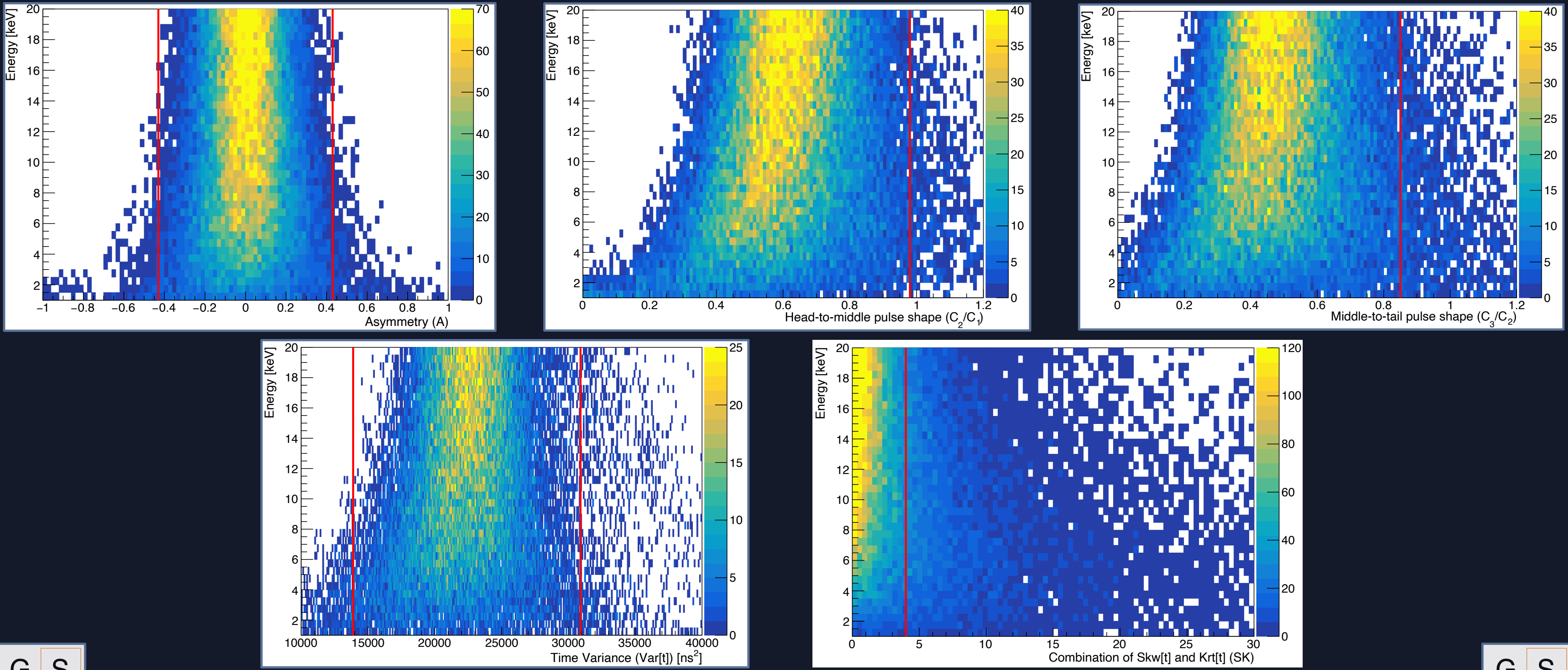

Boosted Decision Trees (BDT)

- **Decision tree:** sequential application of cuts splits the data into nodes, where the final nodes (leaf) classify an event as signal or background.
- **Events selection** done on a **majority vote on** the result of **several decision trees**, all derived from the same training sample by supplying different event weights during the training.
- **Training** is the process to **define cut criteria** for each decision node.
- Depending on how often an event is classified as signal, a "likelihood" **estimator** is **constructed for the event being signal** or **background**.
- The value of the **estimator** is **used to select the events** from an event sample.

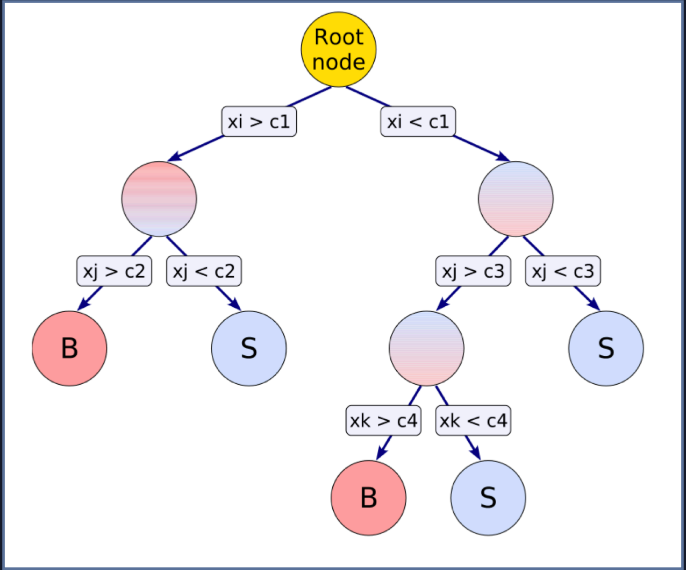

BDT is very efficient in combining several weak discriminating parameters into a single powerful discriminator

BDT training

Using TMVA ROOT package:
https://root.cern.ch/download/doc/tmva/TMVAUsersGuide.pdf

Training sample:

- **Signal** –> ^{108m}Ag calibration run, evt with energy up to 100 keV;
- **Background** –> background data, evt with energy up to 10 keV (dominated by noise)

The analysis was performed by training two separate BDTs.

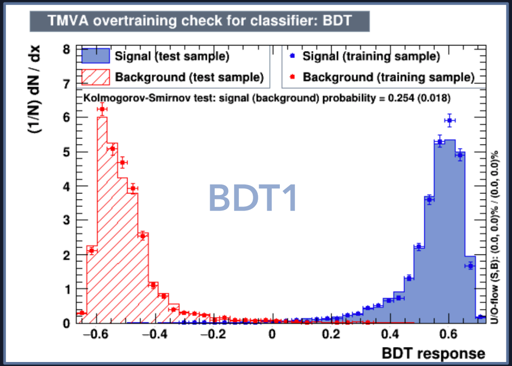

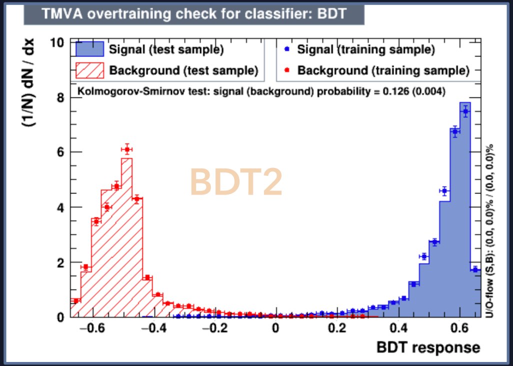

BDT1:
- $< t >_{600}$;
- CoM;
- X_1
- X_2
- A
- C_2/C_1
- C_3/C_2
- Var[t]
- NC

BDT2 (BDT1 variables plus):
- **Skw[t]**
- **Krt[t]**

BDT **classifier output** defined between **-1** (bkg-like) and **1** (signal-like)

Boosted Decision Trees (BDT) analysis

- Selection criteria on the BDT variables tuned on data acquired with the ^{108m}Ag source;
- We select as scintillation events only those passing both thresholds.

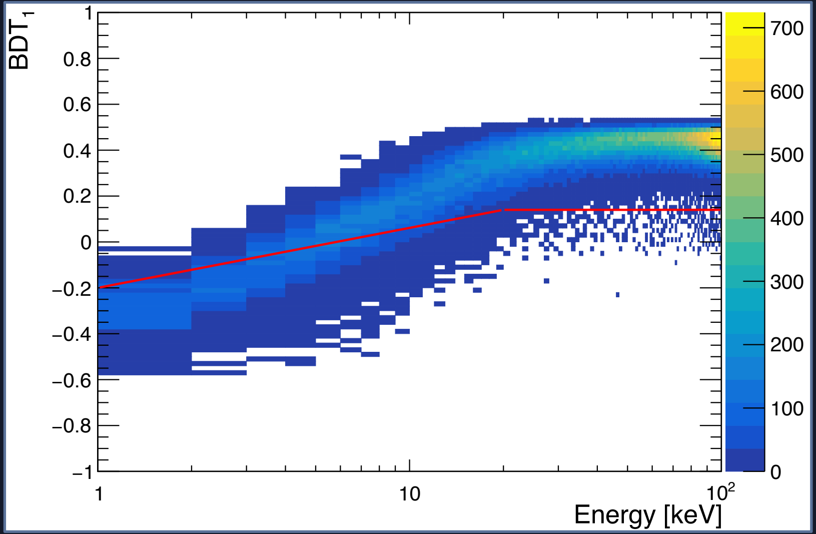

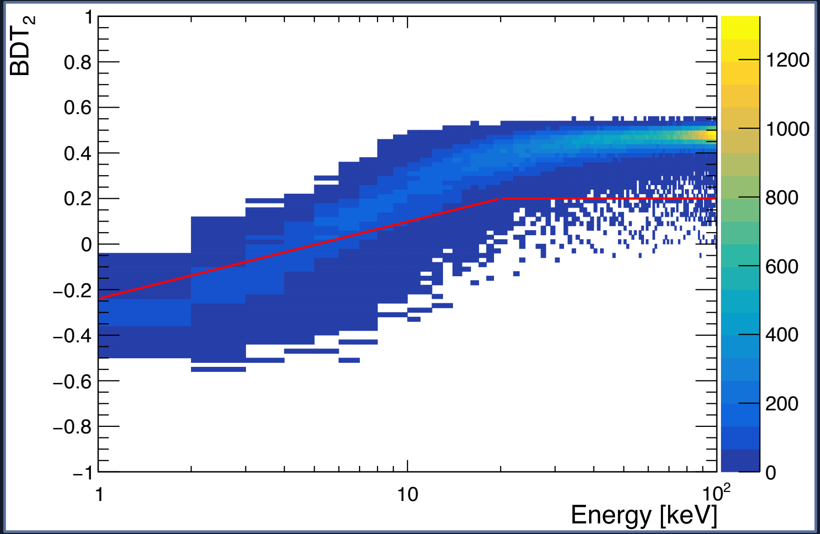

Energy-dependent threshold chosen for the two BDTs in order to ensure an acceptance for each BDT of ~50% (99.8%) in the energy range [1-3] keV ([20-100] keV)

GS SI

GS SI

Hall B results

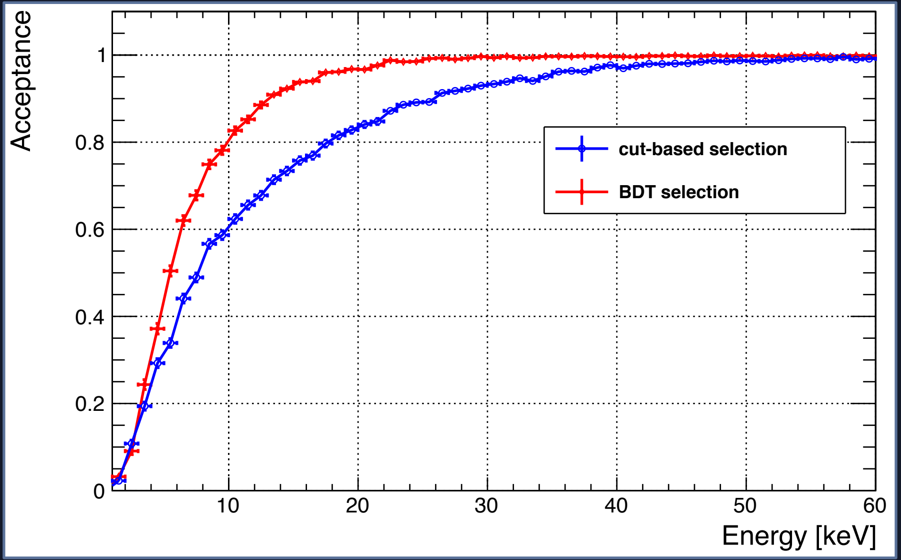

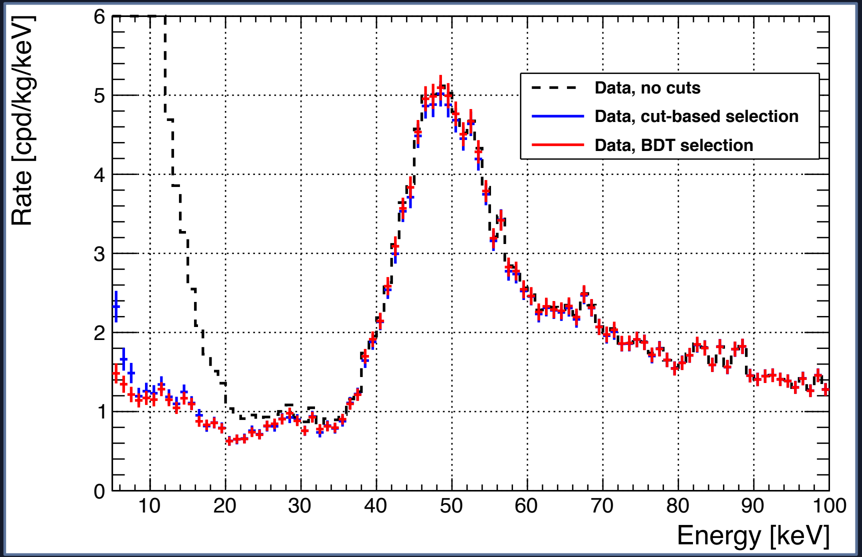

SABRE sensitivity - assumptions

SABRE sensitivity limit calculated under the following assumptions:

- Standard Halo Model:
  - $\rho_W = 0.3$ GeV/cm^3, $\sigma_v = 220$ km/s, $v_{esc} = 544$ km/s;
- Spin-independent WIMP-nucleon interaction;

Model-dependent

- 50 kg of NaI(Tl) crystals;
- 3 years of data taking;
- Background level in the ROI of 0.2 cpd/kg/keV;
- Energy resolution: $\sigma(E)/E = 0.454/\sqrt{E}$ (derived from a ^{241}Am calibration run);
- Detector efficiency: $\varepsilon(E) = a - b/E$, where $a = (1.013 \pm 0.001)$ and $b = (-0.91 \pm 0.02)$ keV;

Experiment-dependent

- Quenching factor for Na measured by Xu et al.;
- Quenching factor for I measured by DAMA (0.09).

Model and experiment-dependent

R. Bernabei et al., *Phys. Lett. B*, 389:757–766, 1996.

Na-recoil QF measurements

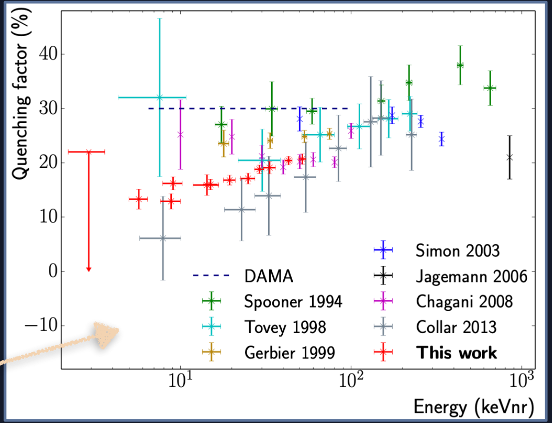

J. Xu et al., *Phys. Rev. C*, 92(1):015807, 2015.

DAMA allowed regions

Obtained from the best-fit to the modulation amplitude measured by DAMA/NaI and DAMA/LIBRA-phaseI in the [2-6] keV energy region

- For every couple of M_W in the range [1-1000] GeV and $\sigma_{SI,n}$ between 10^{-42} and 10^{-38} cm^2:

$$\chi^2(M_W, \sigma_{SI,n}) = \sum_{i=1}^{NDAT} \left(\frac{S_{m,i} - S^{th}_{m,i}}{\sigma_{S_{m,i}}} \right)^2$$

where:

- NDAT number of experimental data points;
- $S_{m,i}$ ($S^{th}_{m,i}$) measured (theoretically expected) modulation amplitude;
- $\sigma_{S_{m,i}}$ uncertainty of the measurement.

$$S^{th}_{m,i}(E_R) \approx \frac{1}{\Delta E} \int_E^{E+\Delta E} \frac{\partial}{\partial v} \frac{dR}{dE_R} \Delta v_E dE$$

Assumptions:

- Standard Halo Model;
- Spin-independent WIMP-nucleon interaction;
- Quenching factor for Na measured by Xu et al. (energy-dependent);
- Quenching factor for I measured by DAMA (0.09);
- Energy resolution measured by DAMA: $\sigma(E)/E = 0.0091 + 0.488\sqrt{E}$

Best values of M_W and $\sigma_{SI,n}$ that reproduce the DAMA experimental data are found minimizing the χ^2

J. Xu et al., *Phys. Rev. C*, 92(1):015807, 2015.
R. Bernabei et al., *Phys. Lett. B*, 389:757–766, 1996.
R. Bernabei et al., *Nuclear Instruments and Methods in Physics Research Section A*, 592(3):297–315, 2008.